

K. F. Dunker
F. W. Klaiber
B. L. Beck
W. W. Sanders, Jr.

Final Report—Part II

Strengthening of Existing Single Span Steel Beam and Concrete Deck Bridges

March 1985

Sponsored by the Highway Division,
Iowa Department of Transportation
and the Iowa Highway Research Board

Iowa DOT Project HR-238
ERI Project 1536
ISU-ERI-Ames-85231

DEPARTMENT OF CIVIL ENGINEERING
ENGINEERING RESEARCH INSTITUTE
IOWA STATE UNIVERSITY, AMES

TABLE OF CONTENTS

	<u>Page</u>
LIST OF TABLES	v
LIST OF FIGURES	vii
1. INTRODUCTION	1
1.1. General Background	1
1.2. Objectives for Phase III of the Investigation	3
1.3. Literature Review	4
1.4. General Research Program	5
1.4.1. Field Testing Program	6
1.4.2. Simplified Design Methodology	7
2. DEVELOPMENT OF STRAIN AND FORCE TRANSDUCERS	11
2.1. Strain Transducer System	11
2.1.1. Literature Review	11
2.1.2. System Design Criteria	12
2.1.2.1. Structural	13
2.1.2.2. Circuit	17
2.1.3. Transducer System Design	19
2.1.4. Transducer System Laboratory Testing	24
2.1.4.1. Preliminary	24
2.1.4.2. Calibration	28
2.1.4.3. Curvature	33
2.1.4.4. Temperature	37
2.2. Force Transducers	40
2.2.1. System Design Criteria	41
2.2.2. Transducer System Design	42
2.2.3. Laboratory Testing	46
2.2.3.1. Preliminary	46
2.2.3.2. Calibration	47
2.3. Force Transducer Field Tests	50

	<u>Page</u>
3. RETESTING OF BRIDGES 1 AND 2	53
3.1. General Background	53
3.2. Instrumentation and Test Procedure	55
3.3. Test Results and Analysis	66
3.3.1. Bridge 1	67
3.3.2. Bridge 2	73
4. THERMAL EXPANSION CONSIDERATIONS	81
4.1. Temperature Transducer System	82
4.1.1. Description of Temperature Transducers	82
4.1.2. Calibration and Testing of Transducers	85
4.2. Field Testing	87
4.2.1. Test Procedures	88
4.2.2. Test Results	91
4.2.3. Analysis and Conclusions	99
5. DEVELOPMENT OF POST-TENSIONING DESIGN METHODOLOGY	103
5.1. Finite Element Model	103
5.2. Distribution Parameters	107
5.3. Force and Moment Distribution Fractions	115
5.4. Ultimate Strength Tests	122
5.5. Analytical Strength Model	127
6. SUMMARY, CONCLUSIONS, AND RECOMMENDATIONS	133
6.1. Summary	133
6.2. Conclusions and Recommendations	136
7. RECOMMENDED CONTINUED STUDIES	139
8. ACKNOWLEDGMENTS	141
9. REFERENCES	143

LIST OF TABLES

	<u>Page</u>
Table 1. Calibration constants for strain transducers: gage factor, $S_g = 2.115$.	32
Table 2. Comparison of strain gage and transducer strain values for a typical curvature effect test.	38
Table 3. Calibration constants for force transducers mounted on 1-inch and 1.25-inch tendons: gage factor, $S_g = 2.09$.	49
Table 4. Comparison of experimental post-tensioning force data: Bridge 1.	71
Table 5. Comparison of experimental truck loading data: Bridge 1.	72
Table 6. Comparison of experimental post-tensioning force data: Bridge 2.	77
Table 7. Comparison of experimental truck loading data: Bridge 2.	78
Table 8. Comparison of experimental and computed strength.	131

LIST OF FIGURES

	<u>Page</u>
Fig. 2.1. Strain transducer details.	21
Fig. 2.2. Strain gage location and electrical circuit layout of strain transducer.	23
Fig. 2.3. Close-up photograph of strain transducer clamped on calibration bar.	26
Fig. 2.4. Typical calibration curve for strain transducer.	30
Fig. 2.5. Curvature effect on transducer performance.	34
Fig. 2.6. Loading apparatus utilized in determining effect of curvature on transducer performance.	36
Fig. 2.7. Force transducer details.	43
Fig. 2.8. U-clamp required for attaching force transducer.	45
Fig. 2.9. Typical calibration curve for force transducer.	48
Fig. 2.10. Location of instrumentation--Bridge 1.	56
Fig. 2.11. Location of instrumentation--Bridge 2.	58
Fig. 2.12. Wheel configuration and weight distribution of test vehicles.	60
Fig. 2.13. Location of test vehicle--Bridge 1.	61
Fig. 2.14. Location of test vehicle--Bridge 2.	62
Fig. 2.15. Variation in midspan, bottom flange beam strains as post-tensioning force is applied to Beams 1 and 4--Bridge 1.	68
Fig. 2.16. Post-tensioning, bottom flange beam strains--Bridge 1.	69
Fig. 2.17. Variation in midspan bottom flange strains as post-tensioning force is applied to Beams 1 and 4--Bridge 2.	74

	<u>Page</u>
Fig. 2.18. Post-tensioning, bottom flange beam strains--Bridge 2.	75
Fig. 2.19. Description of temperature transducers.	84
Fig. 2.20. Temperature transducer sensitivity with respect to time.	87
Fig. 2.21. Determination of transducer response with respect to degree of sunlight exposure.	89
Fig. 2.22. Generally layout of temperature instrumentation-- Bridge 2.	90
Fig. 2.23. Surface temperature of tendons mounted on Beam 4.	92
Fig. 2.24. Surface temperature of tendons mounted on Beam 1.	94
Fig. 2.25. Comparison of average inside and outside tendon temperatures to bottom flange beam temperature of Beam 4.	96
Fig. 2.26. Comparison of average inside and outside tendon temperatures to bottom flange beam temperature of Beam 1.	97
Fig. 2.27. Bridge 2 peak temperatures.	101
Fig. 2.28. SAP IV Finite Element Model.	105
Fig. 2.29. Quarter symmetry composite bridge model.	108
Fig. 2.30. Post-tensioning distribution for a typical eccentric force, right-angle bridge, 51.25 ft. actual span.	110
Fig. 2.31. Force, eccentric force and moment distribution for a right-angle bridge, 51.25 ft. actual span.	112
Fig. 2.32. Effects of several parameters on moment distribution.	114
Fig. 2.33. Regression formula variables.	118
Fig. 2.34. Regression formulas for force and moment fractions.	119
Fig. 2.35. Post-tensioning distribution and interpolation.	121

	<u>Page</u>
Fig. 2.36. Post-tensioning stresses for 51.25 ft. span, 4-Beam Bridge, 100k applied 3 1/4 in. above bottom flange, each exterior beam.	123
Fig. 2.37. Post-tensioned composite beams (Stras).	126
Fig. 2.38. Failure mechanism--Idealized post-tensioned composite beams.	129

1. INTRODUCTION

1.1. General Background

A significant number of Iowa's single-span, composite concrete deck and steel beam bridges cannot be rated to carry today's design loads. This problem was initially addressed in a research project, HR-214, "Feasibility Study of Strengthening Existing Single Span Steel Beam Concrete Deck Bridges" [17,18], henceforth referred to as Phase I. The Phase I research analytically and experimentally indicated that post-tensioning was a viable method for strengthening the composite bridges under investigation. Phase II of this research study, which was reported earlier in "Strengthening of Existing Single Span Steel Beam and Concrete Deck Bridges, Final Report--Part I," [16] was a continuation of the feasibility study (Phase I). The primary emphasis of Phase II involved the strengthening of two full-scale prototype bridges. One of the bridges was a prototype of the model bridge tested during Phase I; the other bridge was skewed and had a larger span.

In addition to the field work, Phase II also involved a considerable amount of laboratory work. As only minimal data were found on the strength of angle-plus-bar shear connectors and on the strength of high-strength bolts utilized as shear connectors, two-slab push-out tests were performed to obtain such data [12,16]. To obtain additional shear connector information, the bridge model of Phase I was sawed into four composite concrete slab and steel beam specimens. High-strength bolt shear connectors were added to one exterior slab-beam specimen and to one interior slab-beam specimen. The other two specimens (one interior

and one exterior) were left as originally fabricated. All four specimens were then tested, thus determining the effectiveness of the additional shear connectors.

As previously mentioned, one of the bridges to be strengthened was skewed. To obtain data on a skewed bridge's behavior and thus verify the analysis being used, a small plexiglas model was fabricated. This model, when subjected to vertical load distribution tests and post-tensioning force distribution tests, provided valuable data.

Phase III of this investigation involved the inspection of the two bridges approximately every three months for approximately two years. After being in service for roughly two years, the two strengthened bridges were retested to determine changes in their behavior, any decrease in the post-tensioning force originally applied (1982), and the existence of end restraint. To facilitate the collection of strain and force data on the two bridges (as well as any other bridges tested in the future) transducers were developed. Another part of Phase III of the research study involved the development of a design methodology for the practicing engineer to use in the design of a post-tensioning strengthening system.

The results of Phase III of the investigation are reported herein as Part II of the Final Report and in Ref. 15 as the conclusion to the overall research study. Because portions of the work of Phase III are a continuation of work initiated during Phase II, the writers do not wish the reports on these phases to be completely independent. Rather than duplicate figures which apply to both phases of the study, this report will refer to figures in the report on Phase II [16]. To assist

the reader in locating the various figures the following numbering system will be used:

Final Report - Part I [16] Figs. 1-69, A-1 and A-2

Final Report - Part II Figs. 2.1-2.38

There is no relationship between the figures of the "Design Manual" (Final Report - Part III) [15] and the other parts of the final report.

1.2. Objectives for Phase III of Investigation

The unifying objective of Phases I and II of the study was to determine the feasibility of the post-tensioning strengthening method and to implement the technique on two composite bridges in Iowa. As a result of the successful completion of the first two phases of this study, Phase III was undertaken with the basic objectives of further monitoring bridge behavior (both during and after post-tensioning) and developing a practical design methodology for designing the strengthening system in question. In line with the overall objectives of Phase III of this study, the following specific objectives were established:

- To develop strain and force transducers to facilitate the collection of data in the field.
- To investigate further the existence and effects of the end restraint on the post-tensioning process.
- To determine the amount of post-tensioning force loss that occurred during the time between the initial testing and the retesting of the existing bridges.

- To determine the significance of any temporary temperature-induced post-tensioning force change.
- To develop a simplified design methodology that would incorporate various variables such as span length, angle-of-skew, beam spacing, and concrete strength.

Experimental field results obtained during Phases II and III were compared to the theoretical results and to each other.

1.3. Literature Review

The reports on Phases I and II of this study [16,17] include literature reviews that covered the following six areas: prestressed steel structures, prestressed composite structures, bridge strengthening, bridge deck analysis, mechanical shear connectors, and effect of skew on bridge deck behavior. Although the majority of these references pertain to the work in Phase III a review will not be repeated herein because of their availability in the other reports [16,17]. Since the issuing of the two reports previously described, two studies have been conducted that involved strengthening by post-tensioning; these will be briefly described in the following paragraphs. Pertinent references on transducer design and finite element analysis, which were used in the completion of Phase III of this study, are given in Chapters 2 and 5 of this report, respectively.

During Summer 1984 a steel-beam composite concrete-deck bridge located in Pasco County, Florida near the intersection of County Road 54 and 1 was repaired and strengthened. This bridge consists of three

simple spans end to end; each span had four beams the same size. As the desire was to increase the rating of the bridge from an H 15 to an HS 20, it was necessary to post-tension all twelve beams. The strengthening system was designed by the consulting firm of Howard Needles Tammen and Bergendoff (Orlando, Florida office). As the bridge to be strengthened was different in several aspects from those strengthened by the authors, Iowa State University proposed a testing program and was retained by HNTB to do the proposed testing. The results of this field work, effect of end restraint, relieved stresses, continuity between spans, etc., may be found in Ref. 4.

California has strengthened seven steel bridges [20] by post-tensioning in the period from 1979-1984 and is planning to strengthen at least twelve more. As the bridges being strengthened have beams all of the same size and thus are all being post-tensioned, lateral distribution of post-tensioning force is not a major problem. To date, all bridges have been strengthened using strand that is enclosed in galvanized pipes and grouted after post-tensioning. All prestressing systems and anchorage hardware must be tested and approved by the Caltrans Transportation Laboratory prior to installation.

1.4. General Research Program

As previously stated, Phase III of the study consisted of both a field investigation and the development of a design methodology to be used by practicing engineers. Details on these two undertakings are presented in the following sections.

1.4.1. Field Testing Program

The field investigation consisted of three major undertakings: One involved the development of strain and force transducers to be used for simplifying data collection procedures; the second involved retesting the two post-tensioned existing bridges; the third involved determining the effect of temperature on the post-tensioned bridges to determine the extent of any change in post-tensioning force due to normal temperature fluctuations.

Transducer design criteria were established with respect to the particular data to be measured and the specimen from which they were to be obtained. Designs were completed for both the strain and force transducers, and a calibration procedure was developed. Both transducers (force and strain) could operate with either a data acquisition system or a commercial strain indicator. Several possible sources of error in both transducers were investigated. A total of 10 strain transducers and 10 force transducers were fabricated and calibrated.

The two existing bridges post-tensioned as part of Phase II were retested. Bridge 1 (a four-beam 50-ft \times 30-ft I-beam right-angle bridge) is located in Dickinson County, 2.2 miles north of Terril on county road N14. Bridge 2 (a four-beam 70-ft \times 30-ft I-beam 45° skewed bridge) is located in Greene County a few yards south of the Greene-Webster County line on Iowa Highway 144. Both bridges were instrumented with strain gages (most of which were applied during Summer 1982), transducers, and direct current differential transformers to monitor their behavior. After employing static truck loading tests similar to the tests conducted during Phase II, the post-tensioning force was

released to determine the extent of any losses in post-tensioning force. The bridges were then re-strengthened by applying a post-tensioning force slightly greater than what had been applied during Phase II. End restraint was closely monitored during all field testing of the existing bridges.

A temperature transducer system was developed so that temperature differences between the steel beams and the post-tensioning tendons could be determined. Temperature fluctuations were measured for the individual components of the beam flange-tendon combination. From these measured values the magnitude of temporary temperature-induced post-tensioning force loss or gain was determined.

1.4.2. Simplified Design Methodology

For preliminary analysis and design in Phases I and II, the authors modified an existing computer program that was based on a series solution to orthotropic plate theory. The orthotropic plate program gave approximately correct results but, for improved accuracy, the authors decided to develop a design methodology specifically for distribution of post-tensioning.

After exploring the theoretical methods--orthotropic plate theory, grillage theory and finite element theory--finite element theory was selected because it could be used to determine the distribution for both the axial force portion and the moment portion of the post-tensioning. Finite element analysis was also much more adaptable to the specific construction of the Iowa composite bridges.

Several series of three- and four-beam bridges designed as standard bridges by the Iowa DOT and several individually designed four-beam

composite bridges were analyzed with a finite element bridge model to determine axial force and moment distribution factors. By means of multiple linear regression, the finite element results were utilized to determine relatively simple distribution factor formulas. The formulas make use of relatively few bridge parameters such as aspect ratio of the post-tensioned region, relative beam stiffness and a deck thickness-to-span ratio to determine the distribution factors. Skew did not affect the post-tensioning distribution as much as expected and generally can be neglected if the skew does not exceed 45° .

The regression formulas give the axial force and moment factors at midspan. For other locations on the span a simple linear interpolation will give a very good estimate of the post-tensioning distribution.

The design methodology is based entirely on service load design. Under service load design, post-tensioning can relieve a certain amount of flexural tension overstress. Post-tensioning must be carefully controlled, however, or it can cause overstress at locations other than the location where stress is being relieved.

Post-tensioning also will increase the strength of a composite bridge, although not to the same extent as it will increase service load capacity. The increase in strength for an individual bridge beam can be computed using a simple analytical model developed by the authors and contained in Section 5.5 of this report. Distribution factors at ultimate load are not available at the time of this writing, however.

Post-tensioning can increase the flexural, service load capacity as well as the flexural strength of a bridge. It does not significantly affect the live-load distribution or bending deflection behavior of a

composite bridge. Bridge deficiencies other than flexural overstress must be corrected by strengthening or repairs in addition to post-tensioning.

2. DEVELOPMENT OF STRAIN AND FORCE TRANSDUCERS

2.1. Strain Transducer System

2.1.1. Literature Review

Numerous types of strain transducers have been developed for use in a variety of applications [11]. Many of these, such as the Huggenberger tensometer, were of the mechanical type. With the advent of the electrical resistance strain gage, the general use of mechanical strain transducers has declined considerably. The electrical resistance strain gage has been employed in strain transducer systems to measure both axial and biaxial strain fields on homogeneous and composite materials [10,19].

The Federal Highway Administration (FHWA) several years ago sponsored research investigating the possibility of using bridges as a means of weighing trucks. A weigh-in-motion concept was developed that utilized portable reusable transducers to measure bridge beam strains. Information obtained from the FHWA concerned application of the transducer to a steel I-beam. During August 1983, Bridge Weighing Systems, Inc., gave a demonstration of weighing trucks on a bridge located near Iowa State University. In this particular application, strain transducers similar to the FHWA model were used to measure strains on the bottom surface of prestressed concrete bridge beams. Data were processed at the site by representatives of Bridge Weighing Systems, Inc.; results obtained were in excellent agreement with pre-determined values.

Past experience during Phase II showed that conventional strain gage techniques were time consuming and required temporarily closing the bridge to traffic to permit proper curing of the adhesive used to bond the strain gages to the beams [16]. An alternate approach to conventional strain gage techniques was needed for measuring the strains in the steel beams resulting from post-tensioning or other types of loading. Thus an objective of one phase of this research study was to develop a strain transducer system that could be used to measure the strains in the steel beams and thus the effectiveness of the post-tensioning strengthening system or the effect of vertical loads. To be considered a feasible alternative, the strain transducer system would have to hold a certain degree of operational advantage over a conventional strain gage system in the areas of ease of use and durability. Also, the strain transducer system would consistently have to give results that were within an acceptable tolerance of correct strain values.

2.1.2. System Design Criteria

The strain transducer system would operate on the same principle as a strain gage; under axial loading conditions the transducer would experience the same tensile or compressive deformations as the material to which it was attached. The change in output voltage from the strain gages in the transducer, caused by the deformations, could be measured and equated to a certain strain in the deformed specimen in which strains were desired. Therefore, the governing criteria for use in the design of strain transducers can be divided into two major areas: Those related to structural design and method of attaching the transducer.

system to the material in which strains are desired, and those concerning the strain gage circuit and electrical recording devices.

2.1.2.1. Structural

Since no clamping method or bonding technique can be guaranteed to hold slip between the transducer and beam flange to an absolute zero reading, determination of acceptable slip tolerances is required. The transducer will be in contact with the beam flange at two points separated by a distance, L , referred to as the gage length. If the beam is stressed uniaxially, this distance L on the beam flange will experience a deformation ΔL_b which is equal to $\epsilon_b L$, where ϵ_b is the average strain along the gage length. The transducer, being clamped to the beam, would experience a deformation ΔL_T . If the amount of slip, "S"--defined as $(\Delta L_b - \Delta L_T)$ --is zero, then there is no error involved due to slip and the transducer output voltage could be related to the exact strain in the beam.

The relationship between percent error of strain reading and slip is

$$\% \text{ Error} = \frac{S}{\epsilon_b L} \times 100 \quad (2-1)$$

In order to understand the physical significance of slip with respect to transducer performance, this equation is applied to the FWHA model transducer which has a gage length of three inches. For post-tensioning work related to this research, the maximum ϵ_b experienced would be approximately 300 microinches per inch [16]. If 5% is considered the maximum tolerable error in the strain transducer system, the maximum

total slip that could occur would be 45 microinches for the 3-inch gage length. Since this amount of slip is extremely small, control of this error must be achieved either through the actual transducer design or by adequate attachment of the transducer to the steel beam flange so that acceptable transducer system performance can be obtained.

As shown in the above equation, one way of controlling the effect of slip on transducer performance would be to increase the gage length L . However, given the stiffness of any particular transducer sensing or spring element, an increase in the gage length would increase the total deformation the spring element would undergo and thus require a larger clamping or bonding force development between the transducer and the steel beam. Also, if the beam strain as measured by the transducer is considered to be the beam strain corresponding to the center of the gage length, an error can be introduced since this measured quantity is the average strain along the gage length and not the strain at a particular point [11]. This error will be present when considering any strain distribution other than one that is linear. If the strain gradient is small with respect to a practical gage length, as would be expected in the post-tensioned beams, the error introduced would be small. Keeping the gage length as short as possible would minimize the effect of this strain-averaging error and require the smallest possible clamping force.

Since minimizing slip between the transducer-beam interface is crucial, the stiffness of the instrumented sensing element of the transducer is also critical. The larger this stiffness, the greater the bonding force that must be developed at the transducer-beam interface

if slip is to be kept at acceptable levels. However, the transducer must have enough structural durability so that it is not damaged during the installation process and its performance is not affected by adverse field conditions. Spring elements that are stressed only in an axial sense have a relatively high stiffness. Spring elements that are stressed principally by flexure, while costing considerably more to machine, can be designed to have a lower stiffness than an axially loaded element when comparing practical designs.

Various possibilities exist for incorporating flexural elements into the transducer design [22]. Decreasing the stiffness of a particular design by adjusting one of the dimensional stiffness parameters, while decreasing the possibility of slip, has the detrimental effect of reducing the spring element's strain and thus the output voltage signal from the transducer. Although a signal amplifier could be used in the circuit, this approach could complicate the system's operation by introducing self-generating voltages due to thermocouple effects or conductors crossing magnetic fields [9]. Therefore, any practical design would have to produce a signal strong enough to be easily recorded by all commercial strain indicators or data acquisition systems. Since achieving optimum transducer performance is so dependent on controlling slip, transducer stiffness rather than the level of signal output voltage is to be regarded as the controlling design factor when comparing these two criteria.

The dimensions of the spring element of the transducer are dictated to some extent by the size of available strain gages. Points of maximum stress on the spring element would need to be wide enough and easily

accessible for strain gage placement and circuit wiring. The configuration of the transducer design would have to be compact enough to be attached to the area in which strains are desired--in this case, beam flanges. Most steel beams used in bridge construction have a coverplate welded to the bottom of the beam approximately two inches narrower than the beam flange. The set-back of the coverplate would require placing the transducer near the center of the beam's bottom flange, thus creating clearance problems between the clamping system and the steel beam's web. Therefore it is necessary to place the transducer on the top surface of the bottom flange. Since the transducer-clamp assembly must fit into the space available on the flange area next to the beam web, the maximum width--dimension normal to the longitudinal axis of the transducer--should be two inches. This would allow the transducer to be easily clamped onto most wide flange sections used in bridge construction.

An aluminum alloy, 2024-T4, was chosen as the material most suitable from which to fabricate the transducers [22]. It had excellent machining properties, good thermal conductivity to dissipate thermal energy from the strain gages, and a relatively low modulus of elasticity, thus giving a low stiffness. While the rated yield stress of 2024-T4 aluminum is 42 ksi, its stress-strain curve displays a curved yielding region with no well-defined yield point. Any transducer design should keep the maximum stress well below this nonlinear region. Minimization of hysteresis, the magnitude of the deviation from linearity of the strain gage system during cyclic loading, will also be achieved if the stress in the transducer is kept low [11,22].

In addition to transducer stiffness and gage length, attachment of the transducer to steel beams became a critical factor in achieving acceptable transducer performance. Strain gage manufacturers have developed epoxies and application techniques to keep slip between the strain gages and specimens at near-zero levels. The practicality of an epoxy bond in a transducer system is questionable. Considerable time would be involved in surface preparation. The epoxy bond would most likely be inadequate in shear if the transducer had some finite stiffness. Therefore, some sort of mechanical means is needed to hold the strain transducer in position on steel beams. The flat surface of a steel beam flange offers a good surface for developing the frictional force necessary to maintain displacement compatibility between the beam flange and the transducer. While surface conditions of the steel beam flange could vary greatly between bridges, the transducer clamping system should operate with a minimum amount of surface preparation.

2.1.2.2. Circuit

Commercial strain gages are readily available in various sizes, with many options for specific applications, and with a common initial resistance of either 120 or 350 ohms. The size of the strain gages used on the transducer should be kept as small as possible while staying within the skill level of those doing the actual instrumentation work. The smaller the strain gage, the larger the deformation it would experience with respect to its gage length, thus creating a larger signal to be picked up by the recording instrumentation. It is anticipated that data from the transducer will be recorded using either a data acquisition system or a commercial strain indicator, both of which

employ a constant voltage power supply. The ratio of output to input voltage for a wheatstone bridge is given by the equation:

$$\frac{\Delta E}{V} = \frac{r}{(1+r)^2} \left(\frac{\Delta R_1}{R_1} - \frac{\Delta R_2}{R_2} + \frac{\Delta R_3}{R_3} - \frac{\Delta R_4}{R_4} \right) \quad (2-2)$$

where

ΔE	= change in bridge output, voltage, measured in volts
V	= bridge excitation voltage measured in volts
r	= ratio of resistance of arm 1 of bridge to resistance of arm 2 of bridge
$\Delta R_1, \Delta R_2, \Delta R_3, \Delta R_4$	= change in resistance of respective arms in bridge, measured in ohms
R_1, R_2, R_3, R_4	= initial resistance of respective arms in bridge, measured in ohms

Thus, the strongest output signal per volt of input will be obtained if 120-ohm resistance strain gages are used [11]. Strain gages with resistance of 350 ohms can be used to reduce bridge circuit current levels if heat dissipation problems occur. Given the good thermal conductivity of 2024-T4 aluminum and the expected physical dimensions of the transducer spring element, the 350-ohm gages were not required.

The output voltage from the strain gages mounted on the transducer is related to the strain on the beam flange by a calibration constant, k . Any slight resistance change in the internal arms of the wheatstone bridge, such as that incurred from changing interbridge lead wire

lengths, alters this calibration constant. Thus, to avoid a change in calibration between each field test, a full wheatstone bridge arrangement was required on the transducer itself. Completion of the wheatstone bridge on the transducer would allow for the use of different lead wire lengths, which would commonly occur during testing at various bridge sites. Quick-coupling electrical connectors were used outside the wheatstone bridge (between the recorder and the transducer) to enhance the system's convenience.

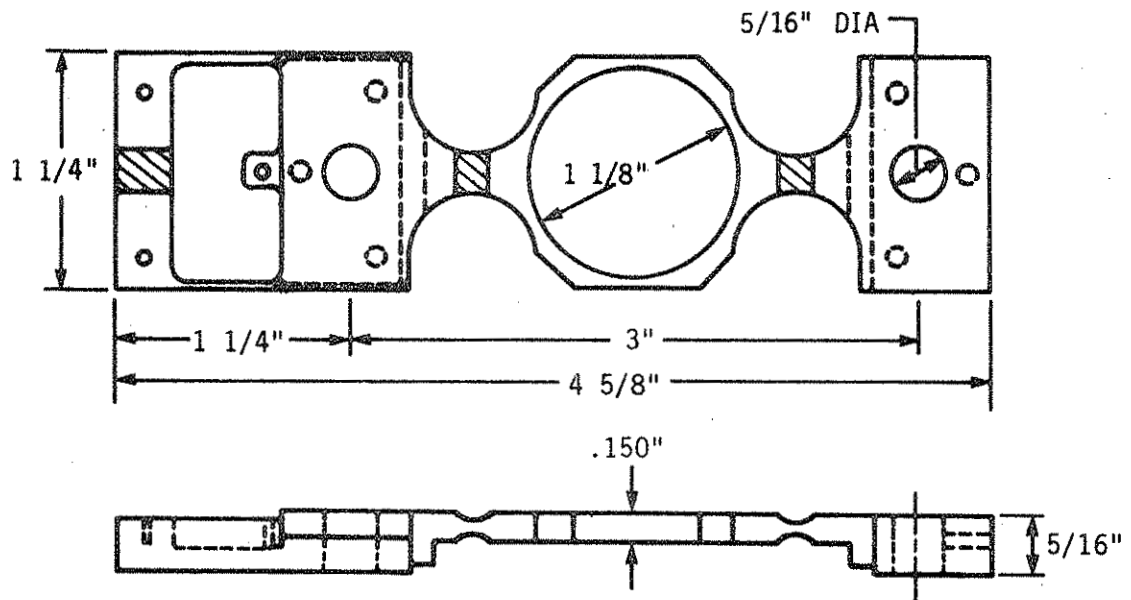
The full-bridge circuit configuration and self-temperature compensating strain gages eliminated all major errors due to temperature changes in the transducer spring element [11]. Although refinement of the circuit through the installation of appropriate internal resistors in the bridge arrangement would have resulted in increased system performance and accuracy, this degree of sophistication was not necessary [13]. Using internal resistors to achieve the conditions of initial bridge balance was not possible since the transducer was preloaded to a certain level during the clamping process. Zero shift or deviation from the calibration factor, k , due to a temperature change could be further minimized with the internal resistors, but the resistors' effectiveness would be reduced if a null-balance type strain indicator was used. Since the transducer would most likely be used with null-balance commercial strain indicators, no internal resistors were used in the transducer circuit.

2.1.3. Transducer System Design

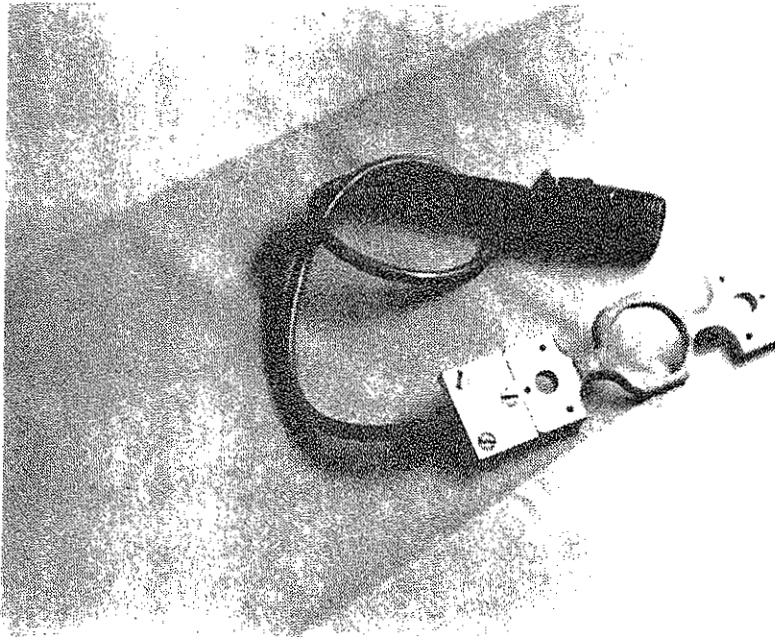
A literature review revealed that the FHWA had developed a strain transducer as part of a weigh-in-motion project that used the strains

in bridge beams as a method of determining truck weights. Although several transducer spring element designs (such as a double fixed-end beam concept) were analyzed, the FHWA model seemed the most promising when judged against the criteria stated in Section 2.1.2. Therefore, this existing transducer design was fabricated and tested to determine its suitability for measuring beam strains when using the post-tensioning method of bridge strengthening. Possible modifications to the transducer were investigated, and a simple clamping technique compatible with this transducer design was developed.

Figure 2.1 gives details regarding the strain transducer's various dimensions. These design dimensions are basically the same as those of the FHWA strain transducer. The overall width of 1 1/4 inches was narrow enough for it to fit on the flange of any steel beam used in composite bridge construction. Actual physical dimensions of the transducer are large enough for easy handling in the field. The symmetric ring design was ideal for a full bridge strain gage configuration and was large enough to allow strain gage placement. Wiring and soldering of the bridge circuit were simplified by the hollow section located at one end of the transducer. The three-inch gage length was short enough to avoid any significant strain averaging errors while still being long enough to allow for a practical clamping method. Analyzing the transducer as a simple ring structure with a constant cross section, we found the axial force required to displace the transducer the maximum amount anticipated during the post-tensioning process was less than 15 pounds [25]. This is a conservative analysis of transducer stiffness because the ring-shaped spring element has a varying



a. Overall dimensions.



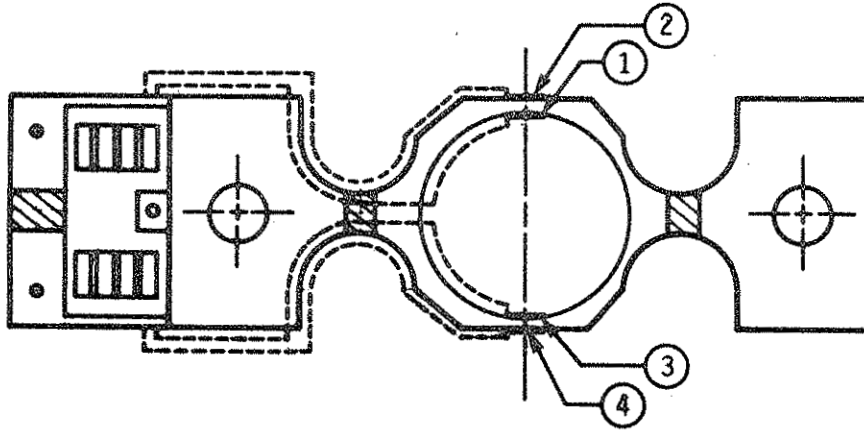
b. Photograph of transducer.

Fig. 2.1. Strain transducer details.

cross section and the total anticipated deformation was applied only to the ring structure and not along the entire transducer gage length. The necked-down region adjacent to either side of the ring structure reduced the transducer stiffness. Using the previously described analysis, the maximum stress in the ring element of the transducer was less than 3 ksi, which is less than 10% of the yield stress of aluminum 2024-T4. Since the transducer's spring element preload stress level caused by the clamping procedure cannot be accurately predicted, this relatively low live-load stress on the spring element was advantageous in assuring that the spring element's total stress remained small.

As can be seen in Fig. 2.1, three 3/32-inch-diameter holes were drilled and tapped at each end of the transducer. A 3/16-inch-long steel set-screw was threaded into each hole. These pointed screws were adjusted to protrude through the bottom side of the transducer's flat bearing surface area; therefore, the transducer itself was not in contact with the beam flange. In this case the points were used alone for displacement transfer. The system was also tested to determine the effect of using only a frictional-type displacement transfer between the beam flange and the flat bearing surface of the transducer.

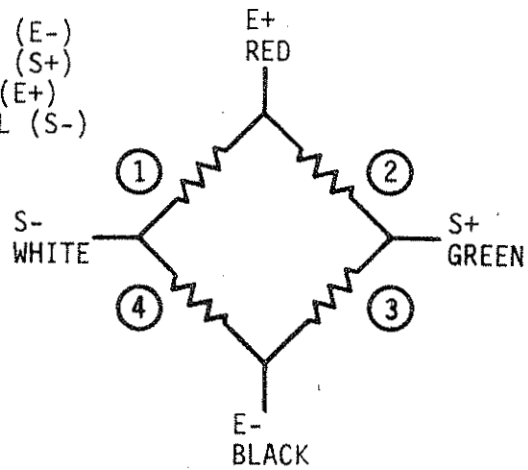
Figure 2.2 describes the electrical circuit used in the strain transducer. Four 120-ohm self-temperature compensating strain gages were placed in a full bridge configuration on the transducer spring element. These gages were mounted on the transducer with a heat-cured epoxy. All strain gages and electrical wiring were covered with a protective coating using standard procedures. A quick-coupling electrical connector was attached to the end of the twelve inches of jacketed four-



a. Gage location

CONNECTOR AND COLOR CODE

PIN	COLOR	DESIGNATION
A	BLACK	MINUS POWER (E-)
B	GREEN	PLUS SIGNAL (S+)
C	RED	PLUS POWER (E+)
D	WHITE	MINUS SIGNAL (S-)
E	SHIELD	



b. Schematic of wheatstone bridge arrangement.

Fig. 2.2. Strain gage location and electrical circuit layout of strain transducer.

conductor lead wire running from the transducer, adding to the system's convenience of operation. The ground in the lead wire was continuous through the quick-coupling connector but was not in contact with the transducer.

Two four-inch C-clamps were used to provide the clamping force to secure the transducer to the beam flange. A 0.30-inch-diameter stud 0.25 inches long, welded to the stationary bearing surface of each C-clamp, fit into the 5/16-inch-diameter hole at either end of the transducer. This kept the clamping force centered on the transducer and in the same position each time the system was used.

2.1.4. Transducer System Laboratory Testing

2.1.4.1. Preliminary

The initial testing of the strain transducer had a three-fold purpose: (1) to determine the best clamping techniques for controlling displacement compatibility between beam flange and transducer, (2) to check the accuracy and reliability of the transducer over a number of identical tests, and (3) to produce a simple test procedure for calibrating the transducer.

Testing and calibration of the transducer was accomplished using an axial loaded tension specimen--a 1/2-inch \times 2 1/2-inch flat steel bar three feet long. Load was applied through the tension mode of a Baldwin Universal testing machine. The bar was instrumented with five strain gages along the mid-length cross section; three were mounted on one side and two on the other side. A slight curvature initially present in the bar was removed as tensile load was applied, thus creating the possibility of an unwanted secondary loading effect on the

transducer (in addition to the ideal pure tensile condition) if not considered in the testing procedure. Strain readings from both sides of the bar were compared to determine that a 14-kip tensile load reduced this curvature effect to a negligible level. The bar was positioned in the tension grips so that the three strain readings across the common cross section gave the same reading, thus eliminating any moment about the bar's strong axis. The testing apparatus and the transducer clamped onto the bar are shown in Fig. 2.3.

After loading the bar to 14 kips (to eliminate the initial curvature effect), the transducer was attached directly over the bar's instrumented cross section and zero readings recorded. One test cycle of the bar-transducer system consisted of loading the bar up to 32 kips (18 kips apparent load on the transducer) and then releasing the load back to 14 kips. This loading produced a strain in the bar of 495 micro-inches per inch, approximately 1.5 times the strain expected in a typical bridge post-tensioning application. Transducer output voltage and bar strain readings were taken at 2-kip intervals throughout the loading cycle. Between tests the transducer was unclamped and then remounted on the bar. Bar strain was plotted against the ratio of the transducer output voltage to the transducer excitation voltage. The slope of the line through the experimental data, calculated using a least-squares linear regression analysis, is the transducer's calibration factor. Slip between the transducer and the bar could be detected by a non-linear data plot or a sudden change in the slope between two data points.

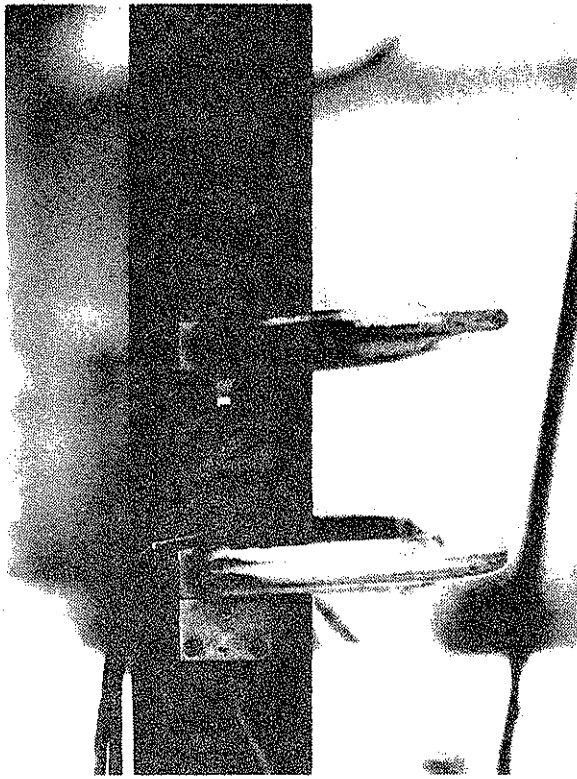


Fig. 2.3. Close-up photograph of strain transducer clamped on calibration bar.

Using the testing procedure previously described, the first tests of the strain transducer were made with the previously described steel points in place. Although various depth settings of the points were tried, a stable and repeatable calibration factor could not be achieved using this approach. With the transducer clamped to the bar, the studs seemed to experience small seating displacements over a long period of time. This caused a significant and continual zero shift in the transducer output voltage. Considerable scatter in the data points occurred during the bar's loading cycle. The idea of using the points for controlling displacement compatibility was considered ineffective and even detrimental; therefore, the points were removed from the strain transducer.

The concept of transferring displacements by developing only frictional force on the flat bearing surface between the transducer and the instrumented test bar was investigated using the previously described test procedures. The repeatability of this approach was excellent, with the average calibration factor from several tests being within 3% of the extreme values. The transducer assembly was easy to attach to the bar and displayed a steady reading under constant load. Each C-clamp was tightened as much as possible by hand. The C-clamps had to be held with one hand while being tightened with the other; otherwise a rotation of the tightened clamp might twist the end of the transducer about the ring element, creating a permanent deformation.

The performance of the transducers was also checked in compression. The test procedure was identical to the one previously described except that the bar was loaded to 32 kips before attaching the transducer.

Once the transducer was in place, force in the bar was reduced to 14 kips and then increased to 32 kips. This simulated a compression load on the transducer. As expected, results from this compression test were in excellent agreement with results from the tension tests.

The strain transducer could be used without being damaged to measure strains anywhere in the elastic region of structural steel. At the yield stress of A7 steel (the typical bridge steel) the stress in the transducer is approximately 9 ksi, or only about one-fourth of the yield stress of the transducer. Preloading of the transducer during the clamping procedure would be expected to produce only minor transducer stress levels relating to the problem of yielding the transducer material.

2.1.4.2. Calibration

Ten transducers were fabricated and instrumented as described in section 2.1.3. The transducers were individually numbered 1 through 10 for identification purposes. In addition, 20 4-inch C-clamps (1 pair per transducer) were modified as described in Section 2.1.3. Each pair of C-clamps was individually numbered 1 through 10 to indicate which pair of C-clamps corresponded to a given transducer. This identification system ensured that a given transducer C-clamp assembly would always be matched to insure greater accuracy. In addition, one C-clamp was marked with the letter A, which indicated it was to be clamped into the hole adjacent to the lead wire end of the transducer.

Small differences in strain gage placement on each individual transducer's spring element resulted in the need to calibrate each transducer individually. Determining each strain transducer's calibration factor

consisted of performing a least-squares linear regression analysis on the data from three separate calibration test cycles, conducted as previously described in Section 2.1.4.1. Figure 2.4 show typical results of a calibration test cycle. Data points were recorded during both the increasing and decreasing load cycles. The slope and y-intercept of this set of data are as shown. The correlation of the data (that is, its degree of deviation from an expected straight-line relationship) is excellent. Transducer output voltage was plotted as a dimensionless quantity (output voltage per unit excitation voltage). This allowed the calibration factor to be applied to all types of instrumentation using any level of direct-current constant excitation voltage. If the recording equipment consisted of a power supply and a digital voltmeter, the beam's indicated strain from the transducer would be given by the equation

$$\varepsilon = \frac{\Delta E}{V} \alpha \quad (2-3)$$

where

ΔE = change in transducer's output voltage, measured in volts

V = transducer's excitation voltage, measured in volts

ε = indicated strain in beam, measured in inches per inch

α = transducer's calibration factor

In the previous expression, α simply relates the ratio of transducer output voltage per unit input voltage to the strain in the beam flange.

A more common form of instrumentation for field use would be a commercial strain indicator. With the indicator set to the gage factor of the transducer's strain gages, the indicator's reading will be

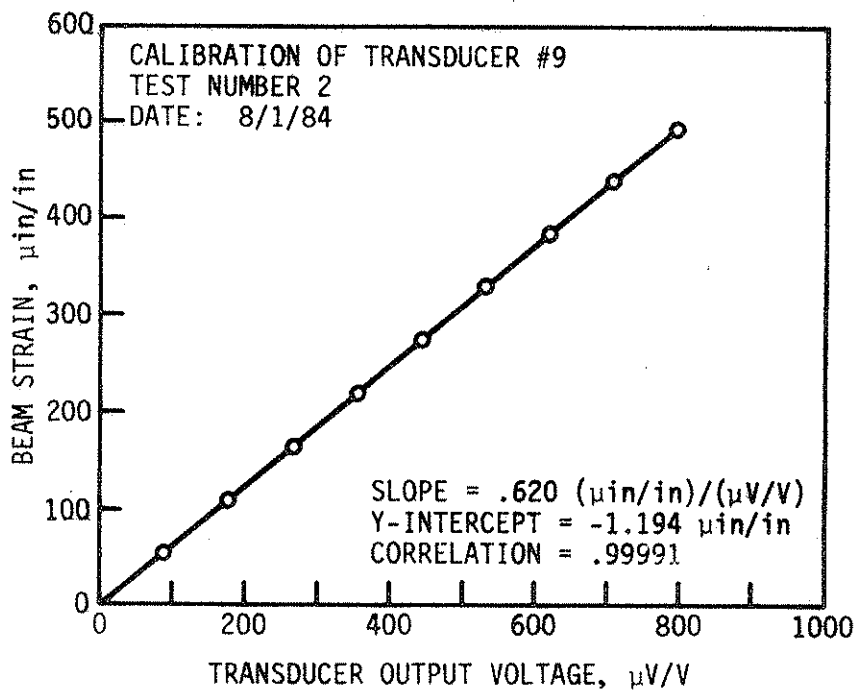


Fig. 2.4. Typical calibration curve for strain transducer.

the sum of the strain from the transducer's four strain gages. The ratio of the transducer's output voltage per unit input voltage is related to the transducer's actual strain by the expression [11]

$$\frac{\Delta E}{V} = \frac{1}{2} S_g (\Sigma \epsilon) \quad (2-4)$$

where

S_g = the gage factor of the transducer's strain gages

$(\Sigma \epsilon)$ = the sum of the strain readings from the transducer's four strain gages, measured in inches per inch

In order to relate the voltage ratio to the beam strain, each side of the above equation is multiplied by the calibration constant, α , resulting in the expression

$$\alpha \frac{\Delta E}{V} = \alpha \frac{1}{4} S_g (\Sigma \epsilon) \quad (2-5)$$

The left-hand side of the equation is now equal to the beam strain as defined by Eq. (2-3). Therefore β , the calibration factor used with readings obtained from a commercial strain indicator, is

$$\beta = \alpha \frac{1}{4} S_g \quad (2-6)$$

and the measured strain in the beam would be

$$\epsilon = \beta (\Sigma \epsilon) \quad (2-7)$$

where β relates the sum of the strains from the transducers to the strain in the beam. The calibration factors, α and β , and the gage factors for the ten strain transducers, are presented in Table 1. In

Table 1. Calibration constants for strain transducers: gage factor,
 $S_g = 2.115$.

Transducer No.	α	β
1	0.621	0.328
2	0.619	0.327
3	0.582	0.308
4	0.616	0.326
5	0.574	0.304
6	0.609	0.322
7	0.637	0.337
8	0.622	0.329
9	0.606	0.320
10	0.595	0.315

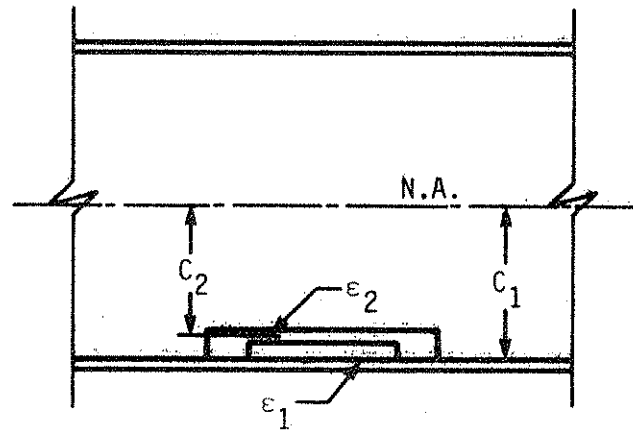
all instances these calibration constants were derived from data that displayed excellent linearity, with the correlation of the data points being very near one.

2.1.4.3. Curvature

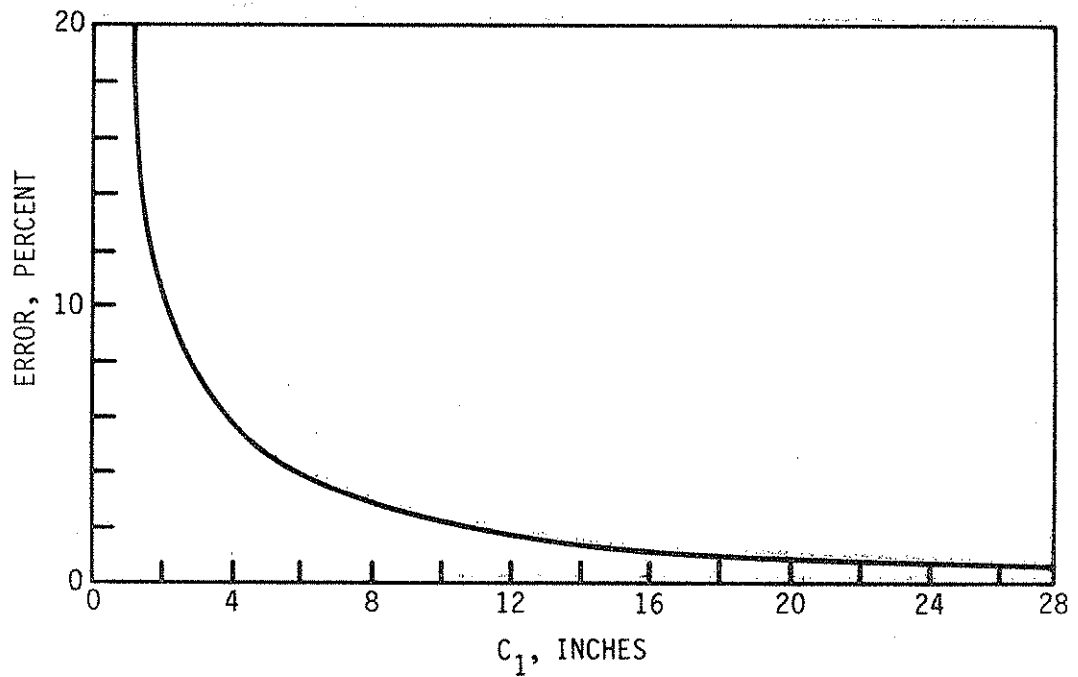
During the calibration tests, steps were taken to eliminate any curvature effect and thus produce a pure tensile loading. However, curvature would be present in the flexural behavior of the steel beams during post-tensioning. This section describes tests conducted to determine the effects of curvature on transducer performance. Figure 2.5a shows a transducer mounted onto the top side of the bottom flange of a steel beam. The distance from the beam's neutral axis to the transducer-steel beam interface is given as C_1 . This surface of the steel beam undergoes a strain, ϵ_1 , when the steel beam is loaded in flexure. Likewise, the distance from the steel beam's neutral axis to the mid-depth of the transducer spring element is given as C_2 ; the corresponding flexural strain at this location is ϵ_2 . The horizontal mid-plane of the transducer spring element is 0.237 inches (see Fig. 2.1) above the top surface of the bottom beam flange; thus, $C_2 = C_1 - 0.237$.

The relationship between the true strain of the flange surface and the transducer's indicated strain, assuming no slip, is given as

$$\epsilon_1 = \frac{C_1}{C_2} \epsilon_2 = \frac{1}{C_2/C_1} \epsilon_2 = \frac{1}{1 - \frac{0.237}{C_1}} \epsilon_2 \quad (2.8)$$



a. Transducer clamped to beam flange.



b. Percent error of beam strain vs. distance from neutral axis.

Fig. 2.5. Curvature effect on transducer performance.

The percentage error due to flexural curvature is defined as

$$\begin{aligned} \% \text{ Error} = E &= \frac{\varepsilon_1 - \varepsilon_2}{\varepsilon_1} \times 100 \\ &= \left(\frac{\varepsilon_1 - \frac{C_2}{C_1} \varepsilon_1}{\varepsilon_1} \right) \times 100 \end{aligned} \quad (2-9)$$

Further manipulation of the above expression reduces the percentage error term to

$$\% \text{ Error} = \frac{0.237}{C_1} \times 100 \quad (2-10)$$

As this expression shows, the percent error due to flexural curvature is a function of the distance C_1 . Figure 2.5b plots the relationship between % Error and the distance C_1 . If this distance C_1 is known, the curvature error can be eliminated by dividing the measured strain ε_2 by the factor $1 - \% \text{ Error}/100$ (as shown in Eq. 2-8). For practical bridge beam sections, this error will be 2% or less.

To simulate bridge field testing conditions, a testing frame and beam specimen as shown in Fig. 2.6 was fabricated. A simply supported W24 \times 94-inch-wide flange beam spanning 13 feet was instrumented at midspan with a strain gage placed on the top surface of the bottom flange two inches in from the edge. A strain transducer was then clamped directly over the gage. To be consistent with proposed field testing plans, no surface preparation was given to the areas where the transducer was in contact with the unpainted beam flange. Using a

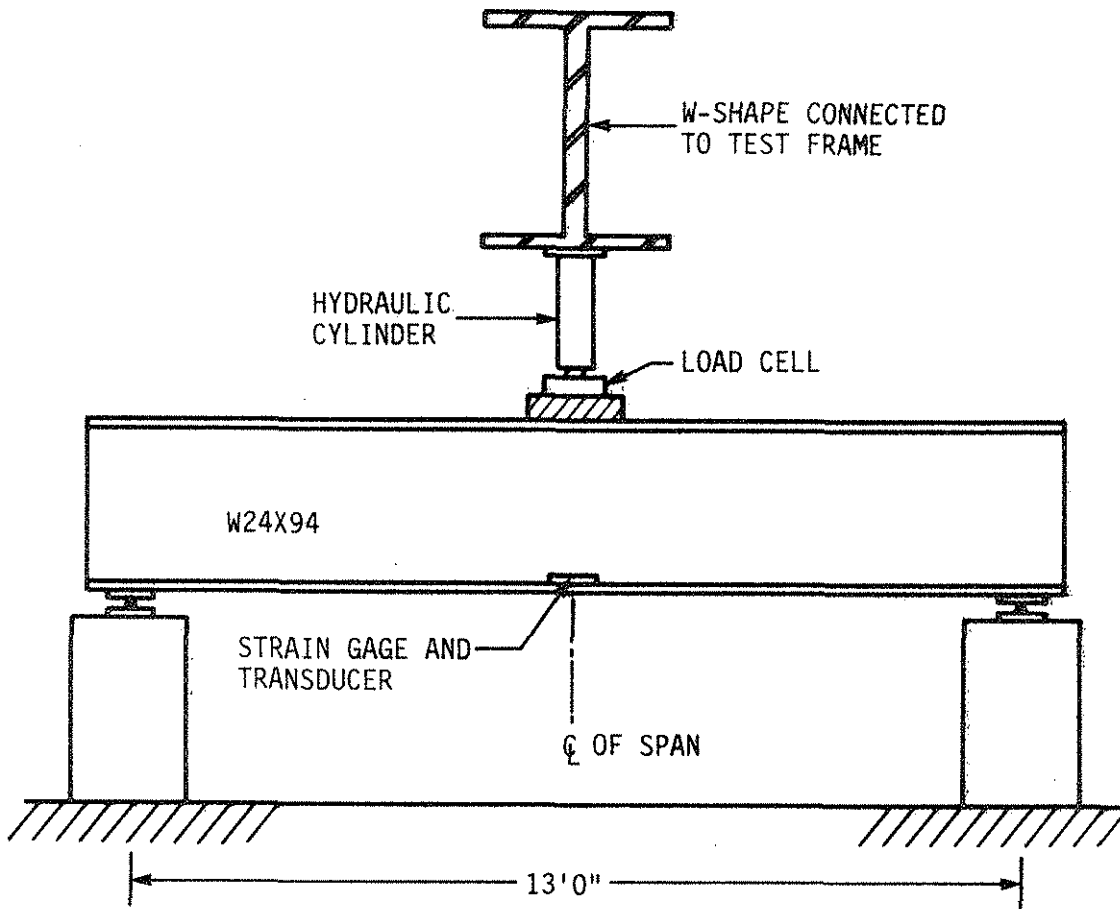


Fig. 2.6. Loading apparatus utilized in determining effect of curvature on transducer performance.

hydraulic cylinder, the beam was loaded at midspan to 16 kips and then released back to zero load; readings were taken at 2-kip intervals. The maximum strain in the beam flange due to this loading was 140 micro-inch per inch; this was approximately equal to the maximum strain values recorded during bridge field testing in 1982.

The purpose of this test was to compare transducer indicated strain, arrived at using a calibration factor developed as Section 2.1.4.2, with that strain measured by the corresponding strain gage. Six tests were conducted in total, all under identical test conditions using the same transducer. The transducer was unclamped and remounted between tests. The results of a typical test are presented in Table 2; as may be seen, the correlation between transducer and strain gage readings was excellent. Transducer strain readings were within 3 micro-inches per inch of strain-gage strain values. No slip between the transducer and the flange was observed. The curvature effect produced no significant errors in the transducer readings. On the basis of results from the calibration tests and the beam test, the strain transducers were expected to give excellent results when employed in the field.

2.1.4.4. Temperature

While the strain gages used on the transducers were self-temperature compensating, a temperature-induced apparent strain could still occur during strain transducer system use. Aluminum has a linear coefficient of thermal expansion approximately twice that of steel: 13×10^{-6} inches per inch per $^{\circ}$ F compared to 6.5×10^{-6} inches per inch per $^{\circ}$ F. With the transducer clamped in a fixed position, an

Table 2. Comparison of strain gage and transducer strain values for a typical curvature effect test.

Load (kips)	Strains (Microinches Per Inch)		
	Strain Gage	Transducer	Difference
0	0	0	0
2	17	16	1
4	36	33	3
6	51	49	2
8	68	66	2
10	85	84	1
12	103	100	3
14	121	118	3
16	138	137	1
14	119	117	2
12	102	100	2
10	84	82	2
8	67	65	2
6	50	48	2
4	33	31	2
2	18	15	3
0	2	0	2

increase in temperature would cause the transducer to expand a greater amount than the beam. The transducer, clamped in place on the steel beam flange, would be placed in compression, and a temperature-induced compressive strain would be included in any strain measurement recorded from the transducer. If a temperature decrease occurred, the result would be a temperature-induced tensile strain introduced into any strain value measured with the transducer system. This temperature-induced apparent strain value ϵ_p would therefore be the differential change in length-per-unit length between the two materials based on their respective temperature changes and linear coefficients of thermal expansion.

Several tests were conducted in the laboratory to determine the temperature-induced apparent strain characteristics of the transducer system. For more details on these tests the reader is referred to Ref. 3. As a result of the laboratory tests, various methods of minimizing the apparent strain effects were determined. After initially clamping the transducer to the beam flange, a 15- to 30-minute period should be allowed for the temperature of the beam flange-transducer system to reach equilibrium. Once this has occurred, a temperature-induced apparent strain of approximately seven microinches per inch (the difference between the linear coefficients of thermal expansion of steel and aluminum) will occur for a 1° F temperature change in the beam flange-transducer system. To minimize the magnitude of any possible temperature change, the transducer should not be clamped in an area exposed to direct sunlight. However, if field conditions should ever require this, the transducer should be shaded by an appropriate material. Also, the time interval between zero readings and any load-

point readings taken during the field test should be kept as short as possible to minimize any error in strain measurements due to temperature fluctuations.

2.2. Force Transducers

One aspect of any post-tensioning work is measuring the force applied to the post-tensioning tendons or strands. Standard practice in the industry has been to measure tendon elongation and relate this change in length to tendon force [23]. During the implementation of the post-tensioning strengthening method an error of 5% or more could occur because of the possible margin of error involved in reading the various measurements required. Jacking pressures can also be measured and calibrated to tendon force; however, this method does not measure the seating losses that occur when the jacking pressure is released. Therefore, the feasibility of developing a transducer to measure the post-tensioning force was investigated. Potential advantages of such a system would be simplifying data collection by the use of electrical equipment and being able to monitor the change in the post-tensioning force due to truck loads on the bridge.

2.2.1. System Design Criteria

The design criteria stated in Section 2.1.2 also apply to force transducers. However, several problems unique to the approach of applying a portable force transducer to tendon force measurement had to be considered. If the high-strength post-tensioning tendons were stressed to 60% of their ultimate strength, the typical strain

would be approximately 3000 microinches per inch. While this large strain would decrease the error due to a given amount of slip, it would also increase the total deformation-per-unit gage length a transducer would experience. Depending upon the stiffness of the transducer, a secure clamping system involving relatively large clamping forces could be required to control slippage. Due to the tendon's irregular surface, the force transducer's clamping system would be more complicated than the clamping technique used in the strain transducer system. Both 1-inch and 1 1/4-inch-diameter Dywidag threadbars were used in this post-tensioning project. These tendons were oval shaped with threads running down two sides; therefore a smooth, flat surface for a frictional-type displacement transfer between tendon and transducer was not present. To be applicable to all possible field conditions, any force transducer and its corresponding clamping technique would have to fit both tendon sizes and be independent of thread orientation. For clearance reasons, the force transducer would have to operate within a 2 1/2-inch radius around the tendon.

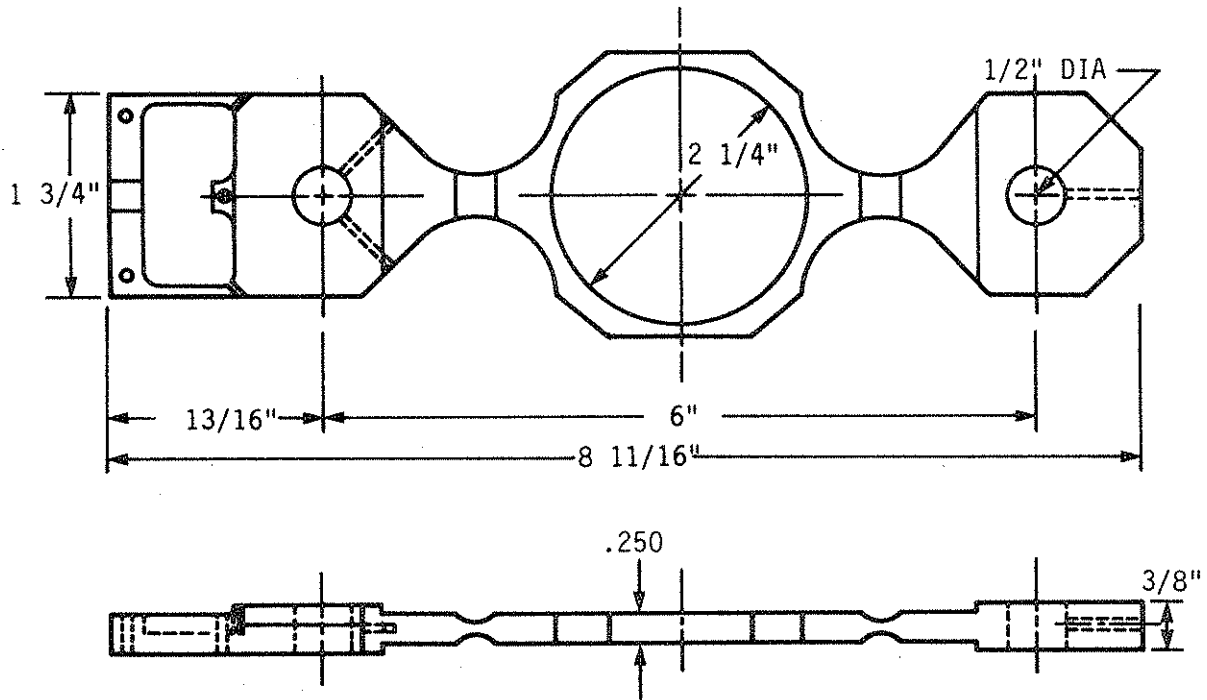
Due to its long unbraced length, the unstressed tendon, when placed in position in the post-tensioning brackets, would sag until it hit the top surface of the lower beam flange along the beam midspan region; this curvature is obviously removed when the tendon is stressed. The curvature effect in the strain transducer system was negligible since the ratio of the distance between the beam's neutral axis and the transducer to the distance between the beam's neutral axis and the monitored surface was close to unity. With the tendons, this same ratio will be significantly greater than one. Therefore, any change

in curvature along the transducer's gage length could have an effect on the axial load reading. To minimize this curvature influence in the force transducer's signal, the transducer system was mounted so the longitudinal axis of the force transducer is in the same horizontal plane as the post-tensioning tendon. Ideally, any flexure of the tendon would have a self-cancelling effect on the symmetrical spring element of the force transducer.

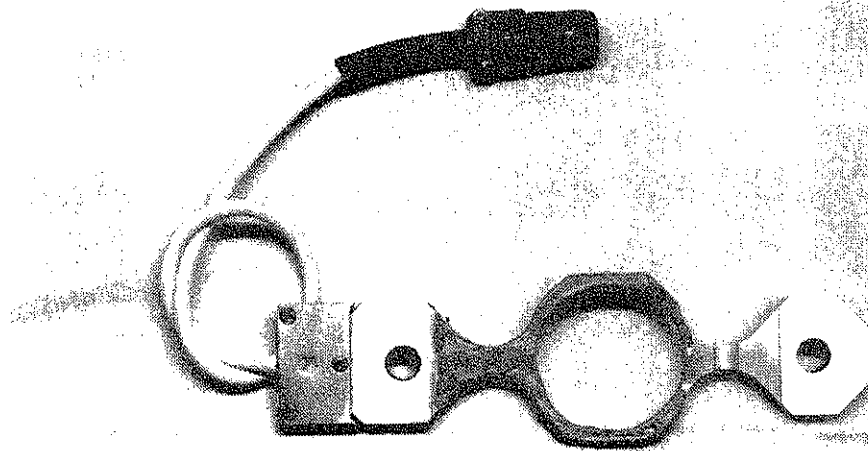
2.2.2. Transducer System Design

Two completely different design approaches were initially considered for the force transducer; one involved a transducer with a very small or "zero" stiffness while the other design required some finite amount of stiffness in the system. The zero stiffness concept is found in commercial tensiometers such as a Huggenberger tensometer. The transducer can be displaced by a very small amount of force; hence clamping forces are minimal, and typically rubber bands or small springs are used to hold the transducer in place. The finite stiffness design would be similar to the strain transducer design; the clamping force would have to be great enough so slip was controlled as the transducer was displaced. The zero stiffness concept was considered to be too fragile for practical field use. Therefore, because of the success of the strain transducer system, the finite stiffness design concept was chosen for the force transducer.

As previously stated, the transducer itself was designed according to the design parameters stated in Section 2.1.2. Figure 2.7 gives the force transducer's configuration and dimensions. Analyzing this force transducer, which was fabricated out of 2024-T4 aluminum alloy,



a. Overall dimensions.



b. Photograph of Force Transducer.

Fig. 2.7. Force transducer details.

as a simple ring structure with a constant cross section, reveals that the axial force required to displace the transducer the maximum amount anticipated during the post-tensioning process was 54 pounds [25].

Using the same analysis approach, the maximum stress in the ring element of the transducer was 14.6 ksi. This stress was slightly more than one-third of the yield stress of 2024-T4 aluminum.

Strain gage location and the electrical wiring for the force transducer are the same as that utilized on the strain transducer (see Fig. 2.2). Actual strain gage placement and wiring techniques are similar to those stated in Section 2.1.2.2.

As with the strain transducer system, the critical part of the force transducer system was the clamping mechanism. The design of the clamp used to attach the force transducer to the post-tensioning tendon is shown in Fig. 2.8. This configuration would be versatile while providing a secure clamping system. The five heat-treated points could be adjusted so that the U-clamp would fit onto either size tendon and could be mounted independently of the tendon thread orientation. The 1/2-inch-diameter stud of the U-clamp was fit into the hole (slightly greater than 1/2 inch in diameter) at each end of the force transducer and locked into a position perpendicular to the longitudinal axis of the transducer by tightening the small set-screws placed in the ends of the transducer. The entire one-piece assembly could then be positioned on the tendon, the 3/8-inch bolts in both U-clamps secured, and the five set-screws in each U-clamp tightened with an allen wrench.

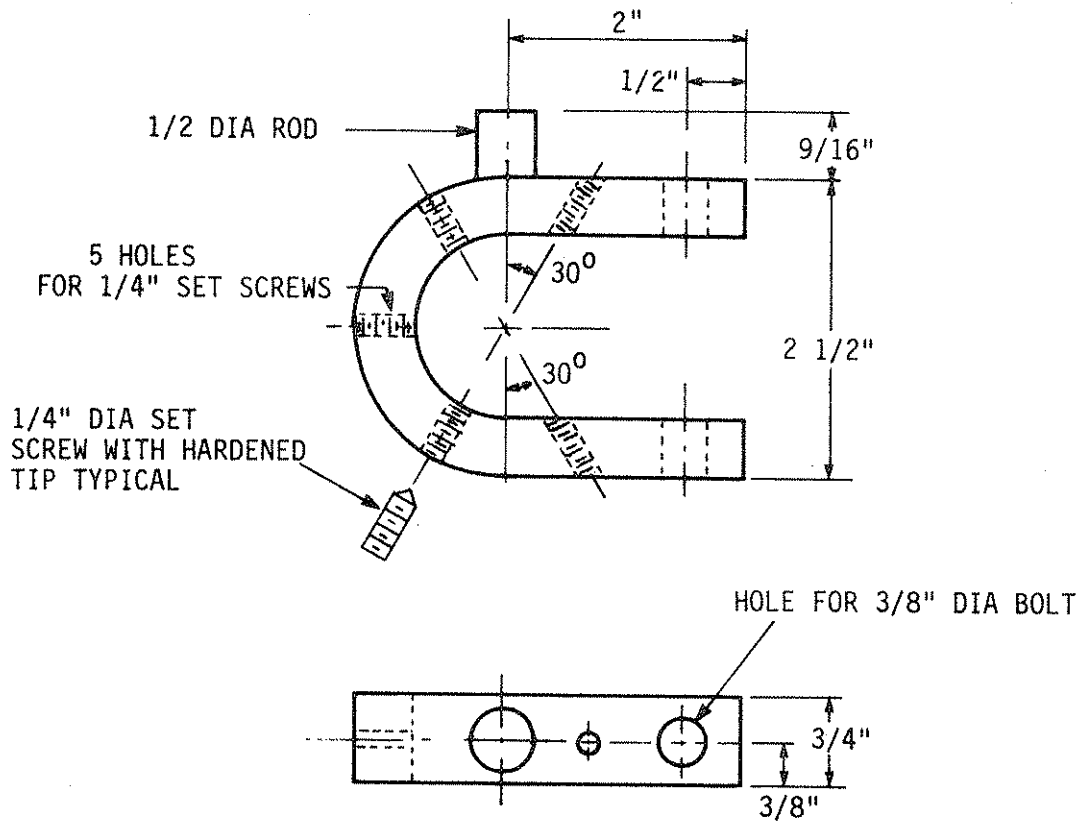


Fig. 2.8. U-clamp required for attaching force transducer.

2.2.3. Laboratory Testing

2.2.3.1. Preliminary

A loading system was devised that served both as a comparative testing procedure and a calibration method for the force transducer design. Two test specimens, a 1-inch-diameter Dywidag threadbar and a 1 1/4-inch Dywidag threadbar each 3 1/2 feet long, were loaded using the tension mode of the Baldwin universal testing machine. After the force transducer assembly had been clamped onto the test specimen, the load was cycled from zero to a load equivalent to 60% of the tendon's ultimate strength. Tensile load in kips was plotted against transducer output voltage in terms of microvolts of signal voltage per volt of excitation voltage. The slope of this line is the force transducer's calibration factor. The force transducer system was removed and reclamped between all tests.

Comparison of results between tests showed that a repeatability of $\pm 5\%$ was obtainable, with most of the variation occurring during the very first part of the loading cycle. Testing of the force transducer system showed its calibration factor to be independent of small position changes with respect to the tendon that would naturally result from removing and reclamping the force transducer on the tendon in between tests. A more significant variation in the data was present if the system was cycled through two or more load cycles without removing and reclamping the system. Temperature-induced apparent force similar to the apparent strain that could occur in the strain transducer could also occur in the force transducer and could be minimized as stated in Section 2.1.4.4.

Stressing the post-tensioning tendons to 60% of their ultimate strength produced a stress in the force transducer of approximately 18 ksi or 43% of the transducer's yield stress. Since a preload stress could exist in the force transducer because of the clamping procedure, this tendon force level should be considered the upper limit for safe operation of the force transducers.

2.2.3.2. Calibration

Ten force transducers were fabricated and instrumented as per Section 2.2.2. Determination of the calibration factors for the force transducers and the use of recording equipment is the same as that described in Section 2.1.4.2 with one exception; only data from the increasing loading cycle of the tests were used in the actual calculations for the calibration factors. The force transducers would not be used in cyclic loading conditions, so this approach was reasonable and resulted in a more accurate calibration factor. A plot of tendon force vs. transducer output voltage for a typical loading cycle is shown in Fig. 2.9. The slope and y-intercept (or zero shift) of the data are as shown. The correlation of the data points for this loading cycle was excellent. For reasons previously stated, transducer output voltage was plotted as a dimensionless quantity (output voltage per unit input voltage). The calibration constants for application of the force transducers on 1 inch and 1 1/4 inch-diameter tendon and gage factors are given in Table 3. Similarly to the strain transducers, these calibration constants were derived from data that displayed excellent linearity with the correlation of the data points being very near one.

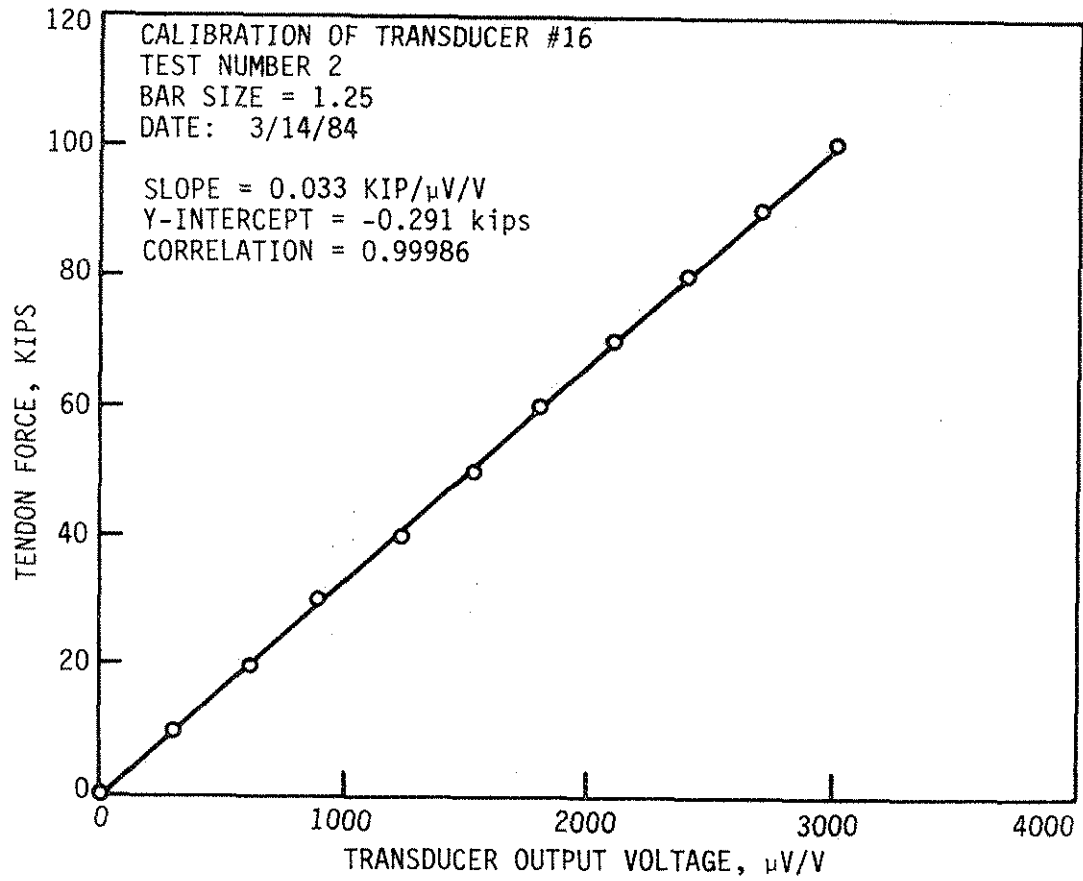


Fig. 2.9. Typical calibration curve for force transducer.

Table 3. Calibration constants for force transducers mounted on 1-inch and 1 1/4-inch-diameter tendons: gage factor, $S_g = 2.09$.

Transducer No.	1-Inch Diameter Tendon		1 1/4-Inch Diameter Tendon	
	α	β	α	β
11	0.0285	0.0149	0.0343	0.0179
12	0.0261	0.0136	0.0341	0.0178
13	0.0262	0.0137	0.0321	0.0168
14	0.0259	0.0135	0.0331	0.0173
15	0.0257	0.0134	0.0338	0.0177
16	0.0246	0.0150	0.0330	0.0172
17	0.0288	0.0150	0.0356	0.0186
18	0.0242	0.0126	0.0339	0.0177
19	0.0259	0.0135	0.0316	0.0165
20	0.0263	0.0137	0.0334	0.0175

2.3. Force Transducer Field Tests

The following section describes the performance of the strain and force transducers during the field testing conducted during Summer 1984 on the two previously mentioned post-tensioned bridges in Iowa. These results are limited for reasons explained later in this section. For a detailed report regarding the strain transducer's performance during actual bridge testing, the reader is referred to Ref. 3.

During the retesting of the two post-tensioned bridges, the strain and force transducers were used in conjunction with the strain gages to monitor both bridges' behavior. Transducer readings were compared with strain gage readings to evaluate both transducer systems' performance under actual field conditions. On both bridges, strain transducers were placed next to the strain gages at midspan and next to the strain gages at the endspan point. All strain transducers were mounted on the top side of the bottom beam flange. A force transducer was mounted at the quarterspan point of each post-tensioning tendon. All post-tensioning tendons were blocked to reduce sag and thus minimize any possible curvature effect on the measured force. All data from the transducers and strain gages were recorded with the data acquisition system. Numerous zero readings were taken throughout the testing program of both bridges to reduce the possibilities of zero shift in the transducer data.

Although both bridges were instrumented with strain and force transducers, a grounding problem with the data acquisition system resulted in the loss of useful transducer data from the testing of

Bridge 1. Thus, the only data available on transducer performance were obtained during the testing of Bridge 2. The strain transducer system was easily and quickly implemented in the field. No beam flange surface preparation was required other than scraping the area free of any loose paint or dirt. Correlations between strain gage and strain transducer readings at midspan were excellent for both the post-tensioning tests and the static truck loading tests. The maximum variance between any corresponding measured strains was 3%. However, correlations between strain gage and strain transducer readings at the endspan points (15 inches from the supports) were poor. No pattern could be detected between the bridge loading and the endspan strain transducer's response. The steel beam's behavior and response to bridge post-tensioning and loading in the vicinity of the supports is more complicated than at midspan. This may have contributed to the strain transducer's loss of accuracy in measuring endspan strains.

Correlation between force transducer data and the tendon force values calculated from strain gage readings was not as close as that which had been achieved during laboratory tests. While some force transducer values were within the $\pm 5\%$ accuracy range that was experienced in previous laboratory work, other force transducer performance was only fair. A greater error was observed in the force transducer readings taken during the initial step of loading or releasing the tendon force than had been observed in calibration tests.

Although it provided a relatively secure clamping arrangement, the clamping mechanism itself proved to be more tedious to operate than had been expected. The close proximity of the steel beam to the

tendons restricted the available working area needed to attach the U-clamps. While still achieving some success, the problems encountered with the force transducer clamping mechanism detracted from the overall efficiency of the system when the mechanism was used to measure the initial application or release of the post-tensioning force.

Considering all factors, the force transducer's performance was less than satisfactory. For practical applications, such as strengthening other bridges by post-tensioning, the force transducers would provide force measurements (force in tendons, seating losses, etc.) within $\pm 5\%$ accuracy. However, if more accurate results are desired, which is usually the case in research, the transducers should not be utilized. For research, strain gages should be applied directly to the tendons for determination of the force in the tendons.

3. RETESTING OF BRIDGES 1 AND 2

3.1. General Background

As previously stated, the testing portion of Phase III of the study consisted of retesting both Bridges 1 and 2. Bridges 1 and 2 were strengthened during the summer of 1982. At that time each bridge was tested to determine the response of the bridge

- to an overloaded truck before post-tensioning
- to post-tensioning
- to the overloaded truck after post-tensioning

Each bridge has been visually inspected essentially every three months since the post-tensioning force was applied.

During these quarterly inspections, no variation in behavior was noted in Bridge 1. The only physical difference observed was a slight increase in the size of the cracks in the wing walls; the change was considered minor.

Inspections of Bridge 2 were also not noteworthy until Summer 1983. Inspection of Bridge 2 during the Summer 1983 revealed that the bridge deck was being rehabilitated. Most of the concrete deck had been removed down to a level slightly below the top layer of deck reinforcement. In addition to this, major portions of the curb section had been removed. Over the east exterior beam, at approximately the quarterspan point, a portion of the deck roughly four feet square had been completely removed. As the post-tensioning force was still in place on the bridge, large upward displacements were visible because of the removal of dead load and the reduction in the effective section.

As the rehabilitation activity was nearly completed before we were aware of it, no instrumentation was in place, and thus no measurements of deflections, strains, etc., were obtained. When the curbs and deck were cast on the bridge later in Summer 1983 and the bridge reopened to traffic, large upward displacements--larger than those measured during Summer 1982--were still observed. More details on this upward displacement will be provided in Section 3.3.2.

During Summer 1984, roughly two years after the initial strengthening, both bridges were retested. The employed test program, which was essentially the same for both bridges, consisted of determining each bridge's response, strains, and deflections to the following five loading conditions:

1. An overloaded truck was placed at the positions used in earlier tests (Phase II, 1982) with post-tensioning force still applied.
2. Post-tensioning force was removed from the bridges.
3. The same overloaded truck was placed at the same positions after post-tensioning force was removed.
4. Post-tensioning force was reapplied to the bridges.
5. The same overloaded truck was placed at the same locations after post-tensioning of the bridge has been completed.

Detailed descriptions of the two bridges in question were presented in the Final Report--Part I [16]. In the Final Report, photographs of the two bridges--with the post-tensioning strengthening system in place--are shown in Fig. 14. The framing plans and midspan cross sections for Bridge 1 and Bridge 2 are presented in Figs. 15 and 16, respectively.

Post-tensioning tendon location and brackets utilized on Bridge 1 are shown in Fig. 19; similar information for Bridge 2 may be found in Fig. 20. Detailed drawings for the brackets used on Bridge 1 and Bridge 2 may be found in Figs. A-1 and A-2, respectively.

In the following sections, details on the instrumentation, test procedures, and test results will be presented.

3.2. Instrumentation and Test Procedure

The instrumentation for the tests consisted of electrical-resistance strain gages (mounted during Phase II of the study), strain and force transducers (developed during this phase of the investigation as mentioned in Sections 2.1 and 2.2), and direct current displacement transducers (DCDT's).

In addition to strain gages already in place on the bridges, a few additional gages were mounted for the purpose of detecting end restraint. An automatic data acquisition system was used to read and record the output from the strain gages, strain and force transducers, and DCDT's.

Because of the similarities in the two bridges, the instrumentation layout, testing program, location of loading, etc., will be discussed together for both bridges. Figure 2.10 indicates the location of the strain gages, strain transducers and DCDT's utilized on Bridge 1. At each of the eight sections instrumented for strain detection, two strain gages were placed on the upper surface of the bottom flanges (1 1/2 inches in from the flange edge) with their axes parallel to the axis of the beam. This position of the strain gages (upper surface of lower

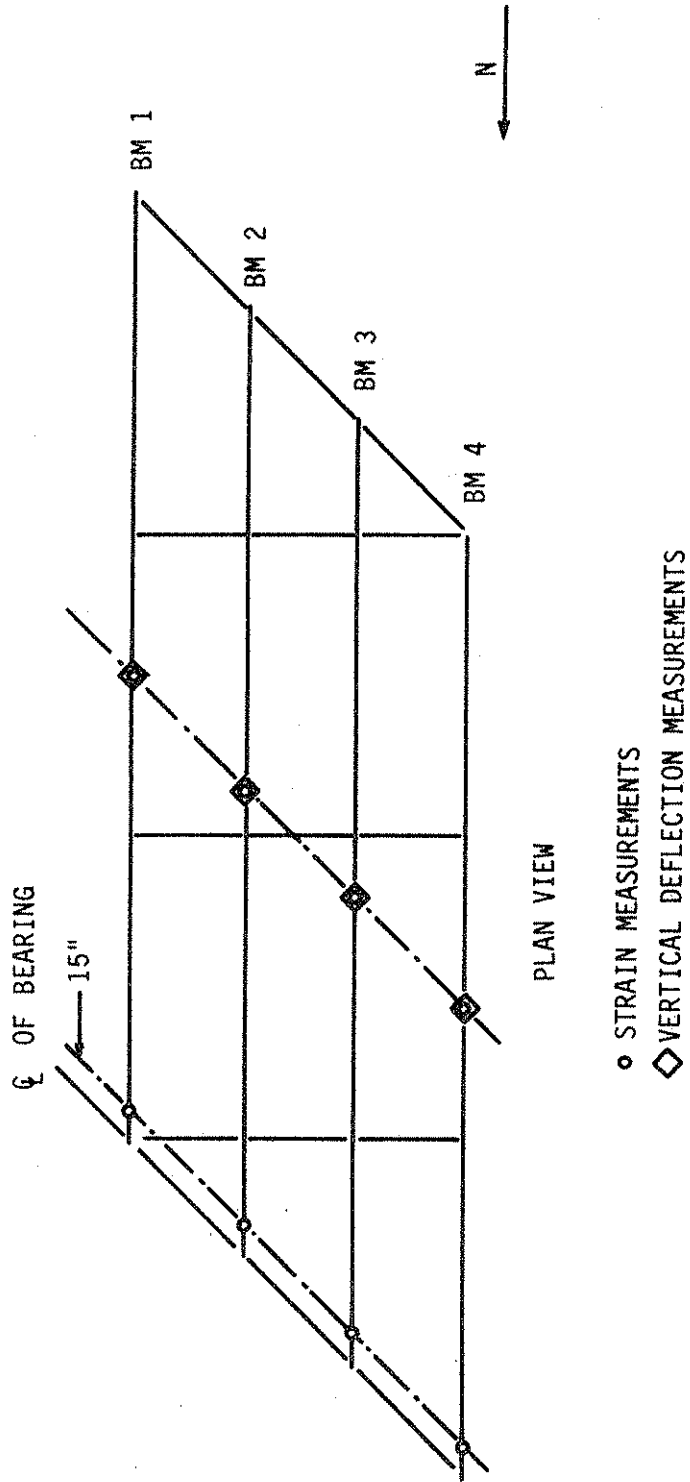


Fig. 2.11. Location of instrumentation--Bridge 2.

Bridge 1. The strain instrumentation 15 inches from the centerline of bearing on the north end of the four beams was used--as was the case on Bridge 1--to estimate end restraint. The telescoping pipe arrangement used on Bridge 1 was also used on Bridge 2 to support the DCDT's.

The field testing program on each bridge consisted of determining each bridge's response, strains, and deflection to the five loading conditions previously described.

The trucks (configuration and weights) used to load the bridges are shown in Fig. 2.12. The same truck was used to load Bridge 1 during the 1982 and 1984 testing. However, because of the amount of sand being carried, the truck was approximately 3440 pounds (60.54^k vs. 63.98^k) heavier during the 1984 testing. Although the vehicle used to load Bridge 2 was slightly longer and heavier than the one used during the testing of Phase II (Fig. 33a vs. Fig. 2.12), for all practical purposes it provided the same loading.

The load points shown in Figs. 2.13 and 2.14 indicate where the center of gravity of trucks (see Fig. 2.13b for Bridge 1 and Fig. 2.14b for Bridge 2) used in the loading of Bridges 1 and 2, respectively, were positioned. Figure 34 vs. Fig. 2.13 (Bridge 1) and Fig. 35 vs. Fig. 2.14 (Bridge 2) show that the positioning of loading used on each of the two bridges this past summer was essentially the same as that used during Summer 1982. Trucks were positioned at these locations with 1982 post-tensioning force in place (load condition 1), with 1982 post-tensioning force removed (load condition 3) and with post-tensioning force reapplied (load condition 5).

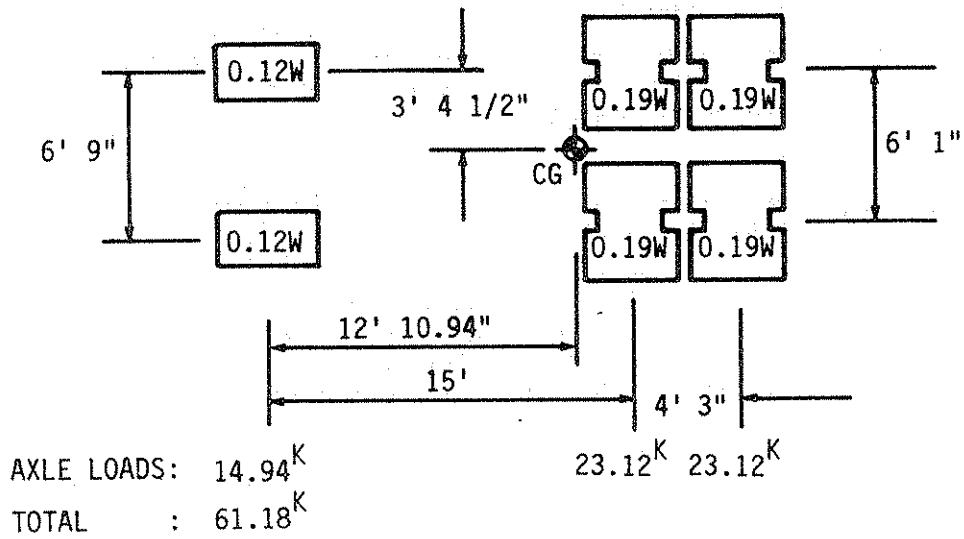
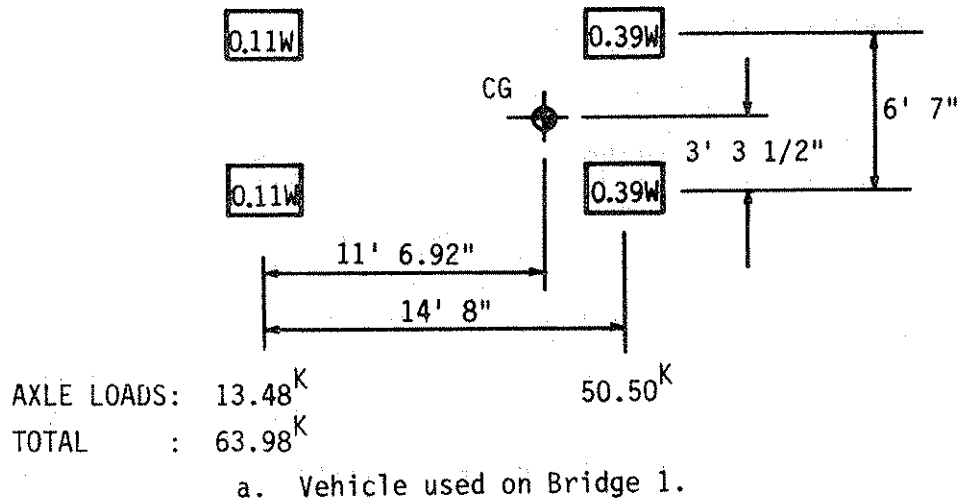
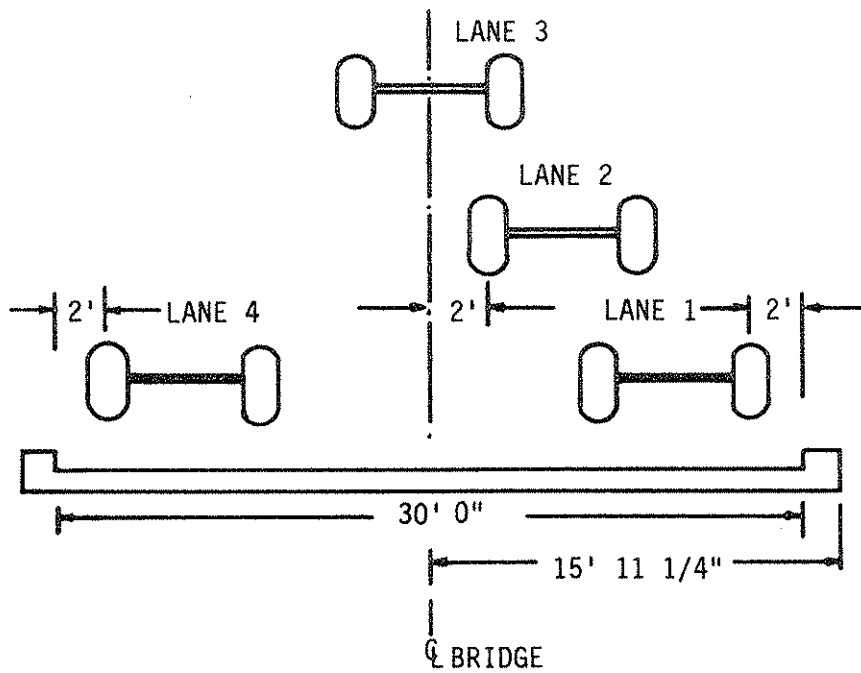
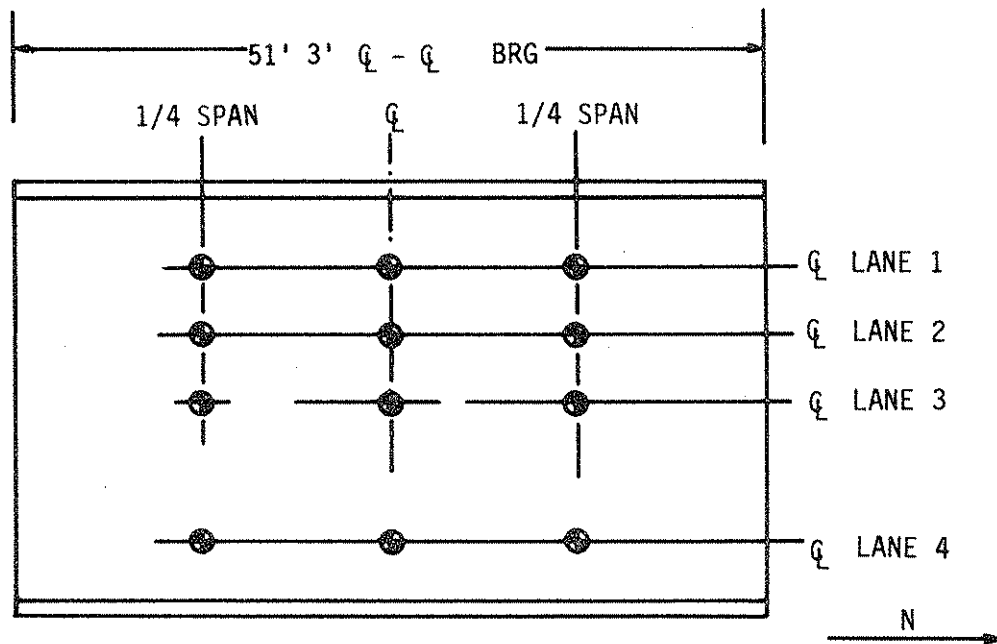


Fig. 2.12. Wheel configuration and weight distribution of test vehicles.

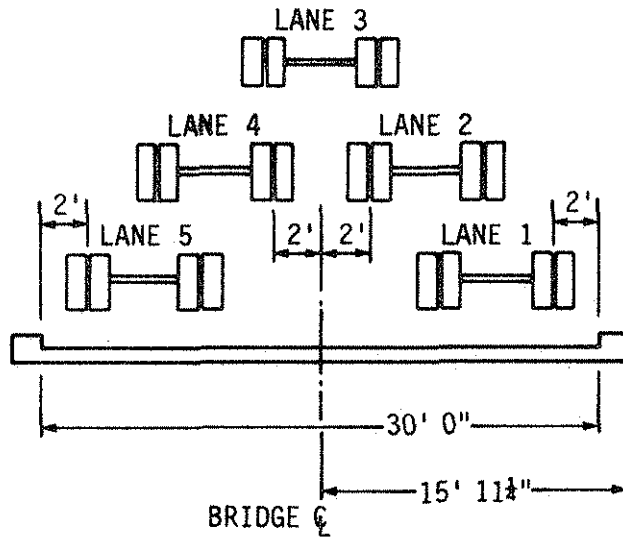


a. Cross-section.

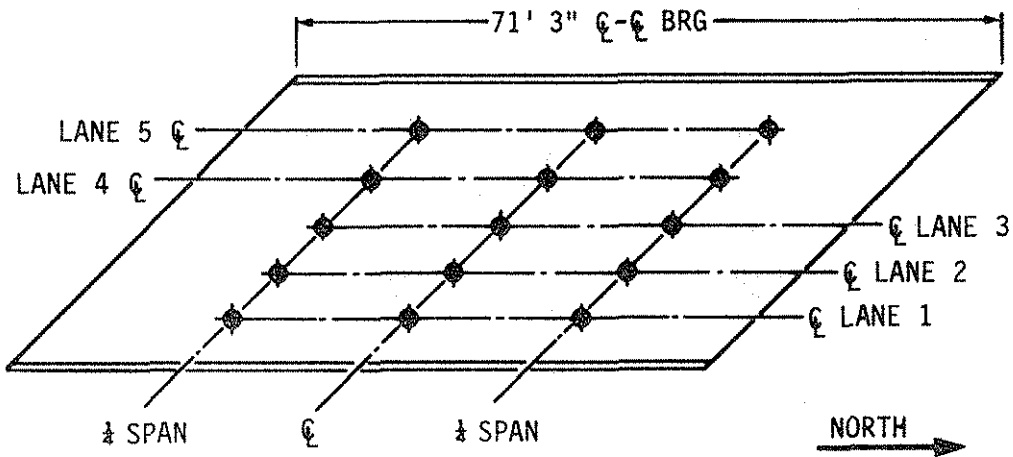


b. Plan view.

Fig. 2.13. Location of test vehicle--Bridge 1.



a. Cross-section.



b. Plan view.

Fig. 2.14. Location of test vehicle--Bridge 2.

On Bridge 1, the truck was positioned over the 12 loading points shown in Fig. 2.13b by having the truck head south in Lanes 1, 2 and 3 and north in Lane 4. The locations of the various lines are shown in Fig. 2.13a. Because of symmetry, the results from the truck in Lanes 1 and 4 should be essentially the same.

The second truck (see Fig. 2.12b) was positioned on Bridge 2 (see Fig. 2.14b) by having the truck cross the bridge in five different lanes and stop so that the truck's center of gravity was at the 15 different predetermined locations. Five crossings (three with the truck headed north and two with the truck headed south) were necessary because of the skew of the bridge. The location of the lanes used by the truck when it crossed the bridge is shown in Fig. 2.14.

Post-tensioning was removed and applied to the exterior beams of the two bridges utilizing 120-kip capacity, 6-inch-stroke hollow-core-hydraulic cylinders, 6 1/4 inches in diameter. The diameter of the cylinders controlled the position of the tendons on each bridge relative to the bottom flange. Only two of the previously described cylinders were available during the Phase II testing (1982). With the purchase of two additional cylinders (for a total of four) the post-tensioning scheme utilized during Summer 1984 was different from that of Phase II. Since the steps in post-tensioning were significantly different for the two bridges, they will be presented separately in the following paragraphs.

As Bridge 1 had four post-tensioning tendons (two per exterior beam) and there were four hydraulic cylinders available, it was possible to remove the post-tensioning force from the bridge in one oper-

ation. The post-tensioning force was removed in three approximately equal increments. After the post-tensioning force was completely off the bridge, deflections and strains were recorded. After a 10-minute period, deflections and strains were again recorded to detect any change in the end restraint. The test vehicle was then driven across the bridge three times; after each crossing strains and deflections were recorded to determine if the truck loading had changed the end restraint. After the previously described vertical loading tests were completed, the post-tensioning force was reapplied to the bridges. Because of end restraint, the post-tensioning force applied to the bridge in Phase II (average 182.01 kip per exterior beam) did not produce the desired strain reduction. Thus it was decided to increase the post-tensioning force applied in 1984 to 200 kips per beam (a 9.9% increase). This force was applied to the bridge in three approximately equal increments, and data were taken after each increment. After seating losses, Beams 1 and 4 had 197.49 kips and 196.10 kips of post-tensioning force respectively. Based on the average of these two values, 196.79 kips, there was 1.6% less post-tensioning force than desired (200 kips per exterior beam). However, the 196.79 kips constitute a 8.1% increase over that applied to the bridge (182.01 kips per exterior beam) in Phase II.

Removing the post-tensioning force from Bridge 2 had to be done in steps as there were eight tendons post-tensioned and only four hydraulic cylinders available. Force was first removed from the four top tendons (1-inch-diameter--see Fig. 20b) in three approximately equal increments with strain and deflection data being recorded after each increment.

Hydraulic cylinders were then repositioned to remove the force from the lower tendons (1 1/4-inch diameter). Similar to the procedure followed on the upper tendons, force was removed in three stages with data taken after each stage. As was done on Bridge 1, data were taken 10 minutes after releasing the post-tensioning force and after having the test vehicle pass over the bridge three times in an effort to detect change in the end restraint. As a result of the end restraint present, the post-tensioning force applied during Phase II (average 305.58 kips per exterior beam) did not produce the desired strain reduction. Thus it was decided to stress each bar to the manufacturer's prescribed working prestress level (76.5 kips for 1-inch-diameter tendons) and 112.5 kips for 1 1/4-inch-diameter tendons (378 kips per exterior beam). Force was applied to the lower tendons first, since they were larger than the upper tendons and thus carried more of the total post-tensioning force. When force was then applied to the upper tendons there were smaller elastic shortening losses to be accounted for because they were smaller and thus carried less force. Force was first applied to the bottom tendons (1 1/4-inch-diameter) in three increments. After seating losses, Beams 1 and 4 had post-tensioning forces of 223.6 kips and 229.6 kips respectively. The hydraulic cylinders were then repositioned, and force was applied to the upper tendons in three approximately equal increments. After seating losses in the upper tendons and elastic shortening of the bridge causing a loss of force in the lower tendons were accounted for, the force on Beams 1 and 4 was 372.4 kips and 370.0 kips respectively. Based on the average of these two values, for 371.7 kips there was 1.7% less post-tensioning force than desired (378 kips

per exterior beam). The 371.7 kips of force, however, are 21.6% greater than those applied to the bridge in Phase II. When the upper tendons were tensioned, there was a 2.7% loss in force in the lower tendons due to elastic shortening of the bridge.

The procedure used to obtain data on both bridges for the trucks in the various locations as well as for the various stages of post-tensioning follows:

1. To record zero strain readings for all strain gages, strain and force transducers, and DCDT's
2. To apply loading (truck, post-tensioning, or truck plus post-tensioning) at desired locations
3. To record strain, force, and deflection readings as in Step 1; to note any changes in bridge behavior
4. To remove truck loading from bridge and check initial zero reading. Obviously this could not be done when the post-tensioning forces were involved
5. To repeat steps 1 through 4 for all loading conditions (see Section 3.1)

3.3. Test Results and Analysis

Experimental results of the various field tests performed will be presented in this section. Detailed descriptions of the bridges and the various tests performed on them have been presented in the preceding sections. In most instances the experimental results will be compared with theoretical results.

In Phases I [17] and II [16] of this investigation, orthotropic plate theory was used in the theoretical analysis. In this phase (Phase III) finite element analysis has been used to determine theoretical results. Thus in this section, experimental results are compared with theoretical values that have been determined utilizing finite element analysis.

Temperature effects are not presented in this section but may be found in Section 4. The effectiveness and reliability of the strain and force transducers have been presented in Section 2.3. Throughout the course of this study questions have arisen as to what effect the post-tensioning forces have on the ultimate flexural strength of the bridge. A discussion of the increase in ultimate flexural strength provided by the post-tensioning is presented in Sections 5.4 and 5.5.

3.3.1. Bridge 1

As stated in Section 3.2, the post-tensioning force was applied to Bridge 1 in three steps. Strains occurring in the bottom flange after each step of post-tensioning are shown in Fig. 2.15. A comparison between the measured post-tensioning strains (post-tensioning force = 196.8 kips per exterior beam) and the theoretical strains assuming both simple supports and fixed ends is shown in Fig. 2.16. Midspan and end bottom flange beam strains are shown in Fig. 2.16a and Fig. 2.16b respectively. As is shown, the measured strains are essentially midway between the two theoretical curves. The significant magnitude of strains measured nine inches from the "simple supports" verifies the existence of end restraint and the resulting effect at midspan. This same end restraint was noted during the testing of Phase II and is

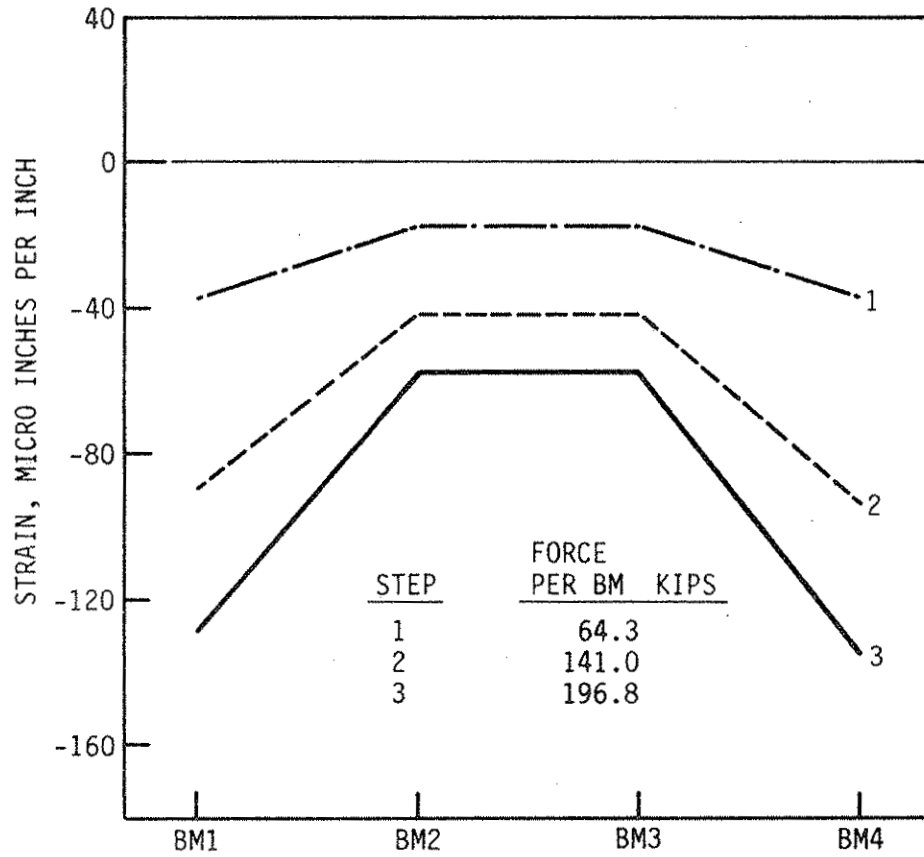
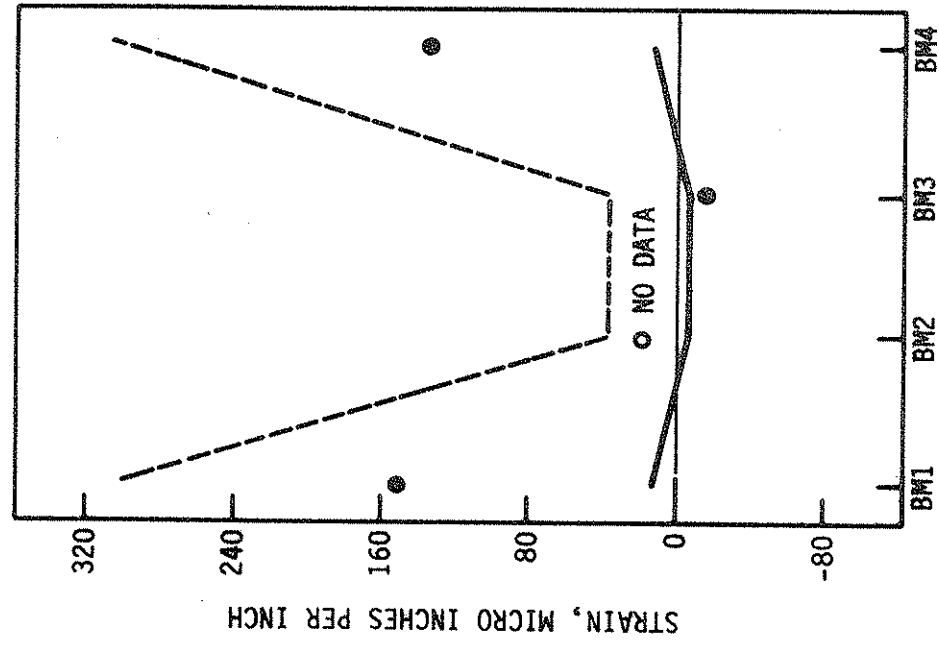
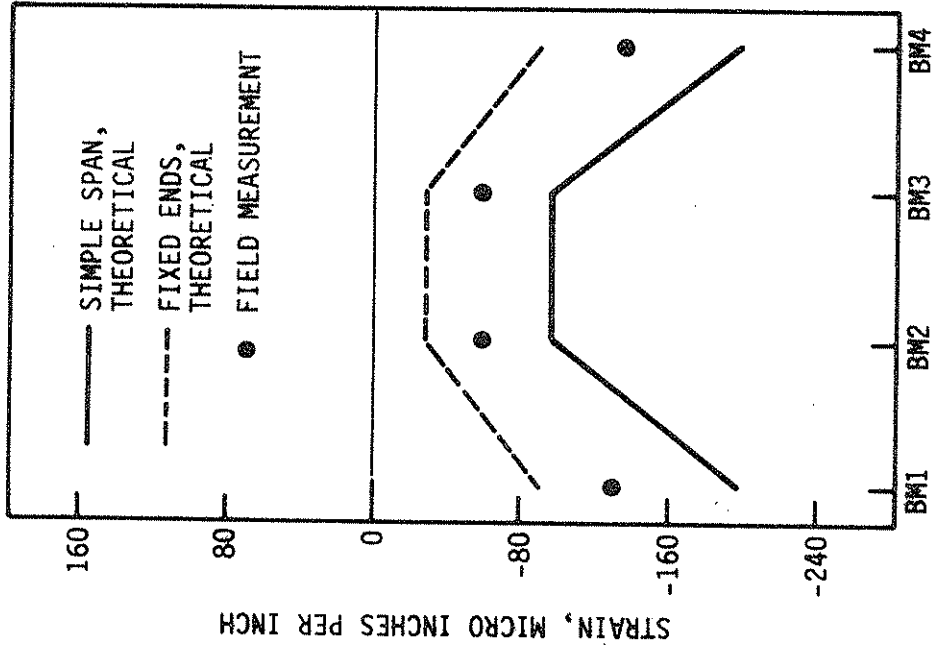


Fig. 2.15. Variation in midspan, bottom flange beam strains as post-tensioning force is applied to Beams 1 and 4--Bridge 1.



a. Midspan.



b. 9" from end.

Fig. 2.16. Post-tensioning, bottom flange beam strains--Bridge 1.

believed to be caused primarily by reinforcing steel extending from the bridge deck and curbs into the abutments. A more detailed explanation of this behavior may be found in Ref. 16.

A comparison between deflection and strain data resulting from post-tensioning during Phases II and III is presented in Table 4. Several observations may be made in reviewing this data. A post-tensioning force of 182.0 kips was applied to the exterior beam of the bridge in Phase II; however, when this force was removed in Phase III a magnitude of only 172.0 kips was measured. This 5.5% decrease is thought to be primarily the result of reduction in the amount of end restraint present. Although a larger post-tensioning force was applied during Phase III than in Phase II (196.8 kips vs 182.0 kips), the resulting deflections and strains in the exterior beams were smaller, although not by a significant amount. The deflection and strains measured in the interior beams during the three cases of post-tensioning were essentially equal. The only explanation for this behavior is the previously noted end restraint. Table 5 presents strains and deflections resulting from the truck loading being applied in Lane 1 (see Fig. 2.13) with and without post-tensioning forces being present during Phases II and III. Values given in this table are only due to the vertical loading and do not include strains and deflections resulting from post-tensioning. Note the excellent agreement in magnitudes of strains and deflections found in the interior beams in the five loading cases. There is also very good agreement in the magnitude of strain and deflection found in the exterior beams. Some of the variations seen are the result of a slight difference in truck weights in Phases II and III

Table 4. Comparison of experimental post-tensioning force data: Bridge 1.

Post-tensioning Force: Kips/ Exterior Beam		Deflection at Midspan of Beam-Inches				Bottom Flange Strains--Microinch per Inch at Midspan of Beam				at 9" from End of Beam				
		1	2	3	4	1	2	3	4	1	2	3	4	
1	PS = 182.0	'82	0.200	0.086	0.087	0.198	-144	-59	-60	-149	a	a	a	a
2	PS = -172.0	'84	-0.145	-0.071	-0.079	-0.162	137	52	55	126	-108	+17	b	-131
3	PS = 196.8	'84	0.181	0.087	0.087	0.175	-129	-58	-58	-135	136	-21	b	152

a = No instrumentation in 1982
b = channel not working on DAS

Table 5. Comparison of experimental truck loading data (truck in lane 1): Bridge 1.

Post-tensioning Force: Kips/ Exterior Beam		Deflection at				Bottom Flange Strains--Microinch per Inch								
		Midspan of Beam-Inches				at Midspan of Beam								
		1	2	3	4	1	2	3	4					
1	PS = 0	'82	-0.206	-0.161	-0.048	0.001	127	90	24	0	a	a	a	a
2	PS = 182.0	'82	-0.187	-0.149	-0.046	0.003	129	93	21	-1	a	a	a	a
3	PS = 172.0	'84	-0.211	-0.152	-0.043	0.003	153	99	22	-2	-64	-41	22	11
4	PS = 0	'84	-0.229	-0.159	-0.047	0.008	162	100	24	3	-42	-40	27	21
5	PS = 196.8	'84	-0.201	-0.153	-0.045	0.003	147	97	21	-5	-73	-43	25	12

a = No instrumentation in 1982

(60.54 kips vs. 63.98 kips). The maximum increase in post-tensioning force, 4.87 kips, as a result of vertical loading was determined when the truck was in Lane 1. This was just slightly less than the increase measured during Phase II of the study. Considering all the variables involved, essentially no difference in behavior was found in the bridge between the testing of Phases II and III.

3.3.2. Bridge 2

The post-tensioning force was applied to Bridge 2 in six steps-- three approximately equal increments of force on the lower tendons followed by three approximately equal increments on the upper tendons. Figure 2.17 illustrates the bottom flange strains measured after each of the six steps. Although the force applied to each beam was essentially equal (average of the two values is listed on the graph), the resulting strain pattern is not symmetrical (with respect to the longitudinal centerline of the bridge). Quite possibly the deck and curb repairs created asymmetrical conditions within the bridge. Theoretical values of midspan and end bottom flange beams strains along with the experimental values are presented in Fig. 2.18. As was the case on Bridge 1, Bridge 2 also had considerable end restraint. In the exterior beams the experimental data are closer to the fixed-end theoretical curves than to the simple-span theoretical curves. This implies the bridge is behaving closer to the fixed-end condition than to the simple span condition. Thus there is a greater degree of end restraint present in Bridge 2 than in Bridge 1. This is the result of the skew plus the end details; Ref. 16 contains a detailed discussion of this. The negative theoretical strains associated with Beam 1,

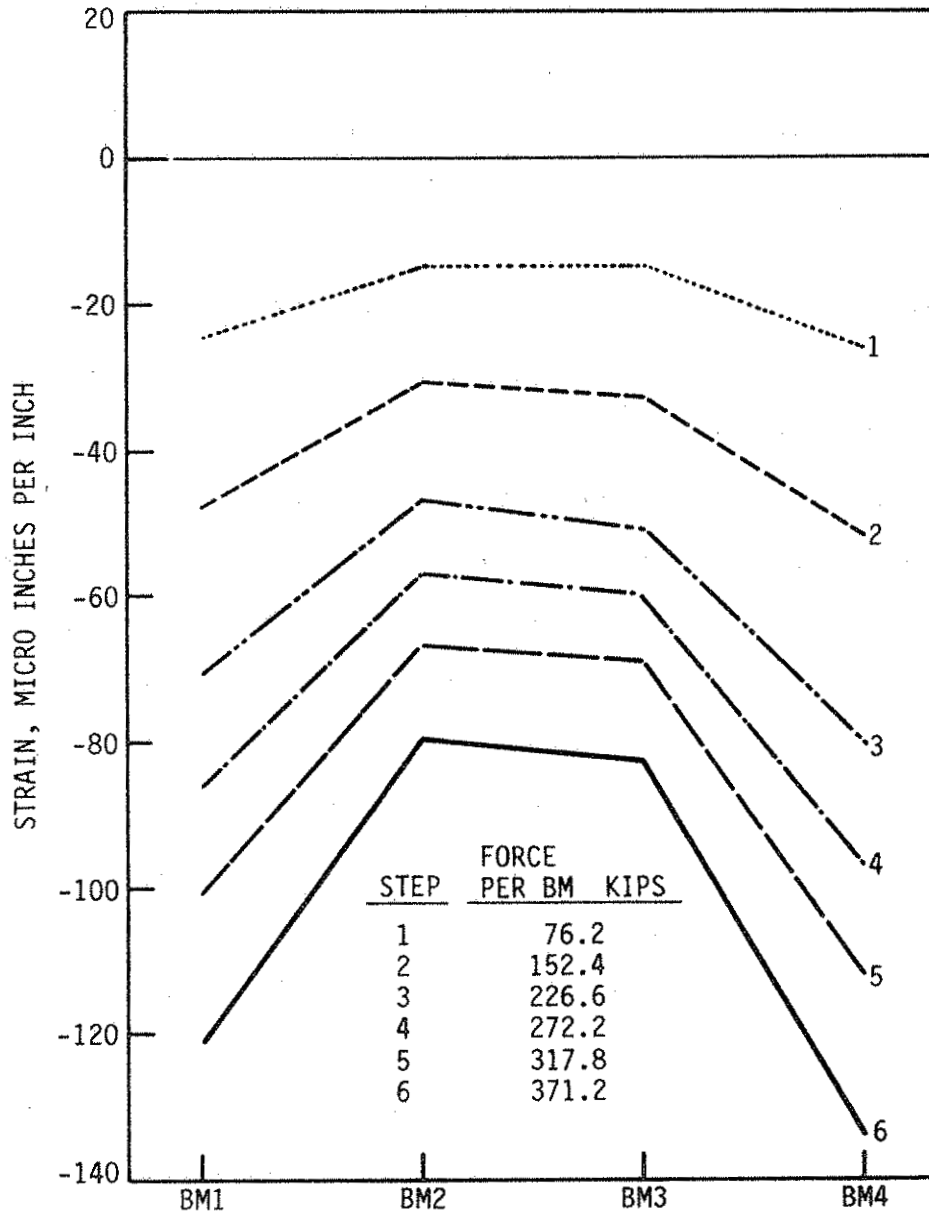


Fig. 2.17. Variation in midspan bottom flange strains as post-tensioning force is applied to Beams 1 and 4--Bridge 2.

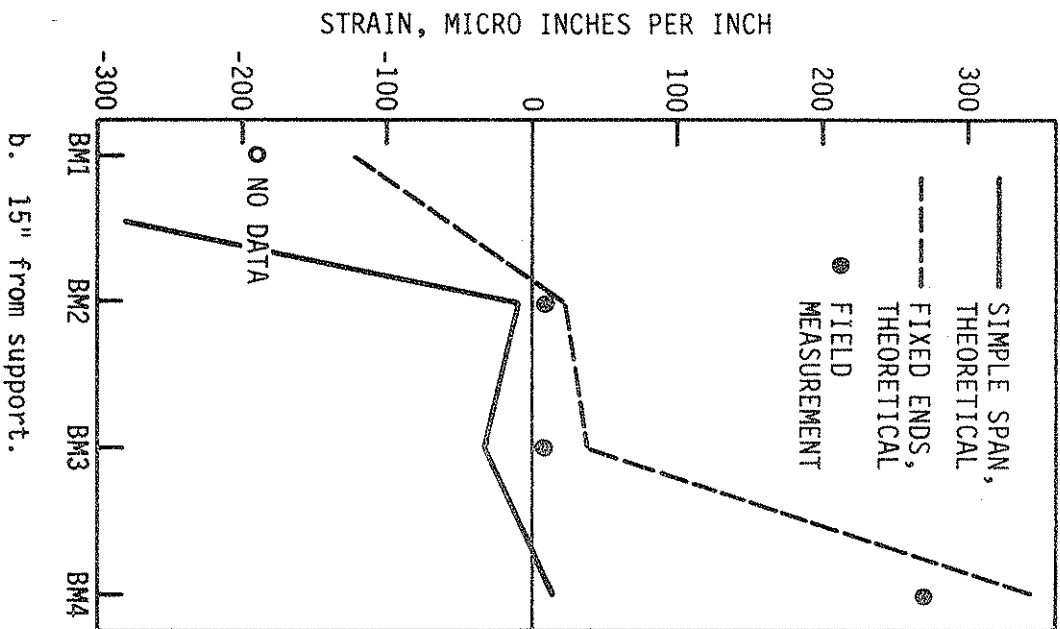
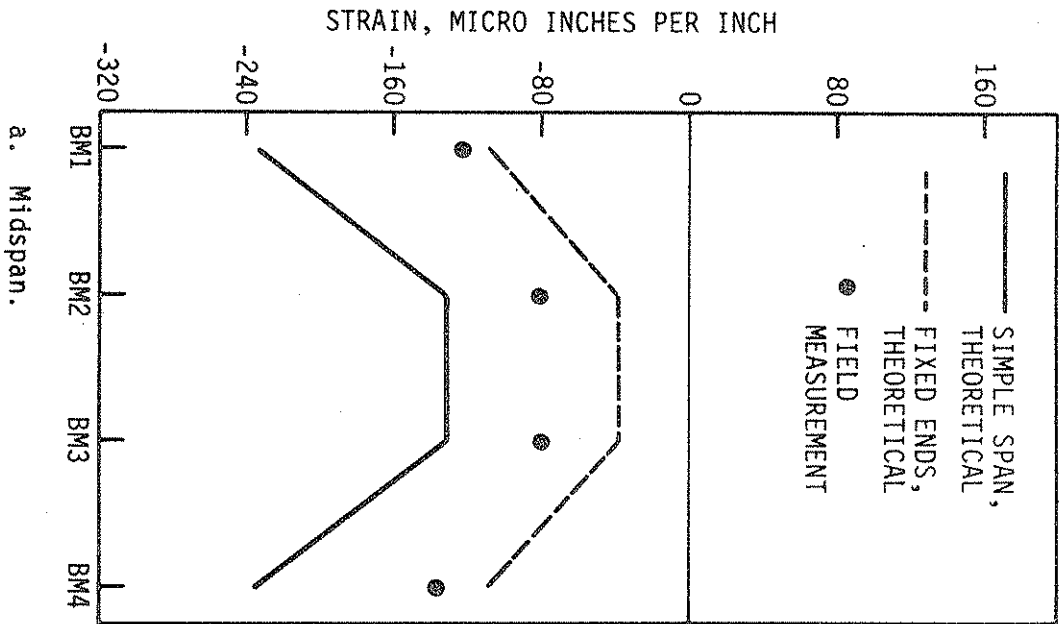


Fig. 2.18. Post-tensioning, bottom flange beam strains--Bridge 2.

shown in Fig. 2.18b, are the result of the section of interest being 15 inches from the end of the support and thus in the immediate vicinity of the post-tensioning bracket (see Fig. 20 of Part I).

Deflection and strain data resulting from post-tensioning during Phases II and III are presented in Table 6. The difference seen between the 1982 and 1984 data is mostly the result of the resurfacing of the bridge during Summer 1983. A brief description of this resurfacing was presented in Section 3.1. In Phase II, a post-tensioning force of 305.6 kips was applied to the exterior beams of the bridge. In Phase III when the post-tensioning force was released, a magnitude of 271.5 kips per exterior beam was measured--a decrease of 11.2%. Most of this decrease was the result of the resurfacing! When the bridge was post-tensioned in Phase III with a force of 371.2 kips per exterior beam (21.5% greater than applied in Phase II), larger strains and deflections resulted, as one would expect; however, the increase was not as large as expected because of the increase in deck thickness as a result of resurfacing.

Strains and deflections resulting from the truck loading in Lane 1, (see Fig. 2.14) are given in Table 7. These data are from both Phases II and III with and without the post-tensioning forces being applied. Also to be noted is that the data are only due to vertical loading and do not include the effects of post-tensioning. There is very good agreement between the deflections and strains from the five loading cases. Although the values measured in case 3 are slightly less than the other four cases, it is not a significant difference. A review of the end strains (15 inches from the beam ends) in this table and Table 5

Table 6. Comparison of experimental post-tensioning force data: Bridge 2.

Post-tensioning Force: Kips/ Exterior Beam	Deflection at Midspan of Beam-Inch				Bottom Flange Strains--Microinch per Inch at Midspan of Beam				at 9" from End of Beam			
	1	2	3	4	1	2	3	4	1	2	3	4
1 PS = 305.6 '82	b	0.120	0.128	0.318	-95	-59	-56	-109	a	a	0	99
2 PS = -271.5 '84	-0.176	-0.090	-0.097	-0.212	125	51	52	98	b	11	b	-205
3 PS = 371.2 '84	0.337	b	0.200	0.323	-122	-81	-80	-136	b	9	3	257

a = No instrumentation in 1982
b = instrumentation not working

Table 7. Comparison of experimental truck loading data (truck in lane 1): Bridge 2.

Post-tensioning Force: Kips/ Exterior Beam		Deflection at				Bottom Flange Strains--Microinch per Inch								
		Midspan of Beam-Inches				at Midspan of Beam at 9" from End of Beam								
		1	2	3	4	1	2	3	4					
1	PS = 0	'82	-0.223	-0.130	-0.044	-0.009	111	51	20	9	a	a	-54	-60
2	PS = 305.6	'82	-0.222	-0.127	-0.041	-0.002	108	47	14	0	a	a	-32	-56
3	PS = 271.5	'84	-0.184	-0.106	-0.019	0.024	98	54	18	6	b	-3	-116	-71
4	PS = 0	'84	-0.192	-0.131	-0.063	-0.016	105	59	20	8	b	0	-80	-82
5	PS = 371.2	'84	-0.204	b	-0.047	-0.003	96	54	15	3	b	c	c	c

a = No instrumentation in 1982
b = instrumentation not working
c = no data taken

indicates that end restraint is present for both vertical loading and post-tensioning loading. In the interior beams, the data indicate there is more end restraint associated with vertical loading than with post-tensioning. The truck weights in the testing of Phases II and III (60.50 kips vs. 61.18 kips) were essentially the same. The wheel spacing on the two trucks was slightly different (see Fig. 33 and Fig. 2.12b); however, since the center of gravity on each truck was used to position it on the bridge this difference would have little or no effect. Thus essentially none of the variation between the various cases in Table 7 can be the result of differences in the two trucks. Vertical loading (truck in Lane 1) caused a maximum increase in the post-tensioning force of 3.8 kips. No increase in post-tensioning force was measured in Phase II because of strain indicator problems. Although the deck and a major portion of the curbs on Bridge 2 had been replaced during Summer 1983, no cracks were observed as a result of the post-tensioning. As was the case with Bridge 1, essentially no change in behavior was found in Bridge 2 (Phase II vs. Phase III) except for effects of resurfacing the deck and replacing the curbs during Summer 1983. However, the resulting bridge behaved essentially the same as in Phase II.

4. THERMAL EXPANSION CONSIDERATIONS

The loss of post-tensioning force due to a possible temporary temperature differential between post-tensioning tendons and beams was addressed in Phase II of this project [16]. It was shown that if the maximum temperature difference that occurred between tendons and beams was 20° F, a temporary temperature-caused loss of 3.9 kips per tendon could occur. This size of loss was considered small enough to be offset by an increase in tendon tension due to a truck passing over the bridge. Therefore, no further investigation into the thermal expansion effects on the post-tensioning force was conducted during Phase II.

In order to check the accuracy of the assumption that 20° F was the maximum temperature differential between the tendons and beams, some sort of verification was required. A thorough analytical investigation of the bridge could be accomplished with the use of a finite element program capable of analyzing three-dimensional, nonlinear temperature gradients through two different materials (steel and concrete). A time surface-temperature response history averaged over several days would be needed to provide program input of member temperatures related to time. This experimental data collection would require extensive instrumentation and either an automatic data recording and storage system or a continuously manned field station. Although this type of analysis is possible, a review of similar investigations found the procedures to be relatively complicated and time consuming [7,8]. Before undertaking the more involved temperature analysis, we decided to conduct simpler experimental tests on the two post-tensioned

bridges to establish a general trend of tendon and beam temperature response relating to the time of day. Depending upon the data obtained in the simpler tests, a decision would be made as to the necessity of a more sophisticated test and analysis.

4.1. Temperature Transducer System

Since this investigation was to provide only a general thermal behavior pattern of the beam flange-tendon system, high-accuracy data collection techniques were not required. Experimental data measured to within a tolerance of approximately $\pm 2^\circ$ F would satisfy the requirements of this analysis. Therefore, a temperature transducer system was developed. Although this system would not be as accurate as if the temperature were measured directly on any beam member itself, the accuracy would be satisfactory to establish conclusions regarding any temporary temperature-induced change in post-tensioning force. This system offered the advantage of being more reliable over long periods of time since permanently attached instrumentation risked loss resulting from weather conditions or vandalism. The versatility of the temperature transducers would also enable temperature data to be collected on either post-tensioned bridge (or other structures) at different testing dates. In the remainder of this section, the temperature transducers will simply be referred to as transducers.

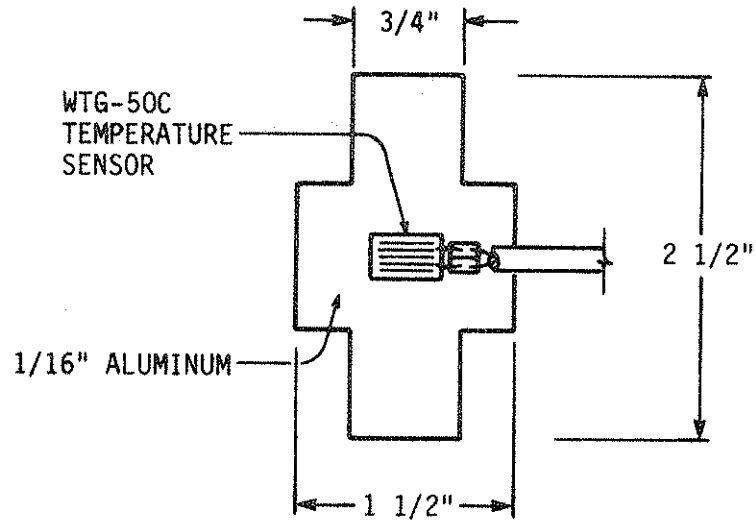
4.1.1. Description of Temperature Transducers

Two types of transducers were fabricated; one for measuring temperatures on the beam flanges and one for measuring temperatures on the

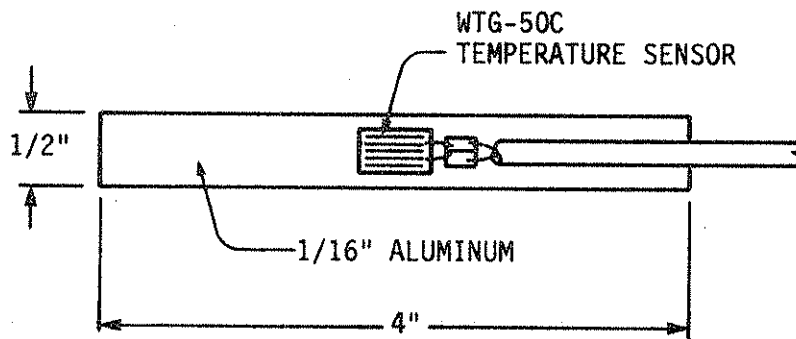
tendons. Both operated on the principle of thermal conduction. If a thin piece of material with good thermal conductivity properties was placed in contact with a bridge member, the predominant temperature gradient acting on the piece of material would come from the bridge member rather than from any other part of the surrounding environment. The piece of material, in this case the transducer, would quickly reach equilibrium with the bridge member's temperature. Temperatures recorded from the transducer would correspond to the member temperature at that location.

Assembly of both the beam and tendon transducers is shown in Figs. 2.19a and 2.19b respectively. Each was fabricated out of 1/16-inch-thick aluminum sheet. Prior to any surface preparation, the tendon transducer was curved in the short direction to allow for more surface contact when placed on the oval-shaped tendon. A Micro-Measurements brand WTG-50C resistance temperature sensor, which resembles a electric resistant strain gage, was bonded to the aluminum using a heat-cured epoxy. After attaching approximately eight inches of two-conductor lead wire to the sensor, the installation area was covered with a protective coating using standard procedures.

A small piece of 3/16-inch-thick polystyrene plastic was bonded to each transducer over the sensor location to provide thermal insulation on the top surface. A small piece of plywood was placed over the insulation and bonded to the aluminum of the beam transducers. This plywood provided a rigid surface for clamping the transducer onto the beam flanges with small C-clamps. The tendon transducers were held in position on the tendons by springs placed over each end of the transducers and hooked around the tendons.



a. Beam temperature transducer.



b. Tendon temperature transducer.

Fig. 2.19. Description of temperature transducers.

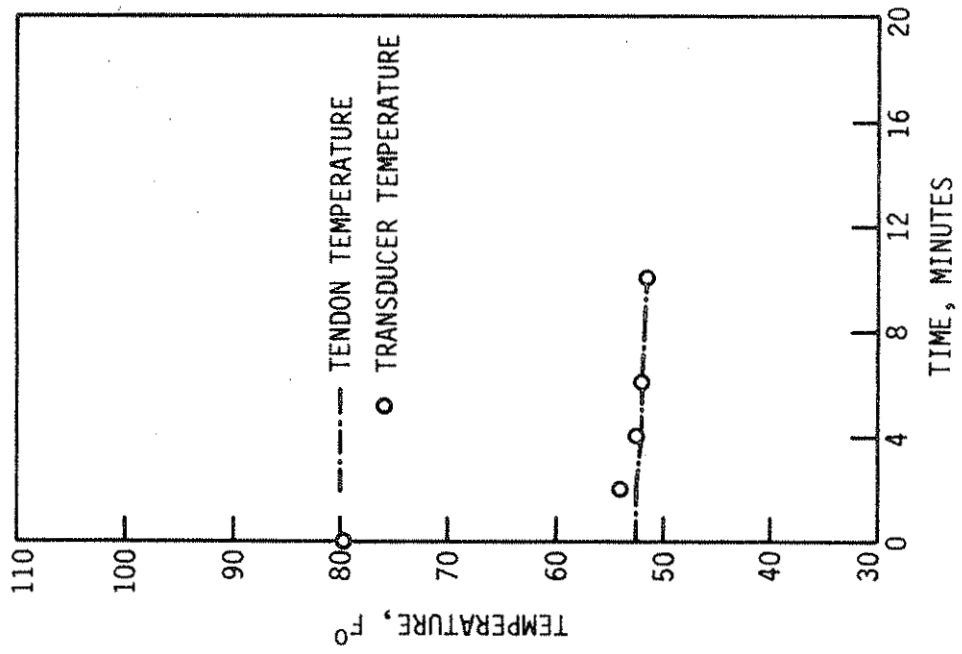
4.1.2. Calibration and Testing of Transducers

The Micro-Measurements WTG-50C temperature sensor is designed such that a resistance of 50 ohms corresponds to a temperature of 75° F. This temperature sensor, which was the actual measuring device of the transducer, was used in conjunction with a Micro-Measurements LST network and a digital strain indicator to read the output signal from the transducer [21]. At the designated gage factor setting, the LST network linearized the electrical output signal from the sensor to a ratio of 100 microinches per inch of apparent strain per 1° F temperature increase. A reference reading was established in the circuit by replacing the transducer with a 50-ohm precision resistor. The digital strain indicator was then set to a strain reading of zero, which corresponded to 75° F. After calibration, the transducer replaced the 50-ohm resistor in the circuit. Thus a bridge member's surface temperature was determined by dividing the indicated strain reading by the ratio of 100 microinches per inch per 1° F and adding this calculated temperature difference to the zero strain reading temperature of 75° F.

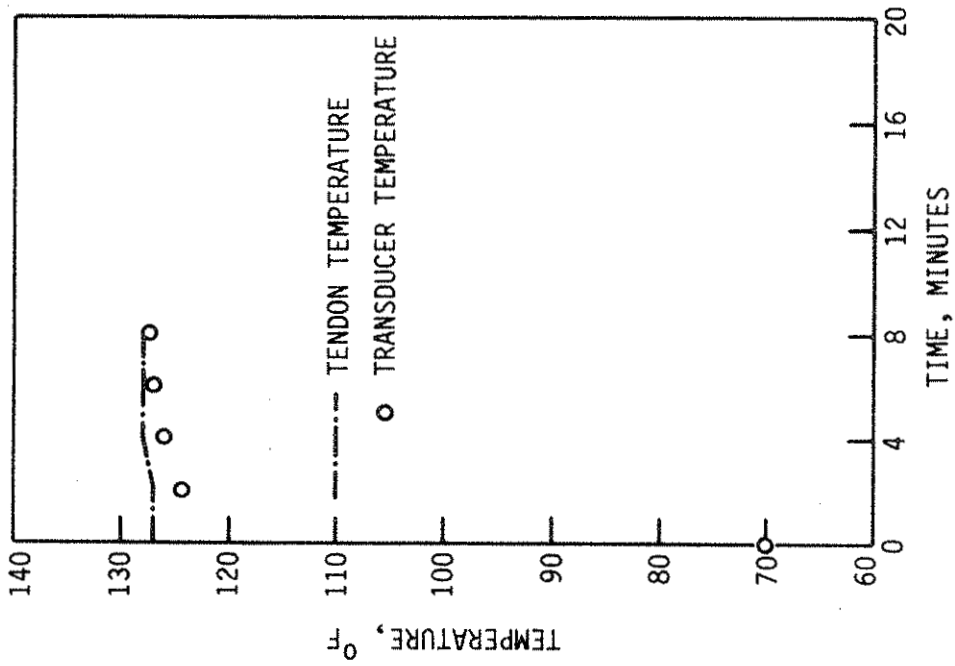
Calibration of the resistance temperature sensor-LST network system was accomplished by using the previously described procedure each time the transducers were used. Therefore, testing of the transducer system concentrated on time response and degree of accuracy. The tendon transducer was used in all tests because its curved shape provided less surface contact between tendon and transducer. The beam transducer, with its flat contact surface, provides results at least as accurate as those of the tendon transducer.

A seven-inch-long piece of 1 1/4-inch-diameter post-tensioning tendon was instrumented with a Micro-Measurements WTG-50C temperature sensor. The tendon, with two springs attached around it, was then placed in a pan of continuously heated water and monitored until the tendon temperature stabilized. After its initial temperature was recorded, the transducer was clamped onto the tendon. The transducer-tendon assembly was then placed back into the water. Temperature response of the transducer related to time was monitored. A representative example from this test series is shown in Fig. 2.20a. A similar test was conducted by placing the tendon in a refrigerator and monitoring the transducer response to a temperature decrease. Results of this test are shown in Fig. 2.20b. By analyzing this time-temperature response data as a first order system with step input, an average accuracy of 99% could be obtained in 2.5 minutes [5]. For practical field applications, the time response of the transducers presented no problem.

Although response time and accuracy were acceptable in the previously described tests, the possibility of the transducer's temperature rising faster than that of the tendon in the presence of solar radiation was still unknown. Three transducers were clamped onto a 1 1/4-inch-diameter tendon; two were mounted six inches apart on one side of the tendon, and the other one was placed 180° opposite the first two. Of the two transducers mounted six inches apart, one was covered with cardboard to shade it from the sunlight while the other one was left exposed. When the tendon was placed in the sunlight, two of the transducers were shaded--one by the cardboard and the underneath



a. Response to higher temperature.



b. Response to lower temperature.

Fig. 2.20. Temperature transducer sensitivity with respect to time.

one by the tendon itself. Although temperature of the tendon was not recorded, the two transducers not exposed to direct sunlight gave readings that were in excellent agreement with the one that was. The results, shown in Fig. 2.21, indicate that the transducers responded to the temperature of the material they were mounted on rather than to thermal inputs from the surrounding environment.

4.2. Field Testing

The transducers previously described were used for data collection during the retesting of both bridges. At a later date in Summer 1984, the two bridges were again instrumented for temperature data collection. Because of cloud cover and mild temperatures the tests of Bridge 1 provided data only for small air-temperature rises. The temperature data taken during the post-tensioning of Bridge 2 did not span the entire day as the post-tensioning tests restricted the time available for the recording of temperature data. The second test of Bridge 2 occurred during ideal weather conditions and produced experimental test results needed to examine the thermal expansion of the bridge due to sun. The transducer location, test procedures, and the recorded data for the testing are presented in the following section.

4.2.1. Test Procedures

Figure 2.22, denoting a cross section six feet from the north end of Bridge 2--Beams 1 and 4 being on the west and east side of the bridge, respectively--shows the location of tendon and beam transducers along with the numbering system employed. As may be seen, there were

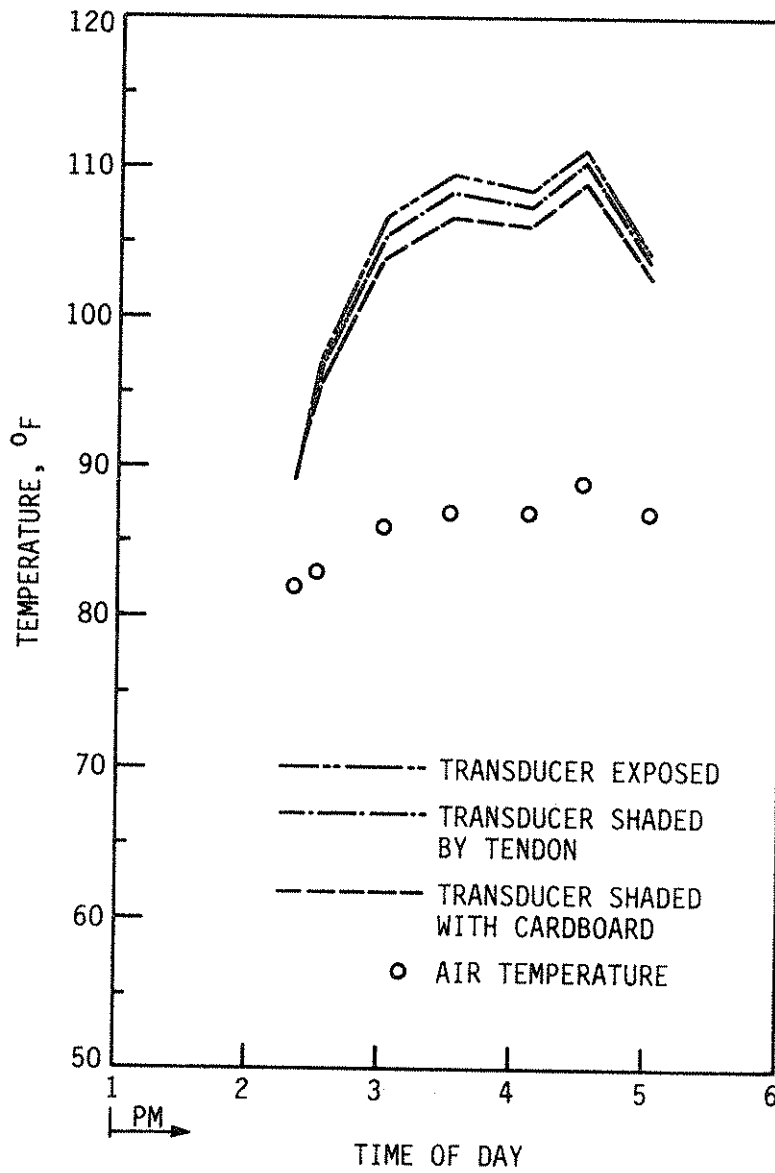


Fig. 2.21. Determination of transducer response with respect to degree of sunlight exposure.

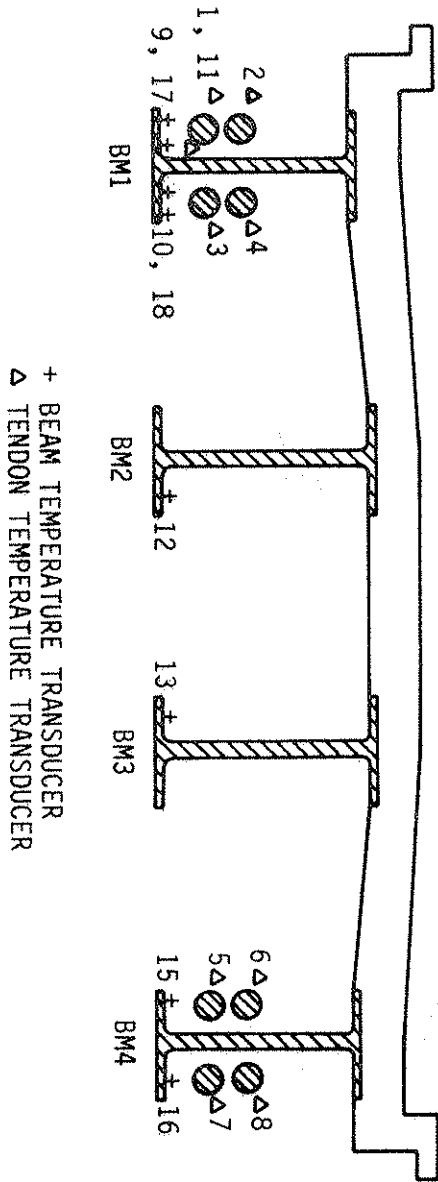


Fig. 2.22. General layout of temperature instrumentation--Bridge 2.

eight transducers on the beams and nine transducers on the tendons. Beam temperatures were measured on the bottom flange and did not consider the temperature at the top of the beam. This is reasonable since the post-tensioning brackets are mounted on the bottom flange, and the thermal expansion in this region of the beam is of most concern. The instrumentation and calibration system described in Section 4.1.2 was used. All transducers except 11, 17, and 18 were placed on bare metal. Transducers 17 and 18 were placed on a painted surface six inches from Transducers 9 and 10, respectively, to determine the effect of the painted surface on transducer sensitivity. Transducer 11 was mounted on a painted section of the outer bottom tendon on Beam 1 at a location 180° opposite Transducer number 1. This was done to again verify that the recorded temperature was not affected by the positioning of the transducer on the tendon. Air temperatures were recorded by shaded thermometers above the bridge near the beginning of the guard rail. Temperature data were taken at half-hour intervals beginning at 9:30 a.m. and continuing until 6:30 p.m. Clear skies were present throughout the entire test.

4.2.2. Test Results

The variation of surface temperature in relation to time of day for the four tendons mounted on Beam 4--the east side of the bridge--is shown in Fig. 2.23. The inside tendons remained at a relatively constant temperature throughout the day. During the morning hours, while Beam 4 was exposed to the sunlight, the inside tendons were approximately 10° F warmer than the air temperature. The outside tendons experienced temperatures of between 30° F and 40° F above air temperature during the

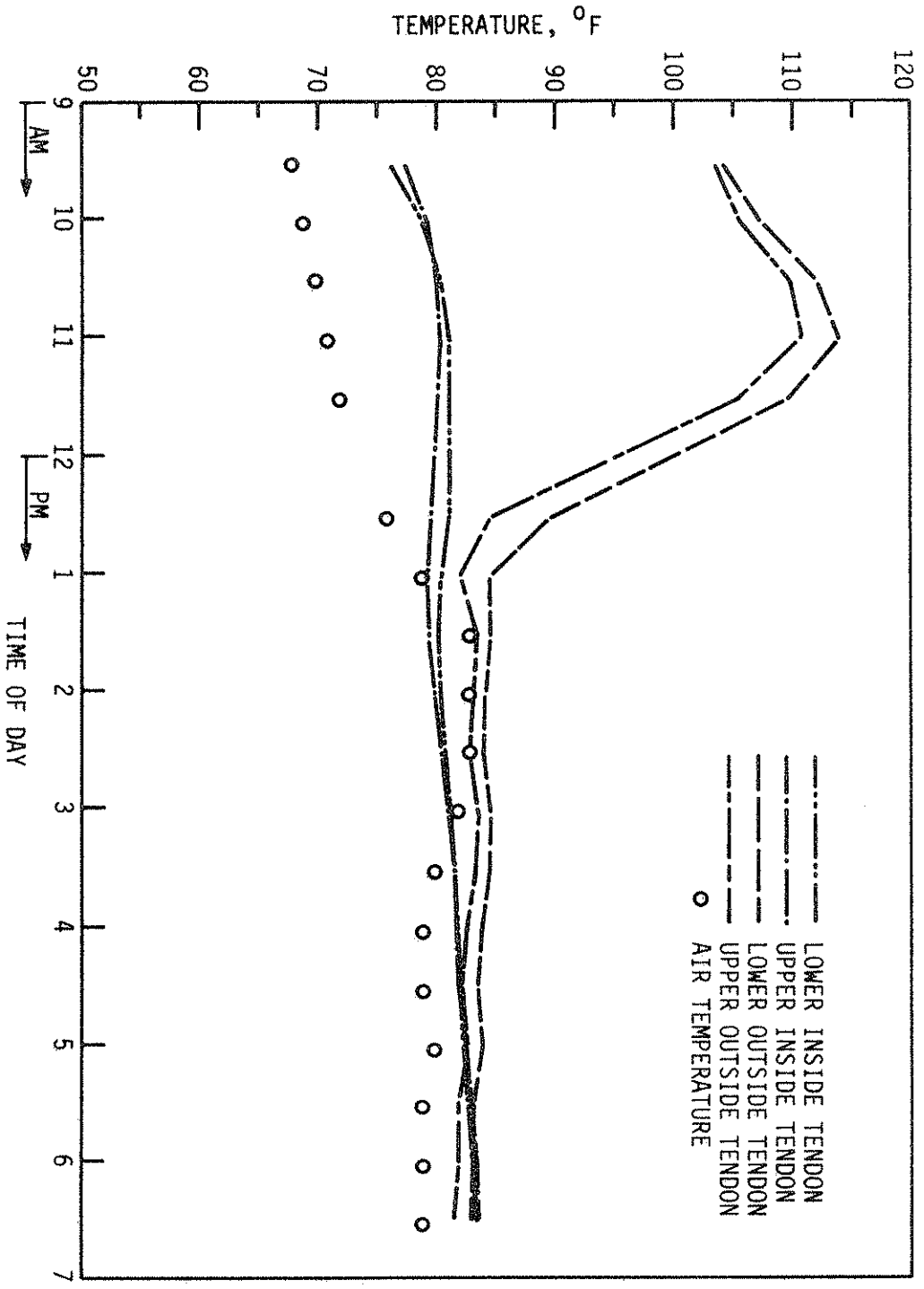


Fig. 2.23. Surface temperature of tendons mounted on Beam 4.

morning hours. The peak temperature on the outside tendons was recorded at 11:00 a.m. after which the tendon temperature decreased rapidly until equilibrium with the air temperature occurred at 1:30 p.m. From this time on, all four tendons were basically in an equilibrium state with the air temperature. The temperature differential between the inside and outside tendons was first recorded at 25° F and reached a peak differential of approximately 30° F at 11:00 a.m. As the exposure to direct sunlight decreased, the temperature differentials between tendons decreased until by 1:30 p.m., very small temperature differentials were noted.

The variation of the surface temperature relating to time of day for the tendons mounted on Beam 1--the west side of the bridge--is shown in Fig. 2.24. The temperature variation trend is, as expected, similar to what was experienced by the tendons on Beam 4, except for the tendon temperature differentials relating to the air temperature occurring in the afternoon. The overhanging deck restricted exposure of the tendon to direct sunlight until about 2:30 p.m. After this time, the inside tendon temperature increased to a value of 5° F above the air temperature. The outer tendons displayed a peak temperature of approximately 40° F above the air temperature. The temperature differential between inner and outer tendons was the same as that recorded for Beam 4 (30° F). However, the peak temperatures in the tendons on Beam 1 were approximately 5° F higher than those temperatures for corresponding tendons on Beam 4. A slight decreasing trend in the surface temperatures for the tendons on Beam 1 was observed by 6:30 p.m.

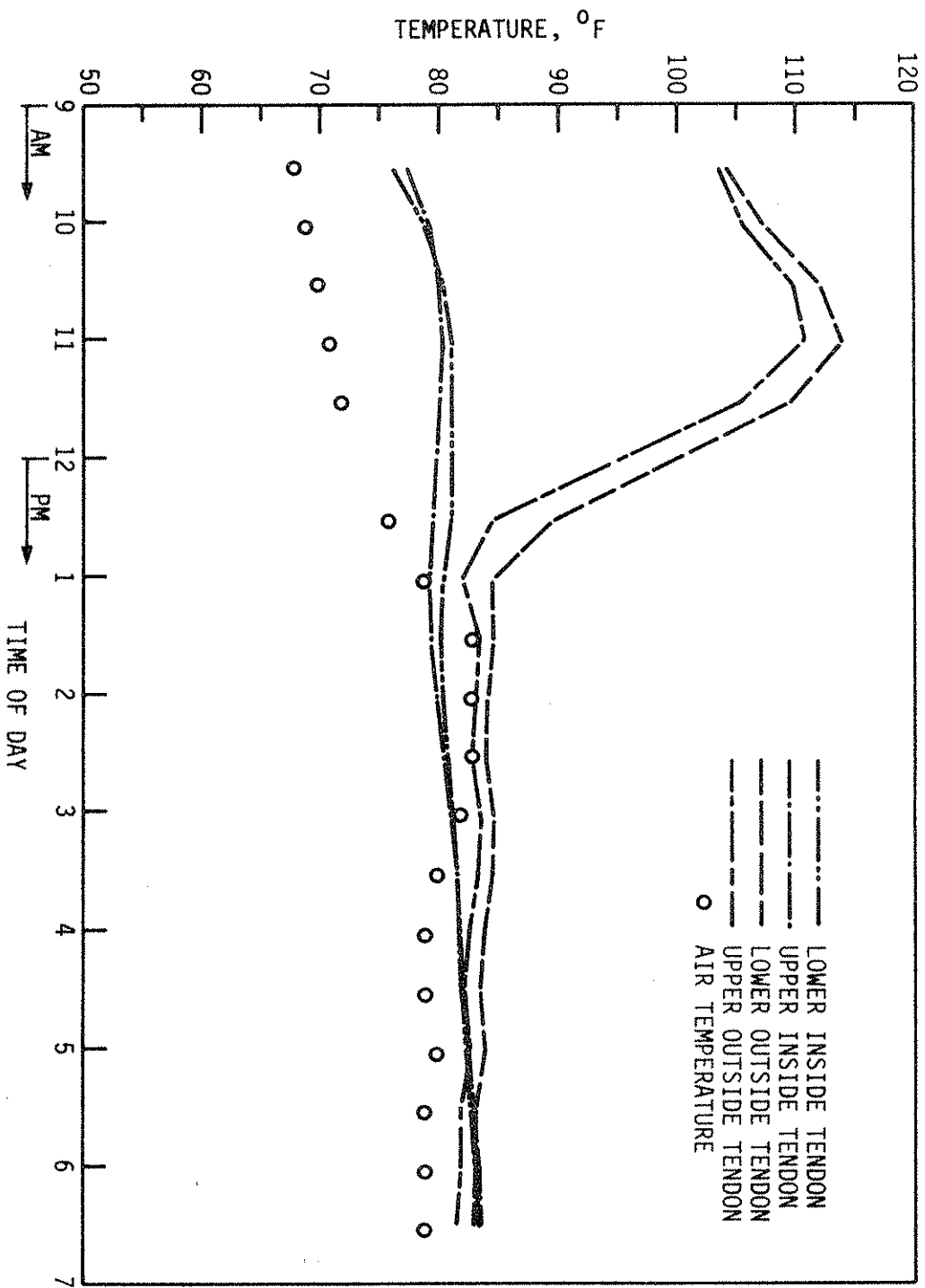


Fig. 2.23. Surface temperature of tendons mounted on Beam 4.

Figure 2.25 compares the inner and outer bottom beam flange temperatures of Beam 4 to the temperatures of the inner and outer tendons on Beam 4. Because the two tendons on either side of the beam had almost identical temperatures at any given time, only the average of the inner and outer tendon temperature is plotted. As can be seen from the graph, exposure to the morning sunlight created a maximum 10° F temperature differential between the inner and outer bottom beam flanges. As Beam 4 became shaded, the temperature differential between the two flanges decreased to zero and the beam basically displayed one temperature throughout the rest of the day. The average outer tendon temperature was only 5° F greater than the outer bottom beam flange temperature and varied from 10° F to 15° F greater than the inner bottom beam flange temperature. The average inner tendon temperature was 15° F less than the inner bottom beam flange temperature and was 20° F to 25° F less than the outer bottom beam flange temperature. While the outer tendons and both bottom beam flanges reached an equilibrium temperature at noon, the inner tendons were still 10° F below this equilibrium value. The temperature differential between the inner tendons and the other members of the beam-tendon system gradually decreased until equilibrium was essentially reached at 4:30 p.m.

Data similar to that shown in Fig. 2.25, but for the beam-tendon system of Beam 1, are presented in Fig. 2.26. Little temperature differential existed between the instrumented members until 2:30 p.m. Subsequent readings revealed a sharp temperature increase in the outer tendons and both bottom beam flanges. All temperature gradients leveled off and displayed a trend toward decrease when the final readings were

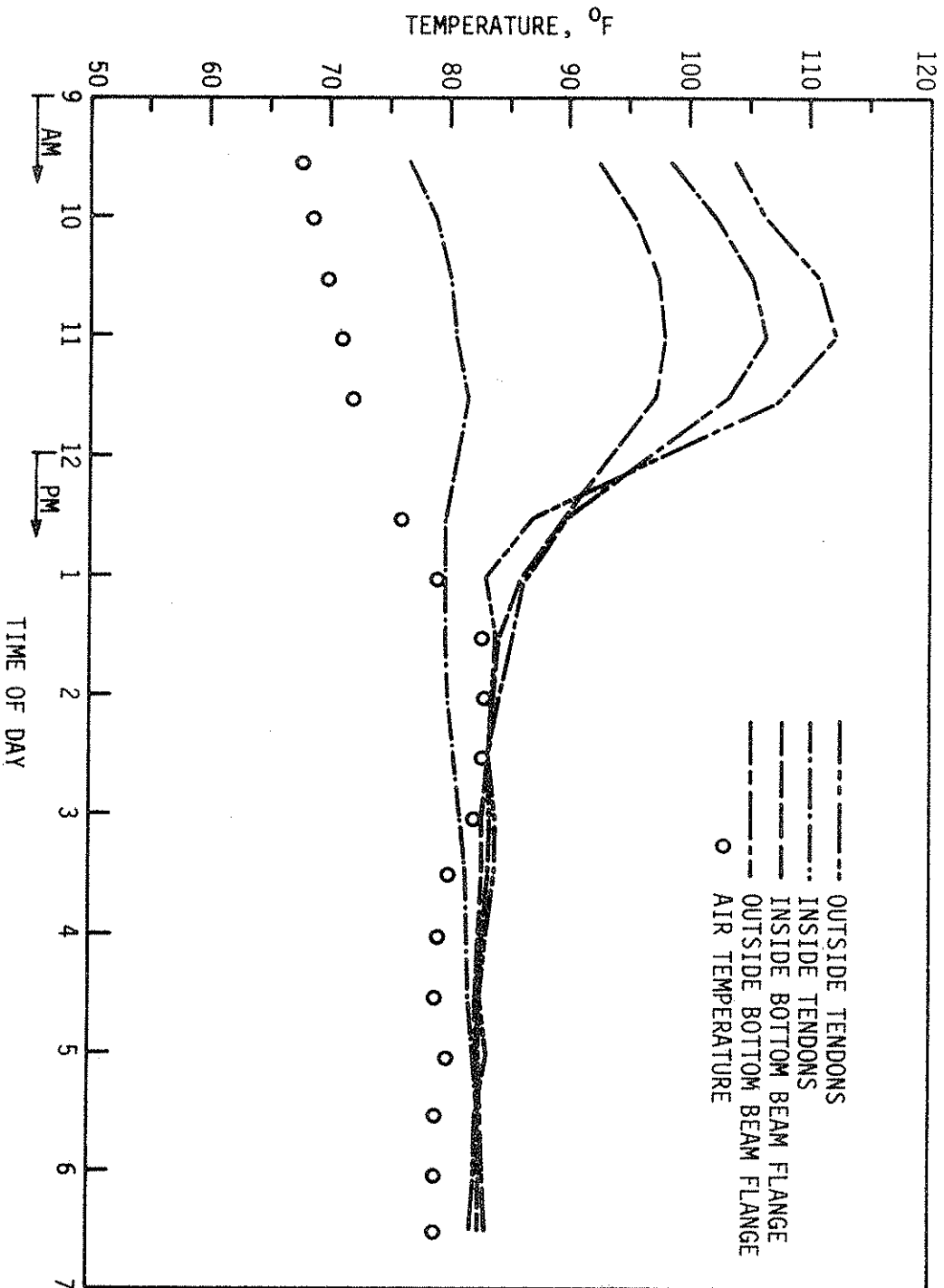


Fig. 2.25. Comparison of average inside and outside tendon temperatures to bottom flange beam temperature of Beam 4.

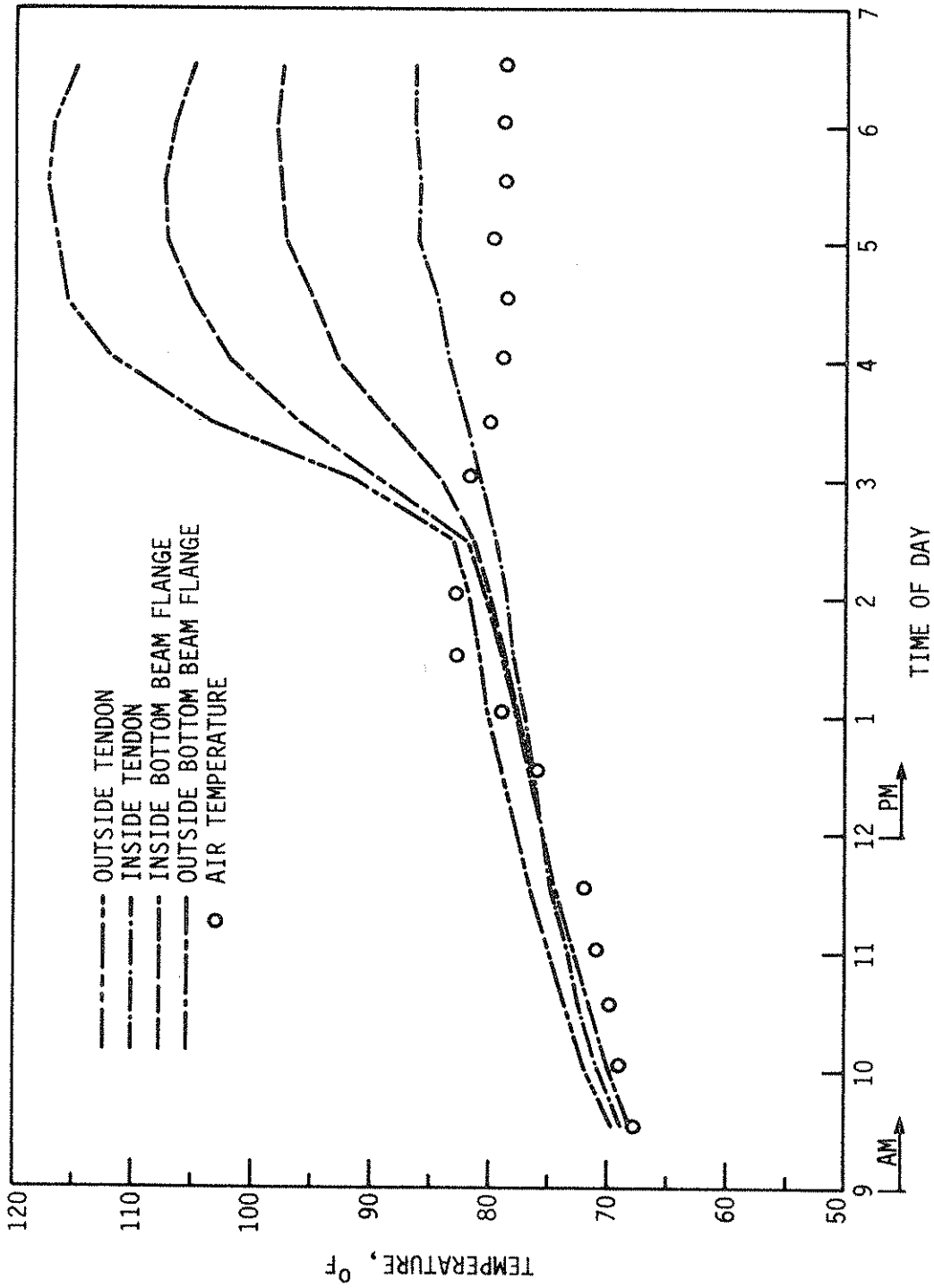


Fig. 2.26. Comparison of average inside and outside tendon temperatures to bottom flange beam temperature of Beam 1.

taken. The maximum temperature differential between inner and outer bottom beam flanges was 10° F. The outer tendons had a temperature reading 10° F greater than the outer bottom beam flange, while the inner bottom beam flange had a temperature differential of 12° F when compared with the inner tendons.

Calculations for the expansion and change in post-tensioning force of the beam flange-tendon system of Beam 1 are based on these assumptions: (1) a linear coefficient of thermal expansion of 6.5×10^{-6} inches per inch for °F for both tendon and beam flange; (2) a modulus of elasticity of all members equal to 29,000 ksi; (3) measured temperatures constant along the entire beam flange and tendon length, and (4) a simply supported structure. Since inner and outer tendon force losses will be based on differential movement between the tendons and the brackets (which are bolted to the inner and outer bottom beam flange), these losses are determined by considering only the corresponding inner and outer beam flange temperatures and the distance between the brackets. For the 10° F temperature differential between the outer tendon and the outer beam flange, the expansion differential was 0.05 inches. Multiplying this term by the axial stiffness of the two outer tendons, a post-tensioning force loss of 3.89 kips occurred on the outer tendons. For the 12° F temperature differential between the inner tendon and the inner beam flange, the length between the brackets expanded 0.061 inches more than the tendons. Therefore a post-tensioning force increase of 4.74 kips occurred in the inner section of the beam flange-tendon system. An overall increase in the post-tensioning force of 0.85 kips occurred in Beam 1. Similar calculations could be applied to Beam 4.

The temperature data recorded from the two interior beams of Bridge 2 indicated their temperatures were influenced by two factors; the trend of the air temperature throughout the day and the conductive temperature gradient coming from the thermal energy stored in the concrete slab. It was determined that the positioning of the temperature transducers on painted or bare metal surfaces, or the orientation of a temperature transducer on a tendon, had no significant effect on temperature readings.

4.2.3. Analysis and Conclusions

As would be expected, the surface temperature of any member of the beam-tendon system increased whenever that member was exposed to direct sunlight. The two tendons on any one side of a given beam displayed little difference in temperature when compared to each other. Whenever one of the steel beams was exposed to direct sunlight, the inner bottom beam flange experienced a temperature increase due to conduction of the solar energy from the outer flange to the inner flange; therefore its temperature lagged behind that of the outer beam flange. Beam flange temperatures were always between the values recorded for the average inner and outer tendon temperatures. From the computations in the previous section it appears that sun-induced temperature differentials increase rather than decrease the post-tensioning on the sunlit beam. The sun, then, should not cause any significant loss for a north-south bridge.

For an east-west bridge, the tendon and beam temperatures for the shaded, north exterior beam would generally follow the temperature fluctuation found in the instrumented interior beams of Bridges 1 and

2. The sunlit south exterior beam would be affected by temperature similarly to the way the east and west exterior beams were in the instrumented bridges. For a post-tensioned exterior beam in a bridge with any orientation, the sun should cause no detrimental temperature effect.

The data collected for Bridges 1 and 2 in all three cases are for situations during which there was only a gradual air temperature rise of approximately 10° F or less over three to five hours. Since the tendons are more exposed to air and not tied directly with the mass of the bridge, they are more affected by changes in air temperature and, if warmed at a faster rate than the bridge beams, will lose post-tensioning force. Higher temperatures for tendons than for beams are shown in the lower right corner of Fig. 2.27. At 11:00 a.m., during the gradual air temperature increase to which Bridge 2 was subjected, the tendons on the shaded exterior beam were warming faster than the beam by an average of 1° F to 2° F, during which time the air temperature was increasing 2° F to 3° F per hour. A similar condition occurred during the air temperature rise on the cloudy days when Bridge 1 was tested.

Because the air temperature increases during the tests conducted on Bridges 1 and 2 were quite mild, those tests cannot be expected to give extreme results for the temperature differentials and losses of post-tensioning. With a sharper air temperature rise, the test results could be extrapolated to give a 10° F temperature differential between tendons and beams. Without further testing, the 10° F adverse temperature differential does give some indication of the potential post-

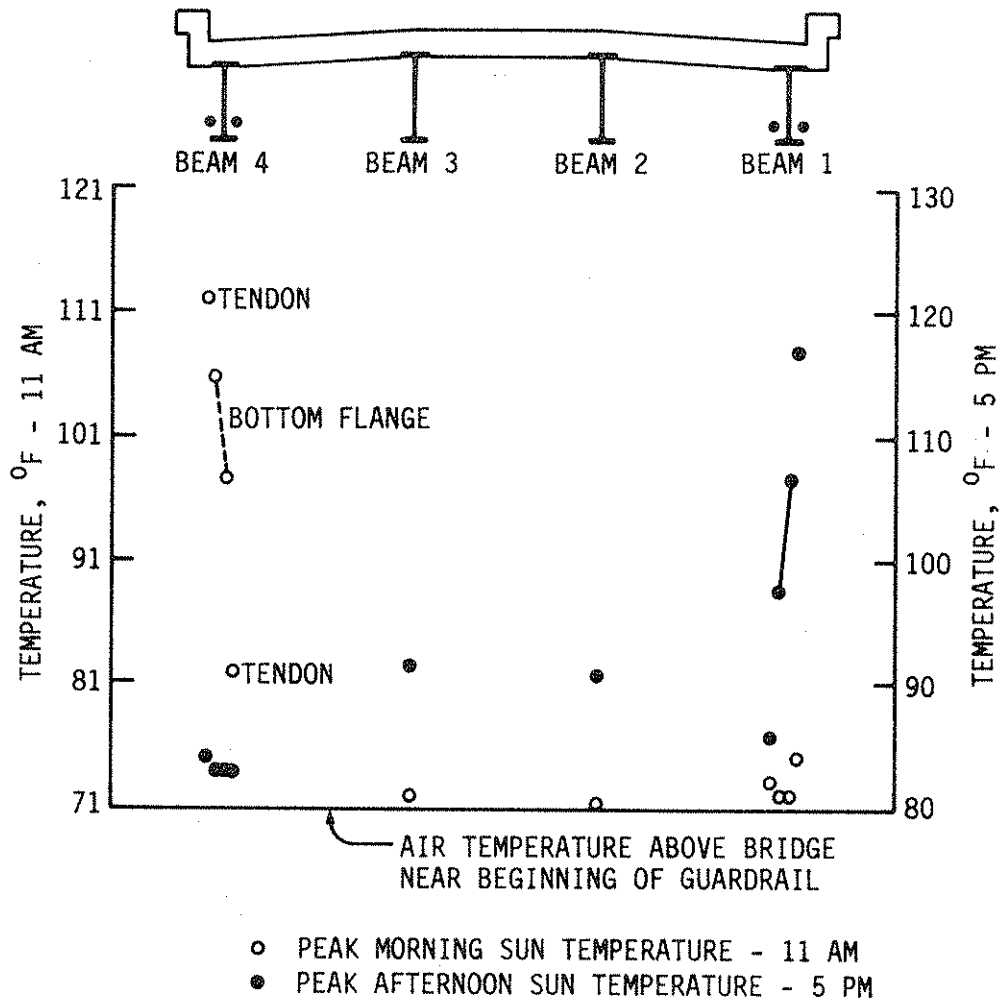


Fig. 2.27. Bridge 2 peak temperatures.

tensioning loss due to air temperature rise. Because of the limited temperature-transducer accuracy, however, this extrapolation should only be taken as the expected trend of the tendon-beam temperature differential with respect to increasing air temperatures.

This analysis was completed on the assumption that the initial temperatures of the inner and outer tendons and the beam were equal before the post-tensioning force was applied. This is reasonable if the post-tensioning occurred in a season or on a day when the solar radiation effects were minimal. If the post-tensioning was completed with temperature differentials existing between bridge members as were measured in the field tests, a loss of post-tensioning force could occur in the inner tendons as the bridge members contracted to a lower uniform temperature. However, a stress increase would occur in the outer tendons so any loss in total post-tensioning force would be minimal. Within the limits of any reasonable initial bridge member temperature, the experimental results support a conclusion that little, if any, temperature-induced loss in post-tensioning force occurs due to sun. Some loss in post-tensioning may occur because of air temperature rise, but the loss should not be as large as estimated in Phase II.

5. DEVELOPMENT OF POST-TENSIONING DESIGN MANUAL

5.1. Finite Element Model

The typical Iowa composite bridge in need of strengthening is a variably stiffened orthotropic plate and, therefore, structurally quite complex. For that reason, in examining the feasibility and in developing a design methodology for strengthening by post-tensioning, the authors have pursued a program of constructing and testing a half-size model of a composite bridge [17], developing a preliminary theoretical model [17], using the preliminary theoretical model for post-tensioning design [16], post-tensioning and monitoring two composite bridges in the field [16] and developing a final theoretical model verified by both laboratory and field data [14,15]. In developing the final model, several theories were selected and examined in detail: orthotropic plate theory, grillage theory, and finite element theory. All three theories can provide information on the flexural behavior of a composite bridge, but only finite element theory can provide information on both flexural and axial behavior of a composite bridge. In order to obtain information on the axial behavior of a bridge as well as to account for variations in construction such as coverplates, diaphragms and curbs, finite element theory was chosen for the final theoretical model.

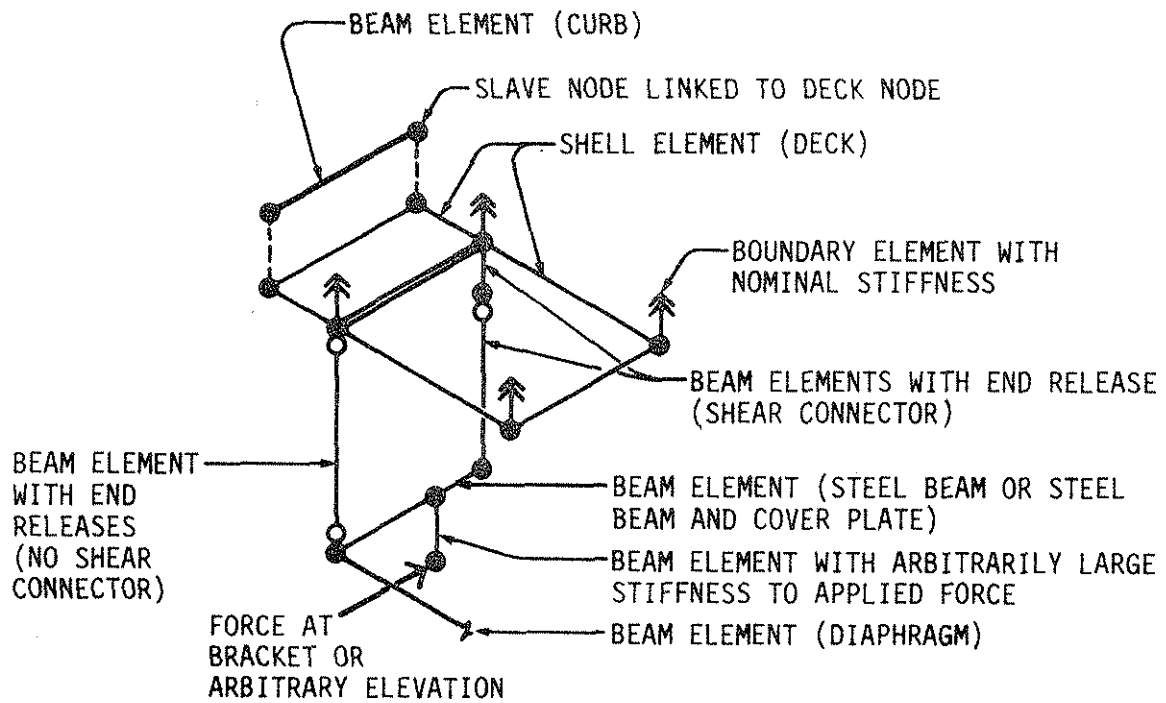
SAP IV [2], a well-known finite element program available to the authors through the Iowa State University Computation Center provided the means by which the bridge model could be assembled and analyzed. Because of the complexity of the bridge model, two preprocessing programs were written--one for a post-tensioned bridge utilizing quarter

symmetry and one for a more general, complete bridge. Several post-processing programs also were written to provide graphical verification of the finite element model and SAP IV analyses.

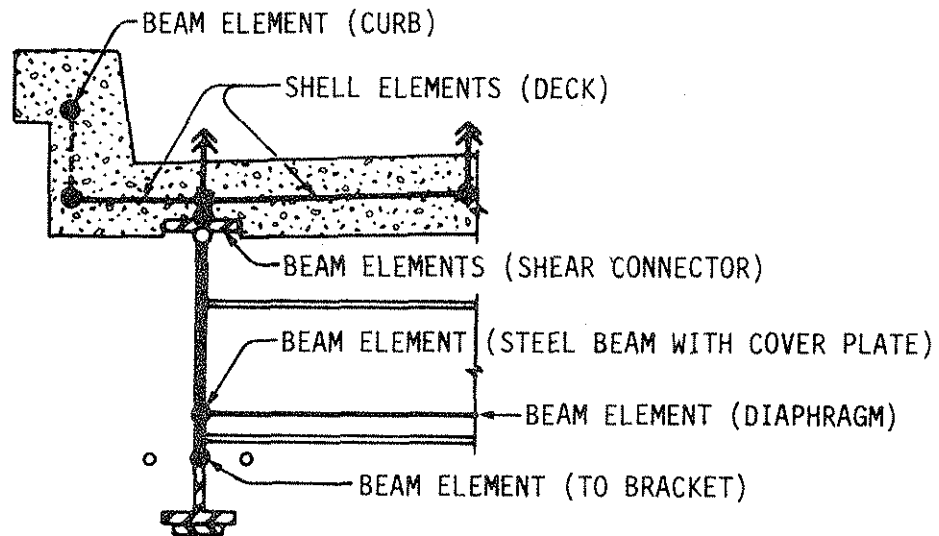
The basic finite element assembly for a composite bridge is given in Fig. 2.28. Experiments with mesh size indicated that reasonable accuracy could be achieved by dividing the concrete bridge deck into approximately 30-inch-square shell elements for right angle bridges or approximately 30-inch parallelogram shell elements for skew bridges. Deck nodes were located to coincide with steel bridge beam locations. Between the exterior beam and curb, a row of shell elements, usually long and narrow, was placed to complete the deck. Deck shell elements were given elastic properties for concrete with a 28-day strength of 3000 psi, except for verification of field or laboratory data when specific concrete properties were known. In order to avoid numerical problems with crowned decks, boundary elements with a small and arbitrary rotational stiffness were placed at deck nodes as required.

Curbs integral with the bridge deck were modeled as beam elements, approximately 30 inches long, with elastic properties based on a 28-day concrete strength of 3000 psi or a known strength. Since there is no significant slip between integral curbs and the bridge deck, curb beam nodes were linked as slave nodes to deck nodes directly below.

Each steel beam and coverplated steel beam was modeled by beam elements having elastic properties as computed for noncomposite beams. Where section properties changed because of presence or absence of a coverplate, beam elements shorter than the 30-inch deck node spacing were linked together. Elevations of the beam elements were changed to



a. Isometric view.



b. Section thru exterior bridge beam.

Fig. 2.28. SAP IV Finite Element Model.

reflect the changes in centroid elevation of the steel beam with or without a coverplate.

Rather than link the steel beam elements directly to the concrete deck shell elements by means of slave nodes, flexible beam elements were inserted for the connection in order to model shear connector slip and to obtain information regarding the forces on shear connectors. The flexible beam elements were given stiffnesses to match the load-slip characteristics of the actual shear connectors. When the shear connector location did not match the 30-inch mesh, the flexible beam link was placed at the nearest set of beam-deck nodes. The modeling error caused by the moved connector link generally had very little effect on the overall model behavior, because a change of connector stiffness generally had little effect. If no flexible beam link occurred at a set of beam-deck nodes, a spacer link without load-slip characteristics was inserted.

Initially, torsional and transverse stiffnesses of the shear connector links were made arbitrarily large, as the stiffnesses would be if slave node connections were used. The arbitrarily large stiffnesses, however, gave poor results for finite element analyses comparable to laboratory or field tests. As a result, torsional and transverse flexural stiffnesses of the steel beam web were given to the flexible and spacer beam links. Experimental and finite element results then were in excellent agreement.

In order to simplify the finite element model, beam elements used to model bridge diaphragms were attached directly to the steel bridge beam elements. The change in elevation of the diaphragm beam elements

generally was only a few inches, and the modeling error, therefore, was minimal.

For post-tensioning brackets or arbitrary elevations of force application, vertical beam elements with an arbitrarily large stiffness were attached to the steel beam elements. Except for a few experiments, the post-tensioning tendons were not included in the finite element model, since inclusion of the tendons adversely affected bandwidth, solution time, and cost.

Right angle bridges symmetrically post-tensioned can be modeled using quarter symmetry and, to reduce cost, the data for post-tensioning distribution factors were generated using the reduced model. Figure 2.29 shows a typical quarter symmetry model. The model in the figure was generated by a preprocessing program written in FORTRAN, which accepts actual bridge data and assembles the SAP IV model. The authors wrote and used a more complex but similar program to generate a full bridge model for skew bridges and asymmetrical loads.

5.2. Distribution Parameters

The experimentally verified SAP IV bridge model provided the means for studying the various parameters that could affect post-tensioning distribution. The half-size laboratory bridge model constructed by the authors was supported so as to eliminate any significant beam rotational restraint at supports. A simply supported finite element model gave stresses and deflections that were in excellent agreement with the laboratory bridge model data. Similar, simply supported finite element

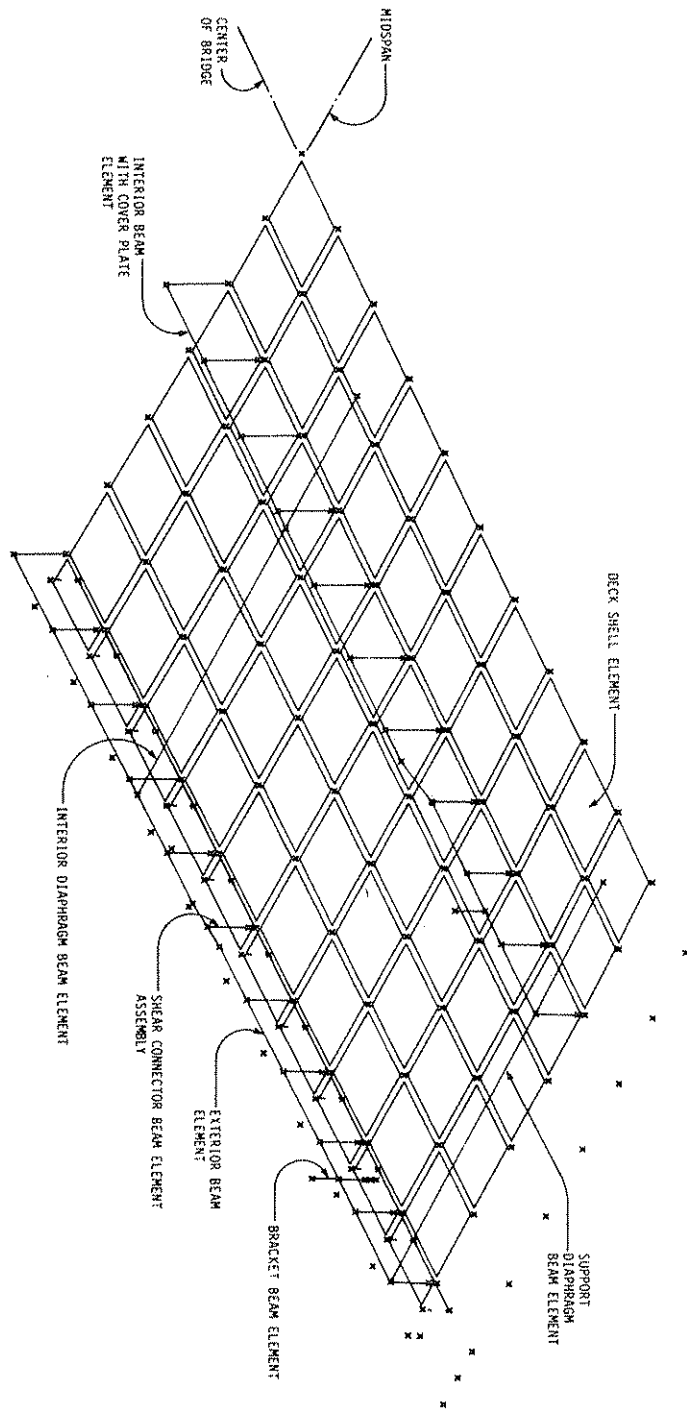


Fig. 2.29. Quarter symmetry composite bridge model.

models did not correlate as well with the composite bridges post-tensioned in the field. Stresses and deflections from simply supported and fixed beam end, finite element models did, however, bracket the field data. Furthermore, when reasonable estimates of support restraints and other restraints present in the field were included in the finite element model, the results from the finite element analysis correlated well with the field data.

Figure 2.30 illustrates the variation in post-tensioning distribution depending on end restraint for a typical composite bridge. Each exterior beam retains approximately 29% of the total post-tensioning effect under simple span conditions, approximately 31% of the effect under field conditions, and approximately 34% of the effect under fixed beam end conditions. It can be noted that the simple span distribution is conservative for the exterior beams with reference to the actual condition.

The partial beam end restraints caused by field support conditions are difficult to quantify and vary from bridge to bridge. The field end restraints generally affect both post-tensioning and live load, although not necessarily to the same degree. Since the simple span end condition is easy to apply, matches usual design practice, and is conservative with respect to the post-tensioning applied to the exterior beams, the authors chose to base all distribution factors on simple span conditions.

Experiments with the SAP IV model showed that shear connector stiffness and coverplate length had little effect on the post-tensioning distribution. Two separate finite element analyses, one

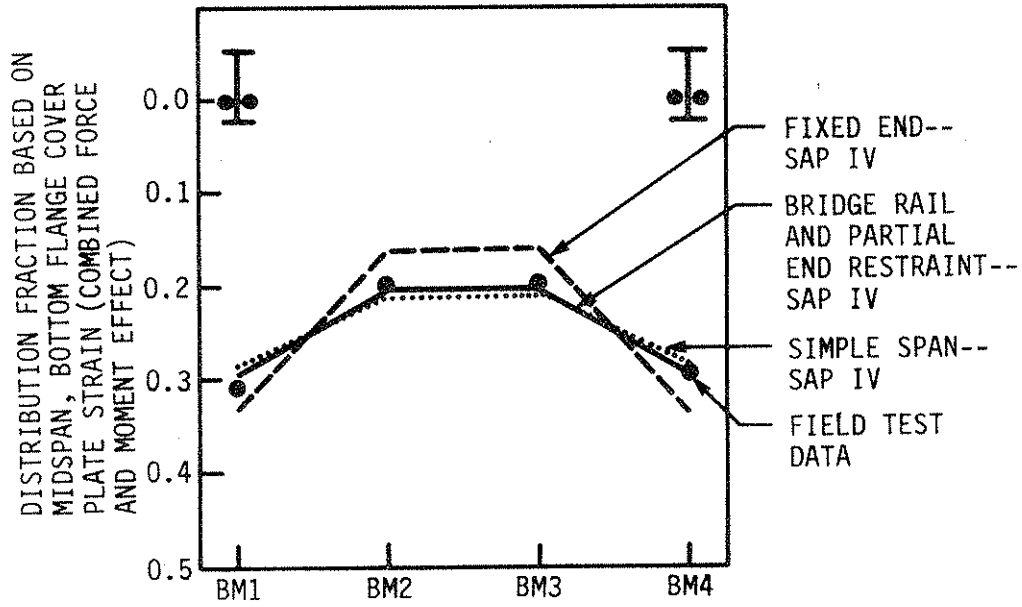


Fig. 2.30. Post-tensioning distribution for a typical eccentric force, right-angle bridge, 51.25 ft. actual span.

utilizing the test load-slip value for shear connectors and one with an arbitrarily large value, gave almost identical beam stresses and deflections. Two separate analyses, one with actual-length cover plates and one with full-length coverplates, differed very little in terms of post-tensioning distribution at midspan.

In the laboratory and field tests conducted by the authors, the post-tensioning tendons were placed above the bottom flanges of the exterior beams with clearance for the hydraulic cylinders. The tendons located in this position cause an eccentric force, which can be resolved into an axial force and a moment. The position of the tendons relative to the neutral axis of each bridge caused the axial compression stresses to be approximately one-third of the flexural compression stresses in the bottom flange coverplate. The ratio of axial to flexural compression stresses was quite consistent in the laboratory and field tests.

It became apparent, however, through experimentation with the SAP IV model, that post-tensioning forces were distributed differently from post-tensioning moments. Figure 2.31 shows the considerable difference in distribution factors depending on whether axial forces or pure moments were applied to exterior beams. The figure also shows that the force fractions and moment fractions bracket the eccentric force fractions.

Thus, in order to give the designer flexibility in choosing the elevation of the post-tensioning tendons, the authors chose to develop two sets of distribution factors: one for axial force and one for moment. Definition of an axial force for purposes of determining dis-

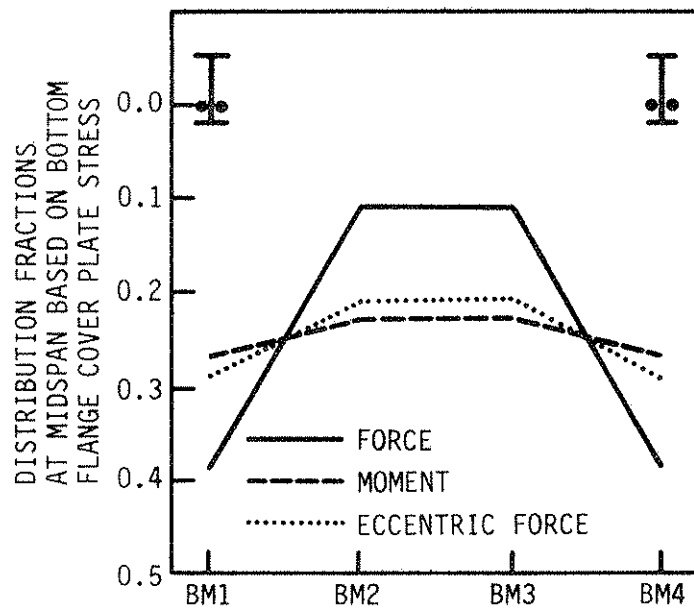


Fig. 2.31. Force, eccentric force and moment distribution for a right-angle bridge, 51.25 ft. actual span.

tribution was subject to judgment. Because of varying, partial-length coverplates and other factors, no elevation of post-tensioning force would give a purely undeflected deck surface or purely axial forces in the bridge beams at midspan. For development of the force distribution factors, the authors defined an axial force as a force placed at the elevation of the midspan bridge centroid and based the distribution factors on the forces in the steel beam elements at midspan.

Several other parameters were examined through use of the SAP IV model. Figure 2.32 shows the effects on moment distribution due to change in bridge span, change in bracket location on a given span, change in relative beam stiffness for approximately equal spans and change in skew for a given span. The greatest change in post-tensioning moment distribution occurs because of change in span length. As Fig. 2.32a shows, the greater the bridge span (for proportionally constant bracket locations), the more the applied moments are distributed away from the exterior beams. Given a constant span as in Fig. 2.32b, as the brackets are moved toward the supports, more moment is distributed away from the exterior beams. The distribution, then, appears to be highly dependent on the length of the post-tensioned region or the distance between anchorages.

Relative beam stiffness has the expected effect. Stiffer beams retain more post-tensioning as shown in Fig. 2.32c. The bridge with all steel beams of equal stiffness [4] retained more of the post-tensioning moment on the exterior beams than the bridge with exterior beams of smaller stiffness. Moment distribution is, therefore, dependent on relative beam stiffnesses.

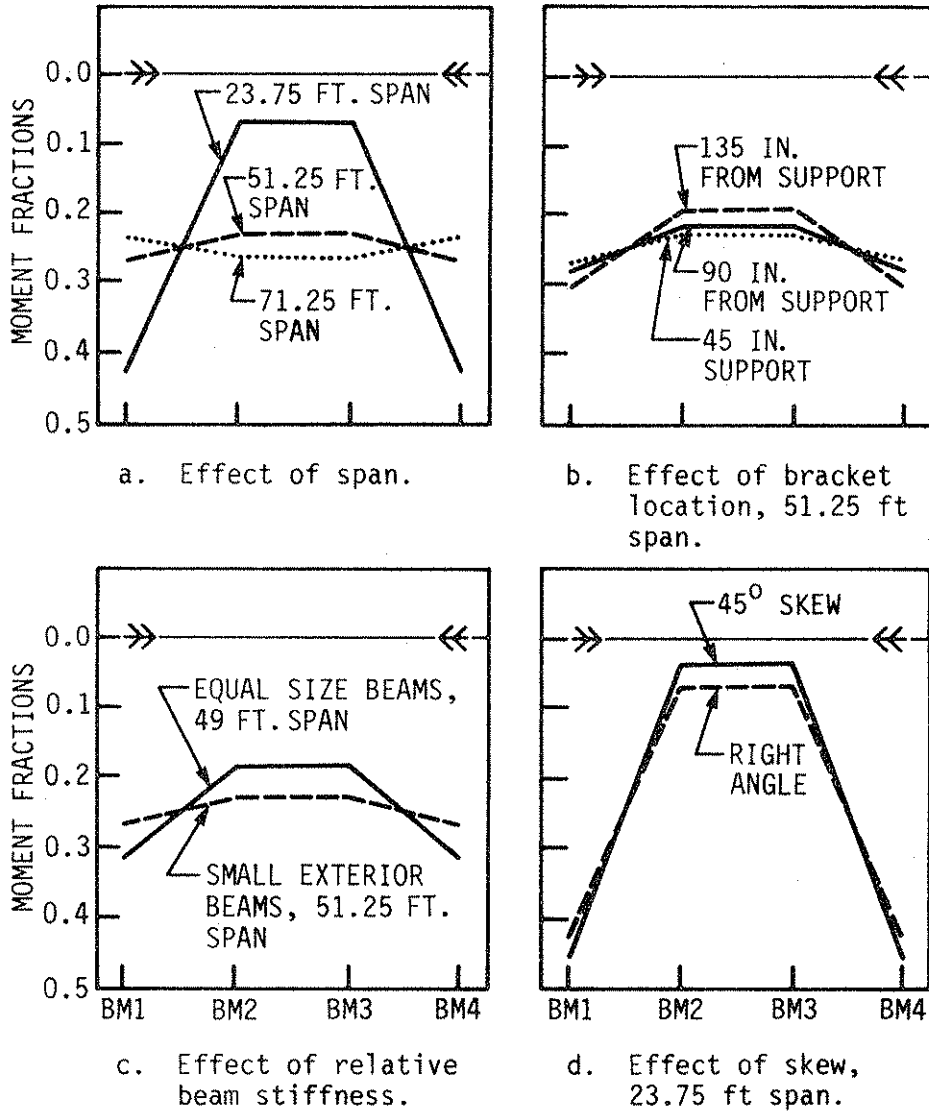


Fig. 2.32. Effects of several parameters on moment distribution.

Skew had an unexpectedly small effect on moment distribution at midspan. Skew tends to add end restraint to bridge beams, and the effect shown in Fig. 2.30 for simple span vs. fixed end conditions is shown again in Fig. 2.32d for the end restraint caused by skew. The maximum effect of skew on moment distribution occurs for short spans, such as the 23.75 ft span in Fig. 2.32d. Because the effect of skew is relatively small at the usual spans for the Iowa composite bridges in need of strengthening, and because neglecting the skew gives conservative moment distribution factors for exterior beams, the authors recommend neglecting the effects of skew for skews of 45° or less.

5.3. Force and Moment Distribution Fractions

The SAP IV model described in Section 5.1 is a general, theoretical model adaptable to a wide variety of composite bridges. However, because of complexity, cost, and lack of availability the model generally would have little practical application. For that reason the authors have developed a simplified design methodology based on midspan distribution fraction formulas derived from a multiple linear regression analysis of the finite element results.

In order for the regression formulas to be applicable to a range of Iowa composite bridges, the authors applied the SAP IV model to several Iowa DOT standard bridge series and several individually designed Iowa composite bridges. The V9, V11, V13, and V15 series for one-lane, three-beam bridges and two-lane, four-beam bridges were included in the data on which the distribution fractions are based.

The SAP IV model experiments reviewed in Section 5.2 provided the basis for choosing potential regression variables. The length of the post-tensioned region, known to be significant, was included in the regression variables as SPANB, the length of the tendons between brackets, and also in AR, an aspect ratio computed from the deck width and SPANB. Relative stiffness of the exterior beams, also known to be significant, was included as IET, the ratio of the total exterior beam stiffness to the total stiffness of the bridge. Because axial stress is dependent on cross-section area, a similar variable, AET, the ratio of the total exterior beam area to the total bridge cross section area, was added to the regression variables.

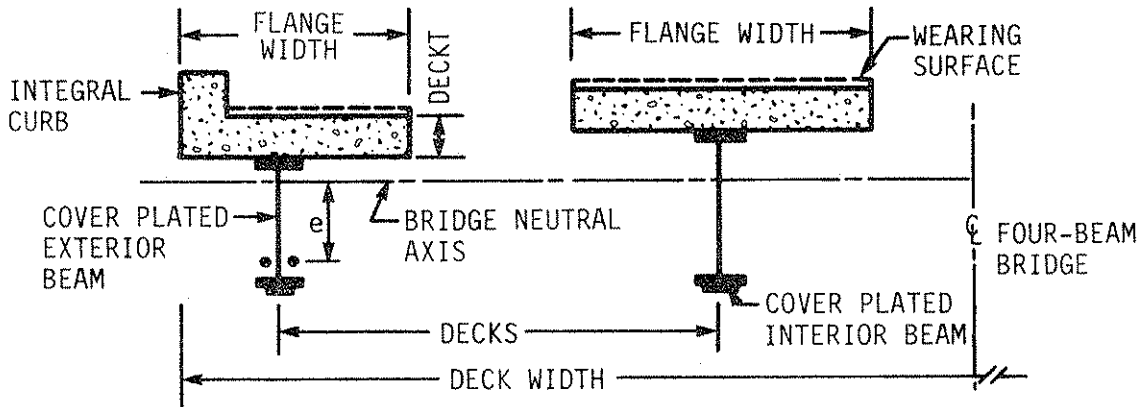
The transverse stiffness of the bridge deck could be expected to affect the post-tensioning distribution. Therefore, DECKT, the deck thickness, and DECKS, the deck span, were identified as potentially significant and were used in the regression analysis individually and in various ratios. Preliminary distribution factors, for design of the field bridge strengthening [16], were computed from orthotropic plate theory. Hence, the orthotropic plate parameter THETA, the flexural parameter and ALPHA, the torsional parameter, were added to the list of potential regression variables. In the event that exterior beam coverplate length had a secondary effect, it was included in a ratio, CPRAT.

All of the potential regression variables listed above were computed for the Iowa DOT standard and individually-designed composite bridges. From those values and the distribution factors computed from the SAP IV model analyses--FF, the midspan force fraction and MF, the

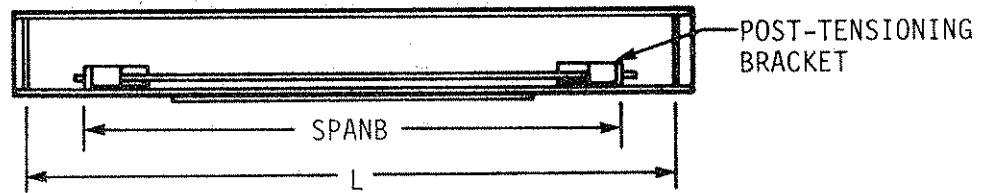
midspan moment fraction--complete data sets for three-beam and four-beam bridges were assembled.

The actual regression analyses was performed by means of SAS, Statistical Analysis System [25], available through the Iowa State University Computation Center. Because the form of an appropriate regression equation was unknown, many experiments with linear, product, logarithmic, and exponential terms were tried. The most effective technique for developing the form of a suitable regression equation proved to be the transformation of variables with a ladder of powers as described in Ref. 6. Variables with the better coefficients of determination were reexpressed in different power forms to linearize the variable in relation to a distribution fraction. Then, sufficient reexpressed variables were included to obtain regression equations with coefficients of determination of 0.95 or greater. A certain amount of engineering judgment was applied in order to keep the formulas as consistent as possible.

The final regression variables are given in Fig. 2.33, and the final regression formulas for distribution factors are given in Fig. 2.34. The variables most related to the distribution factors proved to be the aspect ratio accounting for the post-tensioned region length, relative beam stiffness, deck thickness and span, and the orthotropic plate flexural parameter. The coefficients of determination for the formulas indicate that the moment fraction formulas are more accurate. In most instances, the stresses due to post-tensioning moment will be larger, and thus the better accuracy for the moment fraction equations is desirable.



a. Idealized bridge cross section.



b. Idealized exterior beam.

i = UNIT, AVERAGE LONGITUDINAL FLEXURAL STIFFNESS
 = TOTAL I FOR ALL COMPOSITE, COVER PLATED BEAMS
 ÷ DECK WIDTH

j = UNIT, AVERAGE TRANSVERSE FLEXURAL STIFFNESS,
 INCLUDING INTERIOR DIAPHRAGMS

$$AR = \text{ASPECT RATIO} = \frac{\text{DECK WIDTH}}{\text{SPANB}}$$

$$IET = \frac{I \text{ FOR EXTERIOR COMPOSITE, COVERPLATED BEAMS}}{I \text{ FOR ALL COMPOSITE, COVERPLATED BEAMS}}$$

$$\text{THETA} = \frac{\text{DECK WIDTH}/2}{L} \sqrt[4]{i/j}$$

NOTE THAT ALL SECTION PROPERTIES COMPUTED FOR THE LONGITUDINAL DIRECTION ARE WITH RESPECT TO THE BRIDGE NEUTRAL AXIS.

Fig. 2.33. Regression formula variables.

THREE-BEAM BRIDGES

$$FF = 0.741 - 0.175 \frac{1}{\sqrt{\text{THETA}}} - 0.0624 \frac{1}{\sqrt{\text{AR}}}$$

$$R^2 = 0.986, \text{ ERROR RANGE } +2\%, -3\%$$

$$MF = 0.816 - 0.245 \frac{1}{\sqrt{\text{IET}}} - 0.0755 \frac{1}{\sqrt{\text{AR}}}$$

$$R^2 = 0.991, \text{ ERROR RANGE } +2\%, -2\%$$

RANGES OF REGRESSION	$0.417 \leq \text{THETA} \leq 0.893$
VARIABLES:	$0.456 \leq \text{IET} \leq 0.571$
	$0.306 \leq \text{AR} \leq 1.544$

FOUR-BEAM BRIDGES

$$FF = 0.605 - 0.323 \frac{1}{\sqrt{\text{THETA}}} - 0.0720 \frac{1}{\sqrt{\text{AR}}} + 3.87 \frac{\text{DECKT}}{\text{DECKS}}$$

$$R^2 = 0.954, \text{ ERROR RANGE } +9\%, -6\%$$

$$MF = 0.963 - 0.221 \frac{1}{\sqrt{\text{IET}}} - 0.145 \frac{1}{\sqrt{\text{AR}}} - 2.18 \frac{\text{DECKT}}{\text{DECKS}}$$

$$R^2 = 0.983, \text{ ERROR RANGE } +4\%, -7\%$$

RANGES OF REGRESSION	$0.516 \leq \text{THETA} \leq 1.329$
VARIABLES:	$0.379 \leq \text{IET} \leq 0.600$
	$0.361 \leq \text{AR} \leq 2.246$
	$6.25 \leq \text{DECKT} \leq 8.00$
	$92.00 \leq \text{DECKS} \leq 116.25$

NOTE THAT NEGATIVE ERROR RANGE INDICATES THAT
SAP IV RESULT IS LESS THAN REGRESSION FORMULA-
PREDICTED RESULT

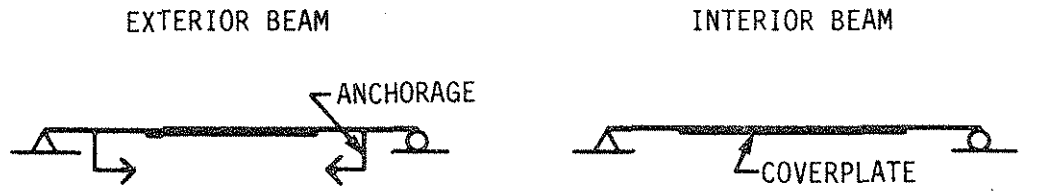
Fig. 2.34. Regression formulas for force and moment fractions.

The force and moment fractions computed by the regression formulas apply at midspan but not at other locations on the span. At midspan, the minimum amount of post-tensioning is retained by the post-tensioned exterior beams, but almost all of the post-tensioning is retained by the exterior beams at the anchorages.

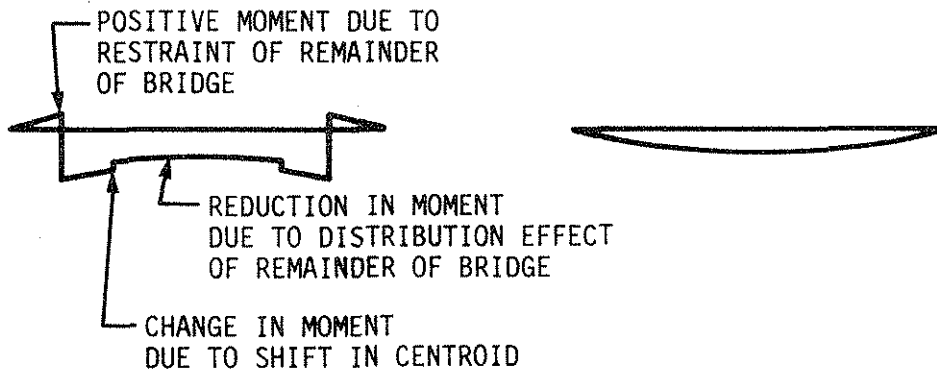
The general distribution of moment (which is similar to the distribution of axial force) is illustrated in Fig. 2.35. The moment applied to the idealized exterior beam in Fig. 2.35a does not remain constant on the span. The moment varies for two reasons: the cover plate on the exterior beam causes a downward shift in neutral axis, thereby reducing the eccentricity of the applied post-tensioning force, and the stiffness of the remainder of the bridge causes moment to be gradually shifted away from the exterior beam to the interior beam. Thus, the moment diagram in Fig. 2.35b shows maximum moments at the anchorages of the exterior beam and gradually reduced moments toward midspan.

In order to account for the change in force and moment distribution fractions for design purposes, the linear interpolation illustrated in Fig. 2.35c is recommended. Because the beam supports are used for known distribution fractions, the anchorage locations are independent of the interpolation, which is an advantage during the design process. Using the supports for the known points also partially accounts for the small positive moments between anchorages and supports.

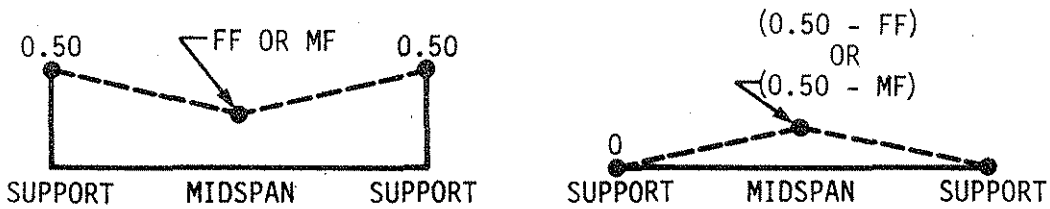
In order to give some indication of the accuracy of the distribution factors computed from the regression formulas and the interpolation procedure, the stresses computed from the SAP IV model and the



a. Idealized post-tensioned beams.



b. Moment diagrams.



c. Recommended linear interpolation

FF = force fraction from regression formula
 MF = moment fraction from regression formula

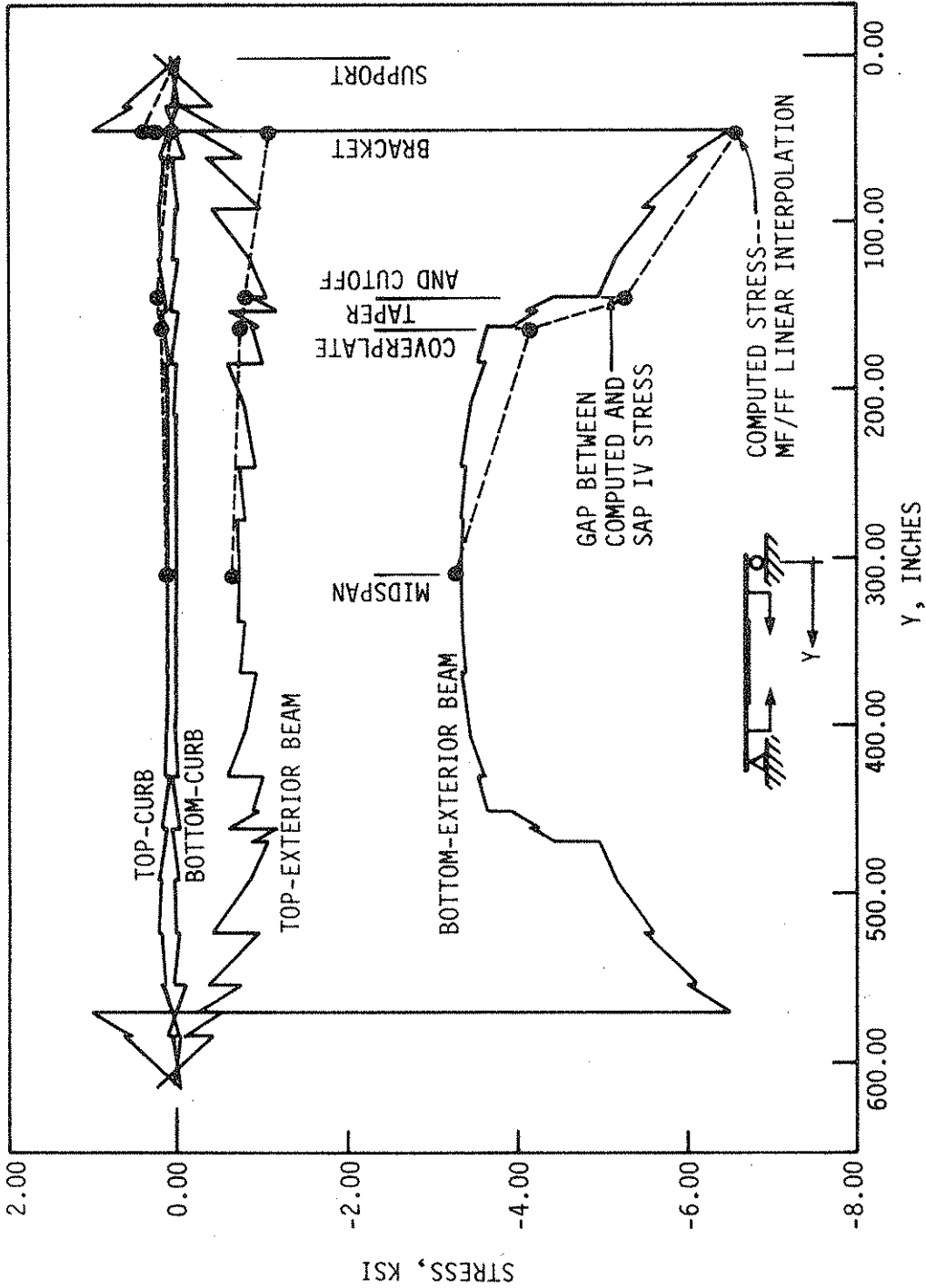
Fig. 2.35. Post-tensioning distribution and interpolation.

formulas and interpolation are compared in Fig. 2.36. The exterior beam stresses in Fig. 2.36a and interior beam stresses in Fig. 2.36b are for a 51.25-foot-span, four-beam bridge post-tensioned with an arbitrary force of 100 kips at 3 1/4 inches above the bottom flanges of each exterior beam. The jagged nature of the SAP IV stress lines is due to the nature of finite element analysis and gives some indication of the accuracy of the analysis. As the graphs for the exterior and interior beams indicate, the stresses from the SAP IV model and the regression formulas are in excellent agreement at midspan. There is good agreement at coverplate cutoffs but, for exterior beams, the interpolation procedure gives stresses unconservative by about 10%. At the brackets, the SAP IV model and interpolated stresses again are in excellent agreement. In general, the regression formula distribution factors and interpolation procedure give stresses that agree very well at critical points on the bridge span.

5.4. Ultimate Strength Tests

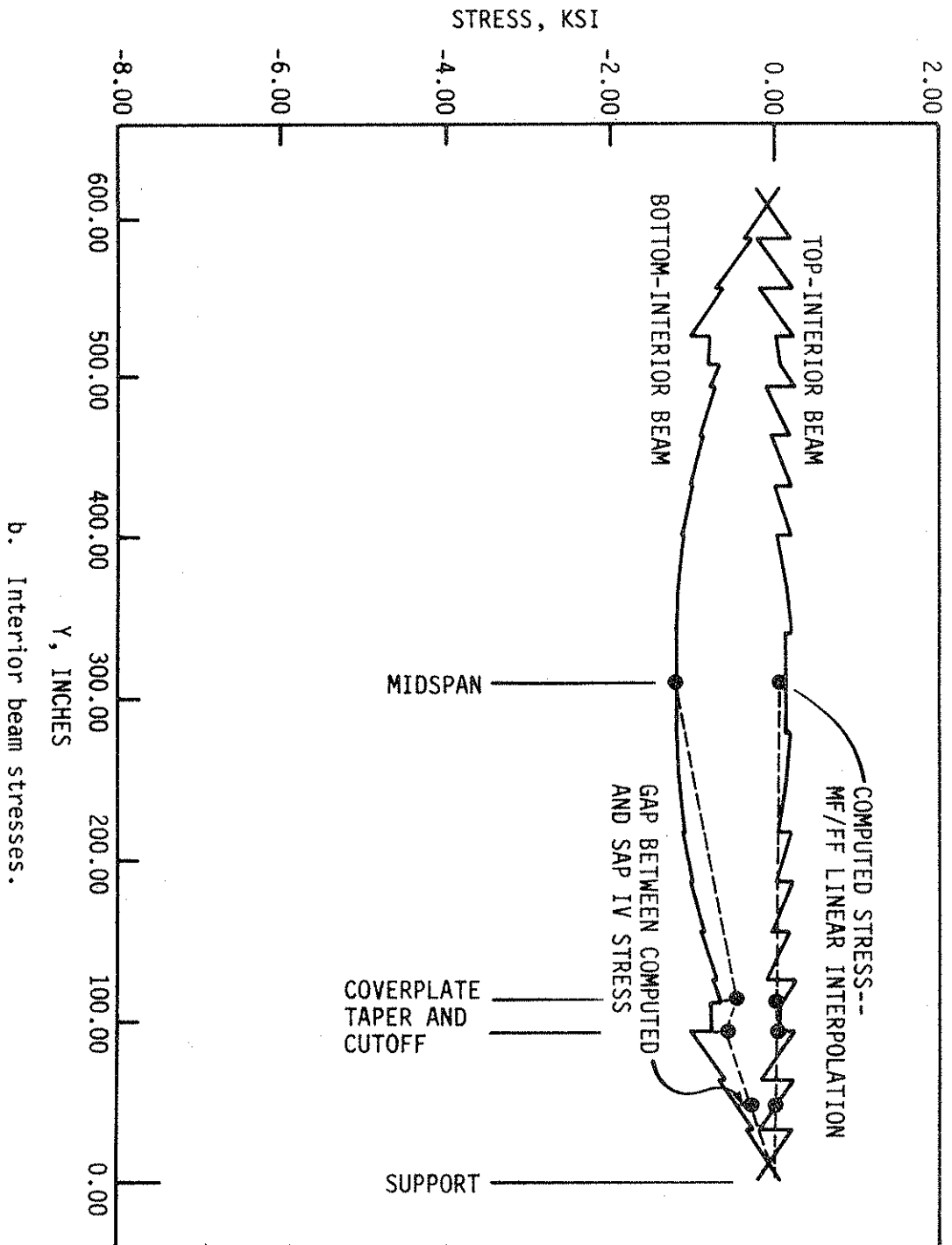
As demonstrated in Section 5.3, post-tensioning can induce compression stresses in the tension stress region of the steel beams in a composite bridge. The final result is to increase the capacity of a bridge according to allowable stress design criteria. The question remains, however, as to whether post-tensioning will increase the ultimate strength of a bridge significantly.

To the authors' knowledge, there have been no tests to failure of complete bridges strengthened by post-tensioning. There have been



a. Exterior beam and curb stress.

Fig. 2.36. Post-tensioning stresses for 51.25 ft span, 4-Beam Bridge, 100k applied 3 1/4 in. above bottom flange, each exterior beam.



several tests to failure of post-tensioned composite beams, however. At Rice University, Stras [27] constructed and tested three beams of the configuration shown in Fig. 2.37. The post-tensioning cable for each beam was placed below the bottom flange and restrained to remain in position with respect to the bottom flange. Shear connectors were oversized but provided stiffening for the top flange of the beam, which was a noncompact section. All failures occurred because of crushing of the concrete slab. The test results raised the question of whether the post-tensioning force in the cable existed at the beginning of the test or whether the beam simply was restrained by the cable.

Recently, at Iowa State University, Dedic tested four post-tensioned composite beams cut from the half-size bridge model constructed in the ISU Structural Research Laboratory (Figures 8-10, 23-26, 40-46 and Tables 2-6 and 13 of Ref. 16). Each beam was post-tensioned with threaded bars of a length less than the span and placed above the bottom flange of the beam. Each beam was coverplated over a region in the central portion of the beam. Two of the beams, modeling exterior beams of the type in the understrength Iowa bridges, had curbs. One exterior beam, Beam 1, and one interior beam, Beam 2, had inadequate shear connectors to simulate the existing bridge conditions. The remaining two beams, the second interior beam, Beam 3, and the second exterior beam, Beam 4, had additional double-nutted, high-strength, steel-bolt shear connectors to simulate a strengthened condition. Although the additional connectors were intended to simulate a full shear connection for a bridge design condition, the connection would be defined as a partial connection because of the place-

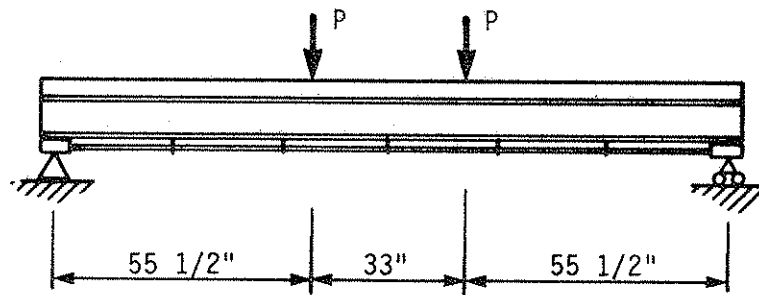
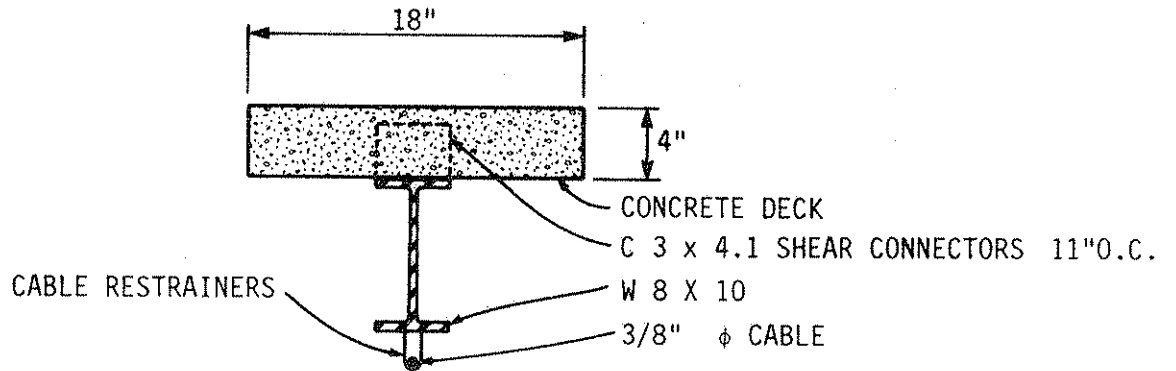


Fig. 2.37. Post-tensioned composite beams (Stras).

ment of the test loads 40 inches each side of midspan. Failure modes included shear connection and apparent yielding for Beams 1 and 2, respectively, and concrete slab crushing for Beams 3 and 4.

Both Stras [27] and Reagan [24] developed analytical, computerized models for elastic and inelastic performance of the three beams tested at Rice. Reagan extended his analysis to typical bridge and building beams. Neither analysis method is convenient to use for determining the strength of a post-tensioned beam during design; therefore, a relatively simple analytical model that can be used with hand computations, refined from the analytical model used by Dedic (Table 13, Ref. 16) has been developed.

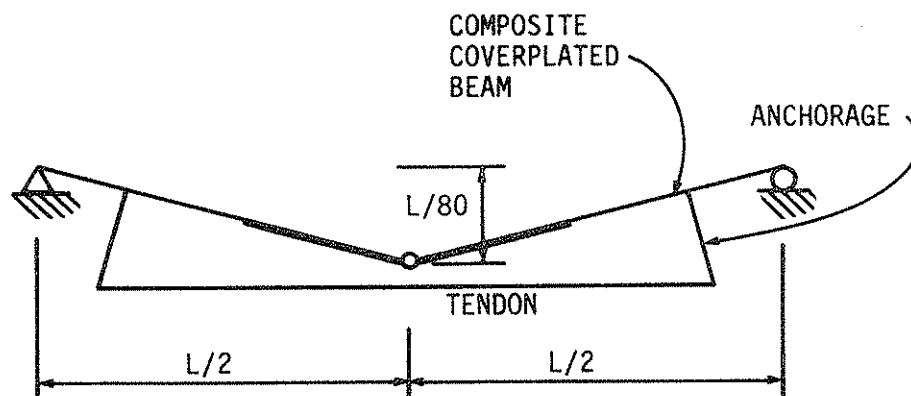
5.5. Analytical Strength Model

A flexural strength model for a post-tensioned composite beam should account for the following types of behavior: steel-concrete composite action, partial shear connection, partial prestress, and unbonded tendons. Some of the behavior can be included in a correct model of the failure mechanism for the beam; the remaining behavior is covered by the AASHTO load factor design rules [1].

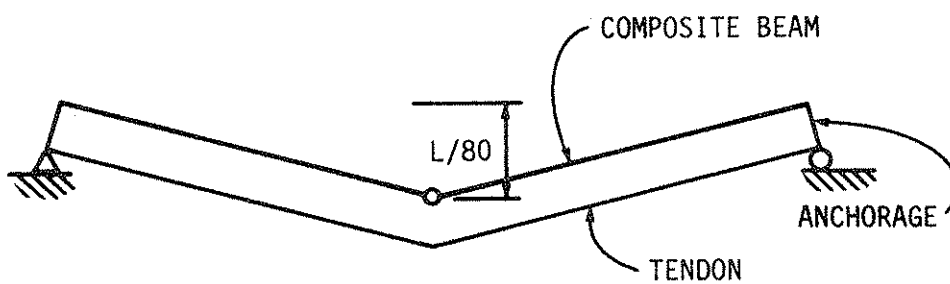
The analytical model proposed is based on the following principles and assumptions:

1. Except for beams with a partial shear connection, the failure mode for beams tested to failure has been crushing of the concrete slab at or near midspan. Therefore, it is reasonable to consider the post-tensioned composite beam behavior to be similar to a beam with a plastic hinge at midspan.

2. The average midspan deflection of the seven Stras and Dedic beams at failure was $L/79$, and the average midspan deflection for the nine beams including two Reagan analytical beams was also $L/79$. For purposes of the deflection at the plastic hinge, the deflection can be taken as approximately $L/80$.
3. The effective beam flange width can be determined according to Ref. 1, Section 10.38.3 (the AASHTO rules for load factor design).
4. The compressive force in the slab can be determined according to Ref. 1, Section 10.50. The AASHTO rules account for slab reinforcing (unlike service load design), relative capacity of concrete slab vs. steel beam, and partial or full shear connection.
5. Tendon strain can be determined from an idealized beam configuration as illustrated in Fig. 2.38. In Fig. 2.38a, in the idealized beam which represents the beams tested by Dedic, the tendon is permitted to rise, and the change in elevation is included in the computations for flexural strength. In the Stras and Reagan beams, the tendon was not permitted to rise, and the tendon strain can be computed from the idealized beam in Fig. 2.38b.
6. Tendon force can be computed from an idealized stress-strain curve for the tendon steel.
7. Shear connector capacities can be computed from the formulas given in Ref. 1, Section 10.38. (For the Dedic beams, the angle plus bar shear connector capacity was based on tests and a modified AASHTO channel connector formula [16].)



a. Dedic beams.



b. Stras and Reagan beams.

Fig. 2.38. Failure mechanism--Idealized post-tensioned composite beams.

The principles and assumptions given above were applied to the average of the Stras beams, two Reagan analytical beams (one of which was a Stras beam) and the four Dedic beams. Results and comparisons for the midspan deflection at failure, change in tendon force, and flexural strengths are given in Table 8. Also given are the moments computed for the beams without post-tensioning.

The largest difference between experimental and computed values in the table is for the midspan deflection values. The actual deflection at failure is often difficult to determine accurately and, in the table, the actual deflection is being compared with an average deflection; therefore, some difference can be expected.

The computed change in tendon force agrees within 12%, and the computed flexural strength agrees within 7% of experimental values or Reagan computed values. In general, the proposed analytical model for computing the flexural strength underestimates the change in tendon force and slightly overestimates the flexural strength. The model is quite accurate considering the variation in tendon type and placement, the variation in beam cross section and the variation in shear connection.

The last column in Table 8 gives the comparison of flexural strength between the post-tensioned and non-post-tensioned conditions. The increase in strength due to post-tensioning varies from 8% to 34%. For exterior beams--Beams 1 and 4, similar to those to be post-tensioned on the Iowa composite bridges--the increase averages 10%. This increase is less than the capacity increase based on service load design, yet still is significant.

Table 8. Comparison of experimental and computed strength.

Author/ Test or Computation	δ_{pe} (inches)	$\delta_{pc} =$ $L/80$ (inches)	$\frac{\delta_{pe}}{\delta_{pc}}$	Δf_{pe} (kips)	ΔT_{pc} (kips)	$\frac{\Delta T_{pe}}{\Delta T_{pc}}$	$M_{u_{pe}}$ (inch-kips)	$M_{u_{pc}}$ (inch-kips)	$\frac{M_{u_{pe}}}{M_{u_{pc}}}$	M_{u_c} (inch-kips)	$\frac{M_u}{M_{u_c}}$ $\frac{pc}{c}$
Stras/avg* of 3 tests post-tensioned	1.90	1.80	1.06	8.99	8.04	1.12	1078	1126	0.96	948	1.19
Stras/avg* of 3 tests restrained	1.90	1.80	1.06	8.99	8.19	1.10	1078	1037	1.04	948	1.09
Reagan (Stras beam)/ computed	1.80	1.80	1.00	8.38	8.04	1.04	1073	1126	0.95	948	1.19
Reagan PH3 computed	12.50	11.85	1.06	97.47	91.67	1.06	42591	42472	1.00	31650	1.34
Dedic/ Beam 1 test	3.57	3.84	0.93	-	35.39	-	4140	4176	0.99	3876	1.08
Dedic/ Beam 4 test	3.36	3.84	0.87	28.83	31.25	0.92	4503	4530	0.99	4036	1.12
Dedic/ Beam 2 test	3.38	3.84	0.88	-	28.04	-	5813	6269	0.93	5561	1.13
Dedic/ Beam 3 test	≤ 5.56	3.84	≤ 1.45	-	27.19	-	6102	6359	0.96	5635	1.13

δ = midspan deflection at ultimate load
 ΔT = increase in post-tensioning force after post-tensioning
 M_u = flexural strength
 *Tests were conducted with loss of prestress. Computations are for extreme conditions: full prestress and no prestress.

subscripts: e = experimental or analysis value by others
 c = computed value, proposed analysis method
 p = post-tensioned

The analytical model described above is accurate for isolated post-tensioned composite beams but does not account for the restraints and load redistribution mechanisms that affect the beam when it is part of a bridge. The authors have done no studies of the post-tensioning distribution at ultimate load and know of no published studies on the subject. The distribution at ultimate load must either be inferred from studies of load distribution at ultimate load or left to the judgment of the designer if the analytical model is to be used with load factor design for a bridge.

6. SUMMARY, CONCLUSIONS, AND RECOMMENDATIONS

6.1. Summary

This report summarizes the work that has been done in Phase III of this study. The work completed during Phases I and II of this investigation has been presented in Refs. 17 and 16. The design manual that was completed during this phase of the investigation (and is briefly discussed later in this section) is Ref. 15. This phase of the study had several specific tasks; the accomplishment of these is presented in the following paragraphs.

For measurement of forces in the tendons used for applying the post-tensioning forces and for measurement of strains in the beams, transducers were designed and fabricated. Ten transducers were fabricated and calibrated for strain measurement, and ten were fabricated for force measurement. The strain transducers were easy to apply in the field and had accuracy of approximately $\pm 3\%$. On the other hand, the force transducers were somewhat difficult to attach and had accuracy of $\pm 5\%$. Both types of transducers--force and strain--can be utilized with either conventional portable strain indicators or data acquisition systems.

Both bridges strengthened during Phase II of the study were inspected every three months; no noticeable changes in appearance or behavior were noted except for some cracks in the abutments of Bridge 1 and the resurfacing of Bridge 2 during Summer 1983. Both bridges were retested during this phase of the study. End restraint was measured on both bridges and found to be of significant magnitude. The end

restraint affected both post-tensioning loading and vertical loading; thus, the effect on both essentially compensated each other. No significant differences in behavior were noted when the bridges were retested from behavior determined during their initial testing in Phase II. Releasing the post-tensioning forces on the bridges revealed that Bridges 1 and 2 had 5.5% and 11.2% less force respectively than that initially applied. The loss on Bridge 1 is thought to be primarily the result of relaxation of some of the end restraint present. The loss in Bridge 2 is thought to be primarily due to the resurfacing during Summer 1983: dead load was removed and net section reduced without removing post-tensioning force.

The question as to loss of post-tensioning force because of differences in temperature due to sun and shading (and thus differences in expansion) between the tendons and beams was resolved. Temperature data was collected on Bridge 2. Although the exterior tendons (those located on the outside of the exterior beams) did increase in temperature more than the beams, the interior tendons (those located on the inside of the exterior beams) were always shaded from the sun and thus were always cooler than the beams. The net effect was a slight increase in the post-tensioning force due to the temperature differential between the tendons and the beams.

A SAP IV finite element model in either quarter symmetry or complete form correlated well with the half-scale laboratory bridge data previously obtained by the authors. Due to guard rails and end restraint in Bridges 1 and 2, the SAP IV model in a simplified form gave results that differed from field data. When the SAP IV model

was used to analyze the bridges assuming fixed beam ends, the finite element analyses fell above and below the field data, thereby indicating that Bridges 1 and 2 were subject to a certain amount of restraint.

Because post-tensioning tendons typically are located eccentrically with respect to the bridge neutral axis, the post-tensioning produces both axial force and moment. In order to determine the post-tensioning distribution most accurately, both axial force and moment distribution fractions are required. Those fractions were determined for typical Iowa three-beam and four-beam composite bridges from a series of SAP IV analyses. By means of multiple linear regression, simple formulas for the fractions were obtained for the typical bridges. Parameters that proved to be the most significant for post-tensioning distribution are an aspect ratio computed from the deck width and distance between tendon anchorages, deck thickness and span between beams, relative stiffness of exterior, post-tensioned beams, and the orthotropic plate flexural parameter for the bridge. Skew had an unexpectedly small effect and therefore may be neglected if it is 45° or less. The axial force and moment fractions at midspan can be used with linear interpolation to determine the approximate post-tensioning distribution at any location on the bridge span.

Post-tensioning does add to the flexural strength of a composite bridge but adds less to ultimate strength than to service load capacity. The increase in ultimate strength for an isolated composite beam can be computed easily from a simple beam with a plastic hinge at midspan, if AASHTO rules for flange width and compression force under load factor

design are followed. The analytical ultimate strength model accurately predicts the strength of the isolated beam but not the strength of a beam in a bridge when not all beams are post-tensioned. The post-tensioning distribution at ultimate load was not determined as part of this project and is not available in the literature to the authors' knowledge.

6.2. Conclusions and Recommendations

The following conclusions and recommendations were developed as a result of this study:

1. Strengthening of single-span composite concrete deck steel beam bridges by post-tensioning has been found (during more than four years of research) to be a viable, economical strengthening technique. Utilizing the design methodology presented in Ref. 15, the required force can be determined relatively easily. Assuming the use of bolted connections, the system can be installed by normal maintenance crews.
2. Behavior of both bridges was similar to the behavior observed from the bridges during field tests conducted under Phase II.
3. The strain transducers were very accurate at measuring mid-span strain. The system was easily attached to the steel beam flange. Associated recording equipment was simple to operate.
4. The force transducers gave excellent results when tested under laboratory conditions but were found to be less effective when used in actual bridge tests.

5. Loss of post-tensioning force due to temperature effects in any particular steel beam-post-tensioning tendon system were found to be small. For sunlit beams a loss of force in a tendon on one side of the beam was offset by a gain in force by the tendon on the other side of the beam; thus, the net effect was a small increase in the post-tensioning force. Air temperature rises do cause loss of post-tensioning force, but based on several tests, the losses should be small.
6. Loss of post-tensioning force over a two-year period was minimal. Any major bridge deck repair (such as that conducted on Bridge 2 during Summer 1983) does adversely affect the total post-tensioning force. Post-tensioning force should be removed and then reapplied after repairs are completed.
7. Significant end restraint was measured in both bridges; this restraint is caused primarily by reinforcing steel being continuous from the deck into the abutments. This end restraint reduced the effectiveness of the post-tensioning but also reduced midspan strains due to truck loadings.
8. The SAP IV finite element model is capable of accurately modeling the behavior of a post-tensioned bridge, if guard rails and end restraints are included in the model. If restraints are neglected, as in usual practice, the finite element model gives approximately correct results.

9. Post-tensioning distribution should be separated into distributions for the axial force and moment components of an eccentric post-tensioning force.
10. Skews of 45° or less have a minor influence on post-tensioning distribution. Skews greater than 45° require further study. Parameters which have major influence are the aspect ratio of the post-tensioned region, the deck thickness and span between beams, relative stiffness of the post-tensioned exterior beams, and the orthotropic plate flexural parameter for the bridge.
11. For typical Iowa three-beam and four-beam composite bridges, simple regression-derived formulas for force and moment fractions can be used to estimate post-tensioning distribution at midspan. At locations other than midspan, a simple linear interpolation gives approximately correct results.
12. A simple analytical model can accurately estimate the flexural strength of an isolated post-tensioned composite beam. The distribution of the post-tensioning among the bridge beams at ultimate load remains to be determined, however.

7. RECOMMENDED CONTINUED STUDIES

On the basis of the literature reviewed and the work completed in the three phases of this study the following areas would be logical for continuation of the strengthening work:

1. The concept of utilizing the post-tensioning tendons in a "king-post" arrangement rather than straight should be investigated. The "king-post" arrangement has the advantage of providing a vertical lift component as well as making possible the required jacking operation from the top of the bridge rather than under it.
2. Post-tensioning strengthening has successfully been applied to single-span bridges and a design methodology developed for its implementation. As there are several continuous bridges that also require strengthening, the problems associated with using post-tensioning for strengthening in the positive and negative moment regions should be investigated.
3. As there are no data available on the effects of dynamic loading on the post-tension strengthened beams or on the fatigue strength of these beams, a laboratory study should be undertaken. The same specimens could be used to determine both of these properties.
4. There have been several methods recently published on how to repair damaged prestressed concrete beams. However, little

or no data are available on the strength of these beams assuming no repair was undertaken. Also, no data or information is available on the lateral distribution of the post-tensioning force used in the repair of the damaged bridge. A study should be undertaken to obtain the information and data previously described.

5. Although in the authors' opinion there should be no fatigue problems with the proposed high-strength bolt shear connectors (HSBSC), a relatively small study should be undertaken to verify this opinion and also to determine if there are any problems with the HSBSC in combination with the two different strengths of concretes [16].

8. ACKNOWLEDGMENTS

The study presented in this report was conducted by the Engineering Research Institute of Iowa State University and was sponsored by the Highway Division, Iowa Department of Transportation, and the Iowa Highway Research Board under Research Project HR-238.

The authors wish to extend sincere appreciation to the engineers of the Iowa DOT for their support, cooperation, and counseling. A special thanks is extended to the following individuals for their help in various phases of the project:

- Charles A. Pestotnik, Bridge Engineer, (retired), Iowa DOT
- Don Schultze, Acting Bridge Engineer, Iowa DOT
- John P. Harkin, Bridge Rating Engineer, Iowa DOT
- Vernon J. Marks, Research Engineer, Iowa DOT
- Robert Younie, Resident Maintenance Engineer, Fort Dodge Office, Iowa DOT
- Kenneth D. Westergard, County Engineer, Dickinson County

Special thanks are accorded the following students for their assistance in various phases of the project: graduate students Robert W. Funke, Jr., and Douglas L. Wood, and undergraduate students Diane O. Viise, J. Glen Hunter, and Michael L. Wright.

9. REFERENCES

1. American Association of State Highway and Transportation Officials. Standard Specifications for Highway Bridges. Thirteenth Edition. Washington: American Association of State Highway and Transportation Officials, 1983.
2. Bathe, K-J., E. L. Wilson and F. E. Peterson. SAP IV, A Structural Analysis Program for Static and Dynamic Response of Linear Systems. Berkeley: College of Engineering, University of California, 1974.
3. Beck, B. L. "Transducers for monitoring of Bridge Behavior." M.S. Thesis, Iowa State University, Ames, Iowa, 1985.
4. Beck, B. L., F. W. Klaiber and W. W. Sanders, Jr. "Field Testing of County Road 54 Bridge over Anclote River, Pasco County, Florida." ERI Project 1730, ISU-ERI-Ames-85417. Ames: Engineering Research Institute, Iowa State University, 1984.
5. Beckwith, T. G., N. L. Buck and R. D. Marangoni. Mechanical Measurements, Third Edition. Reading: Addison-Wesley Publishing Company, 1982.
6. Berenson, M. L., D. M. Levine and M. Goldstein. Intermediate Statistical Methods and Applications. Englewood Cliffs: Prentice-Hall, Inc., 1983.
7. Berwanger, C. "Transient Thermal Behavior of Composite Bridges." American Society of Civil Engineers, Journal of the Structural Division. Vol. 109, No. 10, October 1983, pp. 2325-2339.

8. Berwanger, C. and Y. Symko. "Finite Element Solutions for Thermal Stresses in Steel-Concrete Composite Bridges." *Journal of the Society for Experimental Stress Analysis, Experimental Mechanics*. Vol. 16, No. 5, May 1976, pp. 168-175.
9. Brendel, A. E. "Some Comments on the Evaluation of Transducer Performance." *Journal of the Society for Experimental Stress Analysis, Experimental Techniques*. Vol. 7, No. 5, May 1983, pp. 20-21.
10. Cederberg, A. R. and R. F. Foral. "A Strain Gage Transducer for Measuring Strains in Composite Materials." *Journal of the Society for Experimental Stress Analysis, Experimental Techniques*. Vol. 7, No. 5, May 1983, pp. 22-25.
11. Dally, J. W. and W. F. Riley. Experimental Stress Analysis. New York: McGraw Hill Book Company, 1978.
12. Dedic, D. J. and F. W. Klaiber. "High Strength Bolts as Shear Connectors in Rehabilitation Work," *Concrete International Design and Construction, American Concrete Institute*. Vol. 6, No. 7, July 1984, pp. 41-46.
13. Dorsey, J. "Homegrown Strain Gage Transducers." *Journal of the Society for Experimental Stress Analysis*. Vol. 17, No. 7, July 1977, pp. 255-260.
14. Dunker, K. F. "Strengthening of Simple Span Composite Bridges by Post Tensioning." Ph.D. Dissertation, Iowa State University, Ames, Iowa, 1985.

15. Dunker, K. F., F. W. Klaiber and W. W. Sanders, Jr. "Design Manual for Strengthening Single-Span Composite Bridges by Post-tensioning," Final Report--Part III, ERI Project 1536, ISU-ERI-Ames-85229. Ames: Engineering Research Institute, Iowa State University, 1985.
16. Klaiber, F. W., D. J. Dedic, K. F. Dunker and W. W. Sanders, Jr. "Strengthening of Existing Single Span Steel Beam and Concrete Deck Bridges. Final Report--Part I." ERI Project 1536, ISU-ERI-Ames-83185. Ames: Engineering Research Institute, Iowa State University, 1983.
17. Klaiber, F. W., K. F. Dunker and W. W. Sanders, Jr. "Feasibility Study of Strengthening Existing Single Span Steel Beam Concrete Deck Bridges." ERI Project 1460, ISU-ERI-Ames-81251. Ames: Engineering Research Institute, Iowa State University, 1981.
18. Klaiber, F. W., K. F. Dunker and W. W. Sanders, Jr. "Strengthening of Single Span Steel Beam Bridges." American Society of Civil Engineers, Journal of the Structural Division. Vol. 108, No. ST12, December 1982, pp. 2766-2780.
19. Leahy, T. F. "A Reusable Biaxial Strain Transducer." Journal of the Society for Experimental Stress Analysis, Experimental Mechanics. Vol. 14, No. 3, March 1974, pp. 111-117.
20. Mancarti, G. D. "Strengthening California's Bridges by Prestressing." Transportation Research Record 950, Second Bridge Engineering Conference, Volume 1, 1984, pp. 183-187.
21. Measurements Group, Inc. "Bondable Resistance Temperature Sensors and Associated Circuitry," TN-506-1. Raleigh: Measurements Group, Inc., 1984.

22. Measurement Group, Inc. "Modern Strain Gage Transducers--Their Design and Construction." Epsilonics, Volumes 1-4. Raleigh: Measurements Group, Inc., 1981-84.
23. Nilson, A. H. Design of Prestressed Concrete. New York: John Wiley and Sons, Inc., 1978.
24. Reagan, R. S. "An Analytical Study of the Behavior of Prestressed Composite Beams." M.S. Thesis, Rice University, Houston, 1966.
25. Roark, R. J. Formulas for Stress and Strain, Fourth Edition. New York: McGraw-Hill Book Company, 1965.
26. SAS Institute. SAS User's Guide, 1979 Edition. Cary: SAS Institute, Inc., 1979.
27. Stras, J. C., III. "An Experimental and Analytical Study of Prestressed Composite Beams." M.S. Thesis, Rice University, Houston, 1964.